# Modeling of conduction and natural convection in icewater systems containing porous metal foams

by

# Sylvain Bories

Department of Mechanical Engineering

McGill University

Montréal, Québec, Canada

August 2011

A thesis submitted to McGill University in partial fulfilment of the requirements for the degree of Master of Engineering

© Sylvain Bories, Montréal, Québec, Canada, 2011

#### Abstract

A numerical investigation of heat conduction and laminar natural convection in ice-water systems containing porous metal foams, undertaken in the context of computationally convenient two-dimensional steady-state problems, is presented in this thesis. The overall goals of this work are to provide improvements to available cost-effective mathematical models of these phenomena, solve these models numerically, and investigate the influence of the porous metal foam on fluid flow and heat transfer in ice-water systems. The long-term goal (and the motivation for this work) is to contribute to the development of mathematical models and numerical solution methods for simulations of enhanced ice-water seasonal cold-storage systems.

The proposed mathematical models are based on the local volume-averaging method. A Darcy-Brinkman-Forchheimer model is used for the momentum equations. For the heat transfer, volume-averaged equations governing two intrinsic phase-average temperature fields are used: one for the metal foam and the other for the water (solid or liquid). The following improvements to available two-temperature models are proposed: novel expressions for the interfacial heat transfer coefficient in both the conduction and convection regimes; and modified effective thermal conductivity models that provide consistency between predictions of one-temperature and two-temperature models in the limit of local thermal equilibrium.

A well-established fixed-grid, co-located, finite volume method (FVM) is adapted for the numerical solution of the aforementioned mathematical models. All of the computer simulations are done with rectangular calculation domains, cooled and heated on the opposite side walls, and the adiabatic condition is imposed on the top and bottom walls.

The FVM is first validated by the comparing the predicted results to experimental data for steady-state conduction and laminar natural convection in square enclosures containing pure liquid water and ice-water systems (no foam), with temperatures spanning the density inversion point of water. The problem involving natural convection in pure liquid water is solved using a variable-property model (VPM) and also a constant-property model (CPM), with the constant fluid properties evaluated at several reference (or average) temperatures,

and the reference (or average) temperature that yields the lowest differences between the results obtained with the VPM and CPM is determined.

The FVM is then used to predict laminar natural convection flow fields and average heat transfer rates at the walls in square horizontal enclosures containing liquid water and aluminum foam. The left wall-temperature is fixed at 0°C while the right-wall temperature is assigned two different values above the density inversion temperature of water. The effect of changes in the dimensions of the enclosure is investigated with no foam and the results are compared to those of simulations with five different foams. The effects of thermal dispersion and of the Forchheimer drag term on the computed heat transfer rates are quantified.

Finally, a demonstration problem involving conduction and laminar natural convection in ice-water-metal-foam systems is investigated, for a representative porous foam made of aluminum, and other parameters in ranges relevant to seasonal cold-storage applications. The rectangular enclosure is maintained in a vertical position with respect to the gravitational acceleration vector. Its width in the horizontal direction is 10 cm, its height is varied between 10 to 50 cm, and the imposed cold and hot wall temperatures are -20°C and 20°C, respectively. The computed streamlines, water-ice interface positions, and wall heat transfer rates are compared to the corresponding results obtained with open domains (no foam). The influence of the aspect ratio of the enclosure is also investigated and the results are presented.

#### Résumé

Une étude numérique portant sur la conduction thermique et la convection naturelle laminaire dans des systèmes glace-eau contenant des mousses métalliques poreuses est présentée dans cette thèse. Elle est réalisée grâce à la résolution de problèmes bidimensionnels et stationnaires. Les objectifs principaux de cette étude sont d'améliorer les modèles existants pour ces phénomènes et de les résoudre numériquement afin d'examiner l'influence de l'ajout de mousse métallique sur les écoulements et les transferts thermiques dans les systèmes glace-eau. L'objectif à long terme ayant motivé cette étude est de contribuer au développement de modèles mathématiques et méthodes numériques capables de simuler des systèmes glace-eau optimisés pour le stockage saisonnier de froid.

Les modèles mathématiques proposés sont basés sur la méthode de moyenne sur volume représentatif. Un modèle type Darcy-Brinkman-Forchheimer est utilisé pour les équations d'écoulement fluide. Pour les équations gouvernant le transfert de chaleur, on considère deux champs de température moyennés sur chacune des phases : un pour la mousse métallique et un autre pour l'eau (solide ou liquide). Les améliorations suivantes sont proposées pour les expressions semi-empiriques données aux paramètres de ces équations: de nouvelles expressions pour le coefficient de transfert thermique entre les phases sont développées, à la fois dans le régime de pure conduction thermique et dans le régime de convection; des modifications sont apportées aux modèles de conductivité effective afin d'assurer la cohérence des modèles considérant un seul champ de température et ceux en considérant deux.

Une méthode de type volume fini (FVM dans le texte) à grille fixe est adaptée et toutes les simulations sont réalisées sur des domaines rectangulaires. Les parois de droite et de gauche sont respectivement chauffées et refroidies et celles du haut et du bas sont adiabatiques.

La méthode numérique est tout d'abord validée grâce à une comparaison à des résultats expérimentaux de convection naturelle laminaire dans des cavités carrées contenant de l'eau liquide et des systèmes glace-eau (pas de mousse de métal), dans des conditions stationnaires. Les températures des parois sont choisies de part et d'autre de la température de densité maximale de l'eau. Le problème est simulé avec un modèle à propriétés variables

(VPM) et un modèle à propriétés constantes (CPM). Les propriétés sont évaluées à plusieurs températures de référence, et celle qui implique la plus faible différence entre le VPM et le CPM est déterminée.

Le code est ensuite utilisé pour prévoir les champs de vitesse liés à la convection naturelle laminaire et le transfert thermique moyen depuis les parois de cavités carrées horizontales contenant de l'eau liquide et de la mousse d'aluminium. La température de la paroi de gauche est fixée à 0°C tandis que celle de la paroi de droite prend deux valeurs différentes. L'influence des dimensions de la cavité est examinée en l'absence de mousse métallique et les résultats sont comparés à ceux obtenus avec cinq mousses différentes. Les effets de la dispersion thermique et du terme de traînée de Forchheimer sont quantifiés.

Enfin, un problème de démonstration est simulé. La conduction thermique et convection naturelle laminaire dans des systèmes glace-eau-mousse-métallique est étudiée avec une mousse d'aluminium typique, les autres paramètres étant choisis pour correspondre à des situations de stockage saisonnier de froid. La cavité rectangulaire est verticale, sa longueur fixée à 10 cm, sa hauteur comprise entre 10 et 50 cm et les parois froides et chaudes sont maintenues à -20°C et 20°C respectivement. Les résultats des simulations en termes de lignes de courant, positions de l'interface glace-eau et flux thermiques depuis les murs sont comparés aux résultats de simulations sans mousse métallique. L'influence du rapport d'aspect de la cavité est aussi examinée et les résultats sont présentés.

### Acknowledgements

First, I would like to express my gratitude to my supervisor, Professor Bantwal Rabindranath Baliga, for his constant guidance, wise advice and for the indefectible support he provides to his students. Working under his supervision was an enjoyable and rewarding experience.

I would like to thank the Natural Sciences and Engineering Research Council of Canada (NSERC) for research grants to Professor Baliga. The financial support from the Mechanical Engineering Department and from Ecole Polytechnique in France made this project possible and was much appreciated.

I am also thankful to the staff of the Mechanical Engineering Department for their constant support as regards to practical issues and for their remarkable reactivity. The help that was provided by Joyce Nault, Nozomi Kanekatsu and Mary Fiorilli was essential to make the admission, research and graduation official procedures as smooth as they could have been.

Many thanks to the members of the Heat Transfer Laboratory, Nirmalakanth Jesuthasan, Alexandre Lamoureux, James Medvescek, Jeffrey Poissant, Samer Afara, Raul Palacios-Gomez and Brandon Tulloch, for the wonderful work environment they all helped to create with their constant support and camaraderie.

On the personal front, I would like to thank all the friends I met in Montreal and turned this two-year stay in an unforgettable experience. I am also infinitely grateful to my family and friends back in France who supported my decision to undertake this adventure away from home and constantly encouraged me, especially my parents, Catherine and Alain, my sister, Marion, and my brother, Florent.

# Table of Contents

Abstract		ii
Résumé		iv
Acknowled	dgements	vi
Table of C	Contents	vii
Nomenclat	ture	ix
Chapter 1:	Introduction	1
_	Motivation, overall goals and background	
1.2 I	Literature review	6
1.2.1	Latent-heat thermal energy storage using ice-water systems	6
1.2.2 pheno	Mathematical models of fluid flow, heat transfer, and solid-liquid omena in porous metal foams	
1.2.3	Key textbooks and handbooks	21
1.3	Specific objectives	22
Chapter 2:	Mathematical Models	24
2.1	Conduction and natural convection in ice-water systems in open doma	ins 25
2.2	Conduction and natural convection in ice-water-metal-foam systems	29
2.2.1	Some definitions	30
2.2.2	Governing equations	32
2.2.3	Geometrical characteristics of porous metal foams	39
2.2.4	Comparison and adaptation of effective thermal conductivity mode	els 42
2.2.5 foam	Interfacial heat transfer coefficients for pore-scale heat exchange liquid-water and metal-foam-ice regions	
2.3 I	Dimensionless parameters	59
Chapter 3:	Numerical Method	62
	Synopsis of a Finite Volume Method for steady, two-dimensional, finsfer in open domains	
3.1.1	Governing equations	62
3.1.2	Domain discretization	64
3.1.3	Discretized equations	65
3.1.4	Solution of the discretized equations	66

	Finite Volume Method for simulation of steady, two-dimensional, fluid flow and asfer in Water-Ice-Metal-Foam systems	
3.2.1		
3.2.2	Modifications implemented for computing fluid flow and pressure 69	
3.2.3 temp	Modifications implemented for computing intrinsic-phase-average eratures	
3.3	Continuation method	
Chapter 4:	Results and Discussions	
	Natural convection in liquid water contained in open square enclosures (no foam), nperatures spanning the density inversion point	
	Conduction and natural convection in ice-liquid-water systems contained in open enclosures (no foam)	
4.2.1 illust	Validation of the proposed mathematical model, verification of the FVM, and ration of the proposed continuation method	
	Flow patterns and ice-liquid-water interface shapes for high values of the eigh number	
	Natural convection in liquid-water-porous-metal-foam systems contained in square res	
4.3.1	Comparison of natural convection with and without porous metal foam 88	
4.3.2	Influence of Rayleigh number and five different foams	
4.3.3	Influence of thermal dispersion and Forchheimer drag term96	
	Conduction and natural convection in ice-liquid-water-porous-metal-foam systems ed in rectangular enclosures	
4.4.1	Comparison of results obtained with and without porous metal foam 98	
4.4.2	Demonstration problem	
4.5	Interstitial heat transfer	
Chapter 5:	Conclusion	
5.1	Review of the work and its main contributions	
5.2	Suggestions for extensions of this work	
List of Re	ferences	

# Nomenclature

AR	Aspect ratio of the enclosure
$a_{\scriptscriptstyle P},a_{\scriptscriptstyle NB}$	Coefficients in the discretized equation for $\phi$
$a_{sf}$	Foam specific area
$C_{\scriptscriptstyle D}$	Thermal dispersion coefficient
$c_{\scriptscriptstyle P}$	Specific heat at constant pressure
$d_f$	Fiber diameter
$d_p$	Pore diameter
Da	Darcy number Forchheimer coefficient
$rac{f}{g}$	Magnitude of the gravitational acceleration
$Gr_{d_f}$	Local Grashof number based on the fiber diameter
h	Surface heat transfer coefficient
$h_i, h_l$	Ice and water interfacial heat transfer coefficients
$\overline{h}_{ ext{wall}}$	Average heat transfer coefficient at the walls (left or right)
$H_x, H_y$	Cavity dimensions in the x and y directions
$\stackrel{\cdot \cdot \cdot}{k}$	Thermal conductivity
$k_{_D}$	Thermal dispersion thermal conductivity
$k_{\it eff_i}, k_{\it eff_l}$	Total effective conductivities
$k_{si}, k_{sl}$	Coupled effective conductivities
$k_{ss}, k_{ll}, k_{ii}$	Solid (foam), liquid water and ice effective conductivities
K	Permeability
$\overline{Nu}_{wall}$	Average wall Nusselt number
$Nu_{sf}$	Interfacial Nusselt number
p	Static pressure
<i>P</i> Pr	Reduced pressure
Ra	Prandtl number Modified Rayleigh number
$\operatorname{Re}_{d_f}$	Local Reynolds number based on the fiber diameter
$\operatorname{Re}_{K}^{'}$	Permeability Reynolds number
$S_{u,}$ $S_{v,}$ $S_{E,}$ $S_{T}$	Source terms
T	Temperature
$T_C, T_H$	Cold (left) and Hot (right) wall temperatures
$\Delta T_{melt}$	Melting temperature tolerance
$T_m^*$	Density inversion parameter
u	Darcy velocity
и	Velocity component in <i>x</i> -direction
$\boldsymbol{v}$	Velocity component in <i>y</i> -direction

Cartesian coordinate axes *x*,*y* 3 Porosity  $\alpha_u, \alpha_v, \alpha_P, \alpha_T$ Under-relaxation factors  $\Gamma_{\phi}$ Diffusion coefficient for variable  $\phi$  $\theta$ Enclosure inclination angle λ Second coefficient of viscosity Dynamic viscosity μ Density ρ Dependent variable

### **Subscripts**

0 constant property
i ice
l liquid water
m maximum (refers to the maximum density of water)
melt pertaining to melting temperature of ice (0 °C in this work)
s solid (refers to the foam)
w water (could be liquid water or ice)

### Chapter 1: Introduction

#### 1.1 Motivation, overall goals and background

This thesis is an endeavor of the author, in collaboration with his supervisor, to contribute to ongoing worldwide efforts to develop and implement enhanced thermal energy storage systems. The overall goals of this work are to provide improvements to cost-effective mathematical models of fluid flow and heat transfer in ice/water systems containing porous metal foams, solve these models numerically, and investigate the influence of this additional porous structure on steady-state conduction and laminar natural convection.

Thermal energy storage (TES) has been an active area of research over the last 50 years mainly because it is useful for enhancing the efficiency of energy-conversion and heating/cooling systems, by matching energy (or cold) supply and demand during summer-winter, day-night, and peak-off-peak periods. TES systems are divided into two main categories: sensible systems, in which energy is stored by changing the temperature of a suitable material; and latent-heat systems, in which change of phase of a suitable material is used to store energy. The materials used in latent-heat systems are called phase-change materials (PCMs), and gas-liquid, solid-gas, or solid-liquid phase-change processes may be involved. Solid-liquid latent-heat TES systems are particularly attractive since they provide a high energy storage density compared to sensible TES, and the mass density change of the PCM during the phase-change process is not overly large. For example, the latent heat of fusion of a mass pure water (a popular PCM for so-called "cold storage") is approximately equal to the energy necessary to raise the temperature of an equivalent mass of this substance from 0°C to 80°C; and the change in density of pure ice to pure water at 0 °C is about 10%. Furthermore, the phase-change process for a PCM in a latent-heat TES system takes place at an essentially constant temperature (the melting point), as the related variations in pressure are usually insignificant, so the overall temperature swings during the charging (storage) and discharging (harvesting) periods are relative small compared to those in sensible systems.

Several reviews of latent-heat TES systems and the PCMs used in these systems were written in the last decade. Zalba et al. (2003) gave an overview of different PCMs and their applications. Farid et al. (2004) and Sharma et al. (2009) provided useful reviews of such systems. In the reviews prepared by Khudhair and Farid (2004), Zhang et al. (2006,2007) and Pasupathy et al. (2008) the focus is on applications of latent-heat TES systems for buildings, and Jegadheeswaran and Pohekar (2009) have reviewed the methods that are used to improve the performance of such systems. Saito (2002) focused on cold storage in his review.

Heat and cold storage can be classified as either seasonal (long-term) or daily (short-term; diurnal). The charging (storage) and discharging (harvesting) periods in seasonal and daily TES systems are typically of the order of half-year and half-day, respectively. Daily TES is the most widely used and investigated, but there are also a few examples of seasonal TES in the literature. Özturk (2004) tested seasonal latent-heat TES with paraffin wax as a PCM, for a full-size greenhouse. He concluded that such systems were viable, but proper modeling of the charging and discharging processes was crucial for optimizing them. The work reported in this thesis is relevant for designs of both seasonal and daily latent-heat TES systems.

The choice of the PCM used in a latent-heat TES system depends on the application. Abhat (1983) is the first author to provide a classification of PCMs for such systems. He studied PCMs with melting points ranging from 0°C to 120°C, and grouped them in the following categories: paraffins, fatty acids, inorganic salt hydrates, and eutectic compounds. The key considerations in the choice of a PCM for a particular application are its melting temperature, heat of fusion, thermal conductivity, and mass density. Zalba et al. (2003) provided a summary of these characteristics for some organic and inorganic PCMs which have been studied by different researchers for their potential use in TES systems. Commercially available paraffins are widely used in TES systems for solar energy: they melt at temperatures between 9°C and 112°C [Zalba et al. (2003)], and the stored thermal energy can be used for space heating in buildings. Papers on this class of materials include those by Hong and Xin-shi (2000) and Sari (2004). PCMs to be used for so-called cold storage need to have a melting point below the ambient air temperature.

Examples of such PCMs are salt solutions and pure water. As pointed out in *ASHRAE Handbook*, *HVAC Applications* (2007), water is the most common PCM used for cooling applications of latent-heat TES systems. Ice-water TES systems are attractive because they are reliable, safe and inexpensive, and have a relatively high latent heat of fusion (333 kJ/kg [Zalba et al. (2003)]). The practice of seasonal storage of ice has been around for over two thousand years, dating back to 400 BC in Iran. Until recently, the Hungarian parliament building in Budapest was cooled in the summer using ice harvested in the winter.

In latent-heat TES systems, containment has a strong influence on the heat transfer rate from and to the PCM. As described by Khudhair et al. (2004), three main methods are used in building applications: incorporation, impregnation, and encapsulation. Regin et al. (2008) wrote a useful review on the heat transfer characteristics of encapsulated PCMs. There are many advantages of microencapsulating PCMs, such as increasing the heat transfer area, eliminating adverse interactions with the outside environment (corrosion for example), and controlling PCM volume expansion. But the price of encapsulation makes it undesirable in the context of the present study, in which the focus is on models and methods relevant to inexpensive, and yet efficient, latent-heat systems for cold storage, with applications to residential and small commercial buildings. Additional information on microencapsulated PCMs is available in reviews written by Hawlader et al. (2003) and Alkan et al. (2009).

As was stated earlier, the underlying concept of latent-heat ice-water TES systems for seasonal cold storage, namely, freezing water in suitable containment vessels in the winter and using it for air conditioning in the summer, is not new. However, novel approaches are needed for enhancing the effectiveness of such systems. For example, several techniques for increasing the effective thermal conductivities (and the rates of heat transfer) in such systems are being actively developed (descriptions are provided in the literature review, Section 1.2). One such technique involves the insertion of porous metal foams (akin to that shown in Fig. 1.1) in ice-water systems, for obtaining significant increases in the effective thermal conductivity of both the liquid water and ice, with only small (less than 10%) reductions in their energy density. Optimal thermal

designs of such ice-water-porous-metal-foam systems for cold storage can be obtained using numerical solutions of available cost-effective mathematical models of the related fluid flow and heat transfer phenomena.

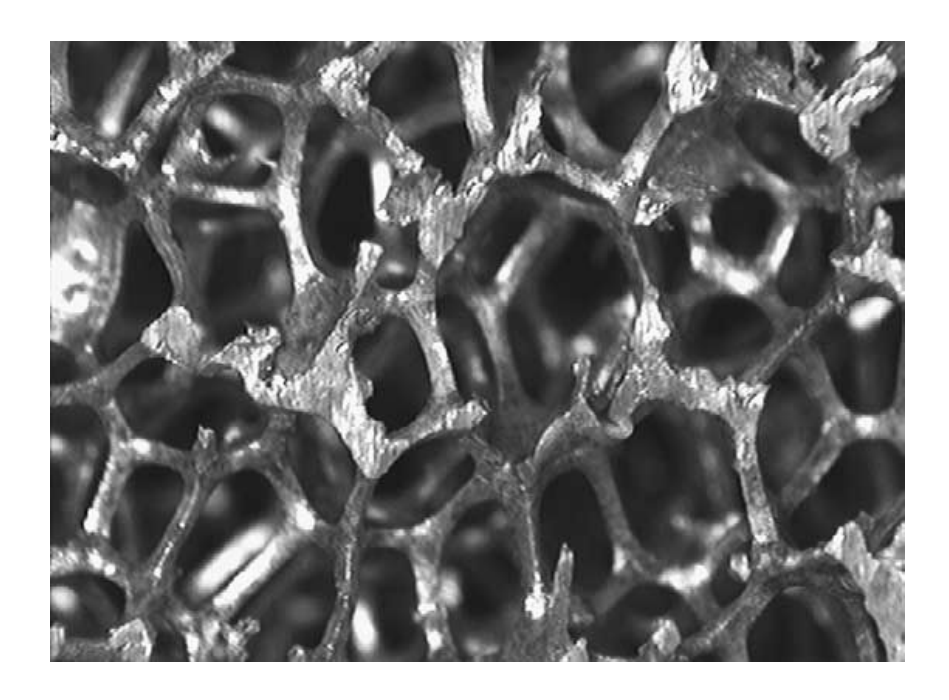


Figure 1.1: Photomicrograph of a porous aluminum foam with ten pores per inch [Tadrist et al. (2004)]

The above-mentioned cost-effective mathematical models of fluid flow and heat transfer in ice-water-porous-metal-foam systems are typically based on local volume-averaging and two intrinsic phase-average temperature fields, one for the metal foam and the other for the water (solid or liquid). They require semi-empirical expressions for the permeability of the metal foam, Forchheimer coefficient (associated with inertial or form drag at the pore level), effective thermal conductivities of the metal foam and water (liquid or solid), dispersion thermal conductivity, pore-level interfacial heat transfer coefficient, and specific interfacial area. The calculation domain geometry and boundary conditions, porosity and pore size of the metal foam, and properties of the metal, ice, and liquid water are provided as inputs to these models. In the work reported in this thesis, the applicability of such models to heat conduction and laminar natural convection in ice-water-porous-metal-foam systems was assessed, in the context of computationally convenient two-dimensional steady-state problems in rectangular enclosures akin to the

one depicted schematically in Fig. 1.2. Improvements to some of the aforementioned semi-empirical expressions were also proposed. A well-established fixed-grid finite volume method (FVM) was adapted for numerical solutions of the mathematical models, and validated using available experimental data of Elkouh (1996) for steady-state conduction and laminar natural convection in pure ice-water systems.

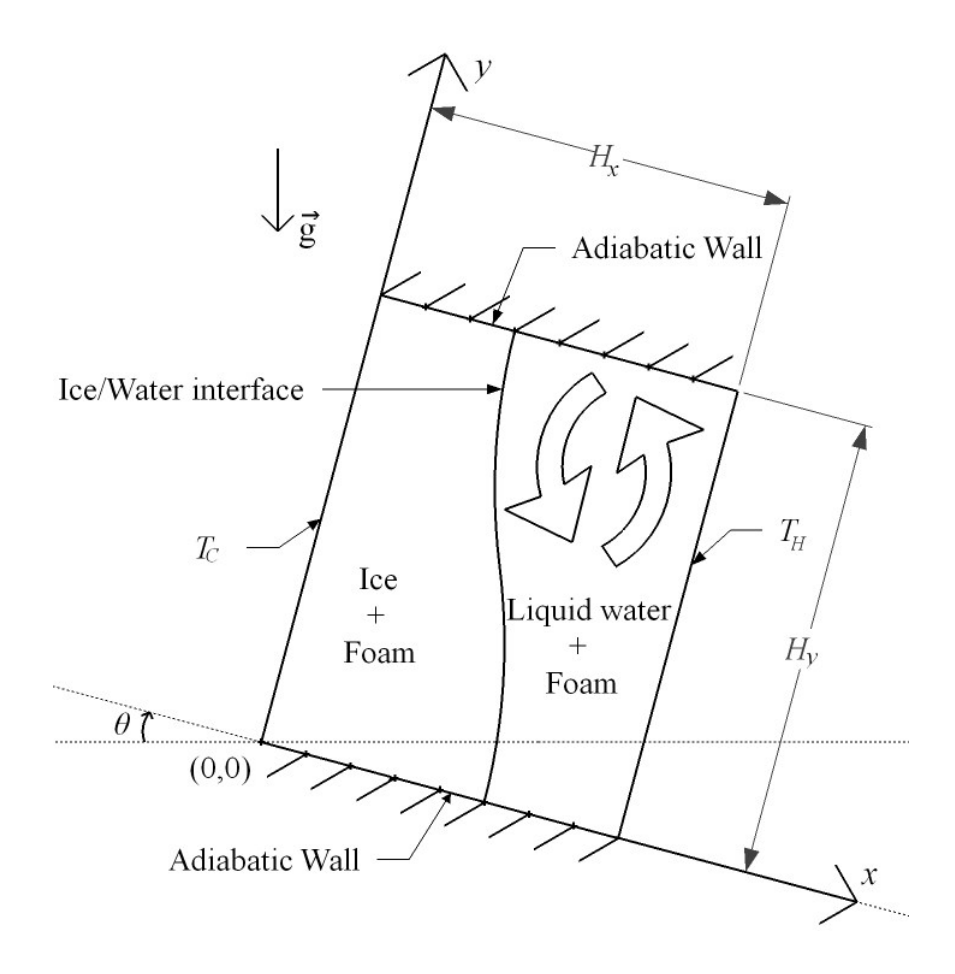


Figure 1.2: Steady-state two-dimensional conduction and laminar natural convection heat transfer in an ice-water-porous-metal-foam system contained in a rectangular enclosure; schematic representation of the calculation domain and boundary conditions used in the numerical simulations.

#### 1.2 Literature review

This section is not intended to be an exhaustive review of the numerous publications on the various areas of interest in this work. Rather, the objectives here are to concisely review some of the key publications directly relevant to this project and provide the interested reader with references to several reviews, textbooks, and handbooks on the areas of interest. This section is divided into three main parts: latent-heat TES using ice-water systems; mathematical models of fluid flow, heat transfer, and solid-liquid phase-change phenomena in porous metal foams; and notes on some key textbooks and handbooks.

#### 1.2.1 Latent-heat thermal energy storage using ice-water systems

Latent-heat solid-liquid TES systems that use water as the PCM are promising, but they have some limitations that have prevented them from being widely used. The methods to overcome these limitations, and some of the research and development works for overcoming them, are discussed in this section.

#### Heat transfer enhancement techniques

Most solid-liquid PCMs used in latent-heat TES systems have relatively low thermal conductivity ( $\leq 5$  W/m.K, [Zalba et al. (2003)]). Several techniques have been proposed to increase the effective thermal conductivity, heat transfer rates, compactness, and efficiency of such systems. The most up-to-date and thorough review of such techniques, and their advantages and drawbacks, is the one by Jegadheeswaran and Pohekar (2009).

Two techniques on which researchers have been mostly focusing in the last decade are the addition of metal or graphite fibers to the PCM, and the use of porous metal foams embedded within the PCM. For useful references on classical techniques such as finned tubes, the reader is referred to the works of Velraj et al. (1999) and Jegadheeswaran and Pohekar (2009).

Fukai et al. (2002) studied composites of carbon brushes and n-octadecane, placed around heat exchanger tubes in a fin-type anisotropic configuration. The transient thermal responses of the composites were measured for different fiber diameters and concentrations. The authors also developed a numerical model that takes account of the anisotropy of the medium. It gave good predictions of the experimental results and allowed them to derive a critical diameter above which further improvement is not possible, due to thermal resistance between the brushes and the tube surface. With a properly chosen diameter, for a carbon-brushes volume fraction of just 1%, the effective thermal conductivity was increased by a factor of five (compared to that of just the PCM).

Xiao et al. (2002) formed a composite paraffin (styrene-butadiene-styrene) PCM with graphite as the agent for enhancing the effective conductivity. They also incorporated thermoelastic elastomers, which provided shape-stability to commercially available paraffin. This innovative material exhibited the same phase-transition characteristics as paraffin and 80% of its latent heat of fusion, while the effective thermal conductivity was significantly increased. Mettawee and Assassa (2007) enhanced the thermal conductivity of a paraffin wax by adding to it a small mass fraction (about 0.5%) of aluminum powder. They compared the progress of the melting surface (front) in both the composite compound and the pure paraffin, as part of a PCM solar thermal collector, and found significant differences. They also found that with the composite compound, the charging time was reduced by approximately 60%.

Frusteri et al. (2005) studied another simple configuration, in which carbon fibers were randomly mixed with a PCM (inorganic PCM44, a eutectic mixture). They measured the effective thermal conductivity of the composites and found that it could be approximated by a linear function of the fiber weight fraction, for up to 10% mass fraction. With 7% weight fraction of the micro-fibers used, the effective thermal conductivity was increased by a factor of about four (compared to that of just the PCM). Randomly-mixed fibers are much easier to use than structured brushes or foams, but this ease of use comes at the cost of thermal performance, because of the lack of contact between the fibers. Furthermore, it

is hard to avoid separation (sedimentation) of the fibers from the PCM. In the aforementioned experiment, the composite was shaken vigorously right before the experiments, a procedure which would be inapplicable or impractical in the case of seasonal or diurnal cold storage.

Cabeza et al. (2002) wrote an article devoted to heat transfer enhancement techniques with water as the PCM. They compared three methods: addition of stainless steel pieces, addition of copper pieces, and use of a graphite matrix. The last technique showed the best results, suggesting that embedding high-conductivity porous foams is good for heat transfer enhancement in solid-liquid latent-heat TES systems.

#### Some issues associated with the use of water as the PCM

A significant amount of information on latent-heat TES systems that use water as the PCM is available in the literature. An excellent synopsis of such systems and related issues can be found in the *ASHRAE Handbook*, *HVAC Applications* (2007). Accurate mathematical models and numerical solution procedures are necessary for designing such systems properly, because of the particular properties of water, such as supercooling, density inversion at 4°C, and random character of crystallization.

Supercooling can have drastic effects on the freezing of water [Angell (1983)]. This phenomenon has been reviewed by Mishima and Stanley (1998) and Debenedetti and Stillinger (2001). The inclusion of a structure such as porous media strongly affects this phenomenon, as pointed out by Warnock (1986), who used optical techniques to measure supercooling in a transparent porous glass.

Supercooling in salt hydrates can be limited by mixing the PCM with other compounds such as nucleating agents (which prevent or limit supercooling) and thickeners (which ensure phase stability). These techniques were summarized in the review by Farid et al. (2004). For pure water, the main works on the control of supercooling were described by Saito et al. (1992). They pointed out that the degree of supercooling is highly dependent on the cooling rate, surface properties, and surface area of the container. Active methods

to control the initiation of freezing of supercooled water have developed over the years, and include application of electric fields and ultrasonic vibrations. A few authors have proposed approaches for including supercooling in numerical simulations of latent-heat TES systems, and a general adaptive solution algorithm has been proposed by Günther et al. (2007). However, in latent-heat ice/water TES systems, the impurities found in potable water or intentional agitation are generally sufficient to initiate nucleation of ice crystals. Residual ice also prevents supercooling. Therefore, the size of ice/water TES systems should be chosen so that some residual ice is always present, at the end of the melting and start of the freezing periods.

Corrosion can cause serious problems in latent-heat TES systems, so the compatibility of the PCM and the container must be carefully verified. Corrosion experiments on salt hydrates as the PCMs were conducted by Cabeza et al. (2001). With sodium carbonate, they concluded that steel and stainless steel can be used without problems, but not copper, aluminum, and brass. With potassium carbonate, steel, stainless steel, and aluminum are all suitable. When the PCM is potassium chloride, only stainless steel can be used for long-term TES applications. The use of steel for the construction of the container results in significant corrosion problems when water is used as the PCM, as in this project, but copper, aluminum, and brass are all fine.

The mass density of pure water reaches its maximum value at the density inversion point,  $T_m = 4$ °C, and has an essentially parabolic variation with temperature about this point. An accurate expression for the variation of water density with temperature in the vicinity of the density inversion temperature was provided by Kukulka et al. (1987). Their expression was used in the work reported in this thesis. Buoyancy-driven natural convection in pure water at temperatures that span the density inversion point is significantly different, in both fluid flow and heat transfer characteristics, from that in fluids with densities that vary monotonically with temperature. A thorough review of the works done on steady-state natural convection in pure water with temperatures spanning the density inversion point can be found in the thesis by Elkouh (1996). From his review and work, it is useful (for the purposes of the work reported in this thesis) to note the

following key points pertaining to natural convection in water contained in a vertical rectangular cavity, with one vertical wall heated and maintained at a hot temperature  $T_H$ , the opposite vertical wall cooled and maintained at a cold temperature  $T_C$ , and the top and bottom (horizontal) walls very well insulated (essentially adiabatic):

- A density inversion parameter,  $T_m^* = (T_m T_C)/(T_H T_C)$ , plays a key role in the fluid flow and heat transfer process. When it is in the 0 1 range, the water along the cold wall has a negative thermal expansion coefficient while the water along the hot wall has a positive one. Therefore, two recirculating cells develop within the enclosure, with fluid flow in opposite directions.
- When the density inversion parameter  $T_m^*$  has a value in the vicinity of 0.5, the fluid flow is particularly sensitive to even minor changes in boundary conditions. The published numerical and experimental results do not agree well for these conditions, due to their sensitivity to intrinsic uncertainties in the experimental data. For a given Rayleigh number, the overall Nusselt number is a minimum when  $T_m^* = 0.5$ .
- There is no consensus regarding the temperature at which the thermophysical properties of water should be evaluated when a constant-property model is used. Elkouh (1996) suggested a zonal temperature, which will be elaborated in chapters 2 and 4.

### 1.2.2 Mathematical models of fluid flow, heat transfer, and solid-liquid phasechange phenomena in porous metal foams

In this section, publications on practical approaches to the mathematical modeling of fluid flow, heat transfer, and solid-liquid phase-change phenomena in porous metal foams are reviewed, along with some key publications on thermophysical properties of such foams.

#### Volume-averaging approach

The most intuitive and exact approach to the modeling of flows in porous media is the complete local or the microscopic-scale description. In this approach, the Newtonian fluid flow and heat transfer in the pores of the porous medium are modeled using the continuity, Navier-Stokes, and energy equations, and the no-slip, impermeability, continuity of temperature, and continuity of heat flux conditions are applied at all fluid-solid boundaries. This approach cannot be used in most practical problems for two main reasons: the computational time requirements and costs are far too large, and the exact description of the geometry at this scale is rarely available due to the high local heterogeneity of most porous structures [Nield and Bejan (2006)].

The most famous early contribution to practical models of flows in porous media was made by Darcy in 1856 [Kaviany (1999); Nield and Bejan (2006)]. In his model, which is now called the Darcy model, a volume-averaged velocity (the so-called superficial or Darcy velocity) is assumed to be proportional to gradient of the intrinsic phase-averaged pressure. The proportionality constant is defined via a geometric property of the porous media, the permeability, which is determined semi-empirically [Kaviany (1999); Nield and Bejan (2006)]. This Darcy model has also been derived theoretically by Whitaker (1999). This model holds only for low values of the superficial velocity, when the values of the pore-scale Reynolds number are smaller or of the order of unity [Nield and Bejan (2006)].

Over the years, the Darcy model has been progressively improved, thanks to numerous experimental and theoretical investigations. Many of these investigations have been reviewed and summarized in classical porous media textbooks, such as the ones by Kaviany (1999) and Nield and Bejan (2006). A thorough derivation of the volume-averaged governing equations is available in Whitaker (1999). The following key improvements and modifications have been proposed: i) inclusion of the Brinkman term (effective diffusion term analogous to the viscous term in the Navier-Stokes equations, which introduces the so-called effective or Brinkman viscosity and enables the

imposition of the no-slip condition at solid-wall boundaries and stress-matching conditions at interfaces with open domains); and ii) accounting of the inertial drag (also called form or quadratic drag) through the inclusion of the Forchheimer term, which brings in a Forchheimer or form drag coefficient. The resulting generalized governing equations, which account for the so-called non-Darcian effects, are referred to as the extended Darcy-Brinkman-Forchheimer equations. There are some limitations to these equations, especially with non-uniform porosity or at the interface between porous and open domains. These limitations, as well as suitable modifications, are described in Kaviany (1999) and Whitaker (1999).

With regard to convective heat transfer in porous media, practical volume-averaged approaches have yielded two types of models. If local thermodynamic equilibrium between the fluid and the solid (porous medium) can be assumed, the conditions for which are discussed in Kaviany (1999) and Nield and Bejan (2006), the local intrinsic phase-averaged temperatures of the fluid and the solid are essentially the same, and a single-temperature or homogeneous model is adequate. However, if the conditions necessary for local thermodynamic equilibrium do not apply, then two separate volumeaveraged energy equations, one for each of the intrinsic phase-averaged temperatures of the fluid and the solid (porous medium), must be used, leading to a two-temperature model. In the two-temperature model, interfacial heat transfer between the fluid and the solid porous medium, at the pore level, must be handled. This is usually done through a semi-empirically determined interfacial heat transfer coefficient and the specific area. Extensive experimental work has been carried out to determine these interfacial parameters in packed beds of spheres [Wakao et al. (1979)], but metal foams have not been studied in similar detail. In both the one- and two-temperature models, the volumeaveraged energy equations involve effective thermal conductivities, which depend on the conductivities of the porous structure and the interstitial fluid. Semi-empirical approaches are necessary for determining these effective thermal conductivities. The numerous attempts to quantify these parameters in porous media are discussed concisely in the next section of this literature review, with special attention to porous metal foams.

In the derivation of the governing equations in the above-mentioned volume-averaged approaches to the modeling of fluid flow and heat transfer in porous media, it is assumed that the pore-scale variations (over a representative elementary volume) of the properties of the fluid can be neglected [Whitaker (1999)]. However, to the best knowledge of the author, in all available publications on this topic, there is no rigorous volume-averaging of the terms in the Navier-Stokes and energy equations that are associated with the variations of mass density, dynamic viscosity, specific heat at constant pressure, and the thermal conductivity of the fluid. Thus, available volume-averaged models of fluid flow and heat transfer in porous media are essentially limited (strictly) to cases in which the properties of the fluid can be assumed to be constant, evaluated at a suitable reference temperature. In the problems of interest in this thesis (conduction and natural convection in ice-water systems containing porous metal foams), the proper choice of this reference temperature is critically important. This point is elaborated further in Chapters 2 and 4.

#### Metal foams and their thermal properties

The manufacturing techniques used for fabricating metal foams, and the difficulties in precisely characterizing their complex structure, have been discussed in a design guide by Ashby et al. (2000) and a review article by Ashby and Lu (2003). At present, most commercially available metal foams are made of aluminum, copper, bronze, steel, and nickel. Ashby et al. (2000) have presented and discussed the mechanical and thermal properties of a great variety of metal foams, and also provided models for predicting these properties. An overview of the applications (including TES and heat exchangers) in which these materials can be used is also presented. Banhart (2001) has also provided a review of metal foams, including a description of the various techniques used to manufacture them, and their possible applications such as acoustic control, water treatment, and heat exchangers.

In cooling applications with water as the working fluid, foams with high values of porosity and specific interfacial surface area are used, and copper and aluminum are the preferred metals. Pure copper is more conductive than pure aluminum (400 W/m.K versus 236 W/m.K), but it is much heavier (8960 kg/m<sup>3</sup> versus 2700 kg/m<sup>3</sup>) and more

expensive. Aluminum is therefore the preferred material for the porous metal foams investigated in this thesis, but the proposed models and solutions methods can be used with porous foams made of any of the other aforementioned metals.

Calmidi (1998) and Calmidi and Mahajan (1999) have presented a model of the effective thermal conductivity of porous metal foams, assuming one-dimensional conduction in the ligaments of an array of hexagonal cells. They experimentally determined a parameter that is needed as an input in their model, the ratio of the radius of the fibers to that of the fibers intersections or bulb. It was found to be approximately 0.3. Their model was validated against experimental data for water-foam and air-foam combinations, with a porosity range of 0.9-0.98 (though it is assumed to be valid for a wider range). Bhattacharya et al. (2002) extended the model proposed by Calmidi and Mahajan (1999), the structure now presenting a six-fold rotational symmetry. The value of fibers to bulb radii ratio was this time determined from microscopic pictures of the foam, rather than from the earlier experimental correlations. They also proposed a simple empirical correlation, assuming that the effective thermal conductivity could be expressed as a weighted average of the parallel-conduction and series-conduction models of effective thermal conductivities [Nield and Bejan (2006)]. Jagjiwanram and Singh (2004) and Singh and Kasana (2004) have also developed their own semi-empirical model, using an approach similar to the one adopted by Bhattacharya et al. (2002).

Boomsma and Poulikakos (2001) independently developed their own model of effective thermal conductivity of porous foams, using semi-empirical approaches. In their model, the porous structure was assumed to be composed of tetrakaidecahedrons with cubic nodes. The required geometrical data was obtained using experiments conducted on aluminum foams, successively saturated with water and air. Their model gave very accurate predictions, and they pointed out that in their experiments, the thermal conductivity of the fluid (water or air) had only little influence on the effective thermal conductivity of the porous structure.

Wang and Pan (2008) developed a random-generation growth model to simulate the fabrication of metal foams, and used it to compute their effective thermal conductivity

from the solution of the microscopic (as opposed to volume-averaged) energy equations in two-dimensional projected microstructures. Their first model ignored radiation and gave rather poor results, but they improved it by including this effect. Their final model predicted quite well the effective conductivity of the tested foams. Their results showed that the effective conductivity of metal foams is much higher than that of a rock-bed structure of the same porosity, thanks to their net-like (connected) morphology. This article illustrates the possibilities offered by complex computational models of metal foams. In the previous works, foams were modeled as periodic repetitions of representative modules or portions, ignoring heterogeneities in pore size and shape.

Bodla et al. (2010) also departed from the periodic models, proposing a precise network-based thermal conductivity model. They considered one-dimensional conduction in the fibers, but numerically built up the structure from X-ray micrographs of the metal foams. From this representation, they could extract statistical distributions of pore and fiber diameters, which were then used to estimate the effective thermal conductivity of different types of foams.

The papers discussed in the previous two paragraphs use the most realistic representations of metal foams, but no simple and general expressions for effective conductivity can be extracted from the works reported in them. Thus, in this work, the semi-empirical models described earlier in this section were assessed and compared. However, these semi-empirical models need to be suitably adjusted before being used, because in all of the cases discussed, the sum of the solid (foam) and fluid effective thermal conductivities (needed separately in the two-temperature model) is not equal to the effective thermal conductivity of the foam-fluid composite (needed in the one-temperature model). This consistency issue is discussed in detail in Chapter 2.

#### Investigations of fluid flow and heat transfer in metal foams with no phase change

Calmidi and Mahajan (2000) conducted experiments on forced convection in aluminum foams with porosities ranging from 0.89 to 0.97. They measured heat transfer rates from the bottom of a rectangular box filled with metal foam, subjected to a fully-developed transverse air flow, and an adiabatic top wall, and then compared these measurements to numerical results obtained with a model based on the extended Darcy-Brinkman-Forchheimer momentum and the two-temperature energy equations. The effect of thermal dispersion was included, using an expression proposed by Hunt and Tien (1988). The interfacial heat transfer coefficient was estimated by adapting the classical correlation of Zukauskas (1987) for forced convection from single cylinders in uniform cross-flow. The dimensionless coefficients involved in the aforementioned correlations were adjusted using the experimental data. They obtained very good agreement between the experimental and numerical results, which validated these choices. However, their parameters and correlations could not be directly used in the work reported in this thesis, since the velocities encountered in forced convection are significantly greater than those involved in natural convection.

Phanikumar and Mahajan (2002) numerically studied natural convection in an enclosure heated from below, with metal foam in a corner. They used a model based on the Darcy-Brinkman momentum equations and the two-temperature energy equations. Their results were validated using data from experiments with different foam-fluid combinations, including aluminum-air and aluminum-water (away from the density-inversion temperature of water), and several different foam structures. They also used the Zukauskas (1987) correlation, for forced convection from cylinders in uniform cross-flow, to estimate the interfacial heat transfer coefficient between the solid matrix (porous foam) and the fluid, even though the values of pore-level Reynolds number encountered in their natural convection simulations were quite low. They used the same thermal dispersion correlation as Calmidi and Mahajan (2000), and observed that its effect could account for up to 10% of the heat transfer. Heat transfer enhancement up to a factor of 16 was observed for aluminum foam filled with water. These authors pointed out that the

single-temperature model resulted in significant errors even in natural convection simulations.

Zhao et al. (2005) investigated the influence of natural convection on heat transfer in metal foams heated from below, isolating the influence of the Darcy and Rayleigh numbers, thanks to both numerical and experimental investigations. They used a classical natural convection correlation provided by Churchill and Chu (1975) for estimating the local interfacial heat transfer coefficient. This assumption was, however, not justified. In the case of air as the working fluid and for the conditions of their experiments, natural convection was found to account for up to 50% of the total heat transfer. Zhao et al. (2006) used the same mathematical model as that of Zhao at al. (2005) to predict heat transfer rates for a heat exchanger, with metal foams on both the cold and hot sides. They investigated the influence of pore size, porosity, and geometrical size and predicted an optimum foam-area ratio for a counter-flow tube-in-tube heat exchanger filled with porous metal foam.

#### Investigations of fluid flow and heat transfer in metal foams with phase change

Phase change in porous media is a vast subject, which could involve changes in gas, liquid, and solid phases of the substance in the void spaces of the porous medium. The structure of the porous medium may be rigid or change its shape as a result of the phase-change phenomena. In this part of the literature review, the focus is on solid-liquid phase-change phenomena in rigid porous metal foams. However, the numerical method used in this work for predicting heat transfer in ice-water systems containing porous metal foams was tested by first applying it to such systems without the porous metal foams. Thus, a very brief review of some publications on problems involving solid-liquid phase-change of pure substances without porous metal foams is presented next.

Multidimensional melting and freezing of pure substances is a classical problem that has been the subject of numerous investigations. Lazaridis (1970) was one of the first researchers to present a multidimensional numerical solution to such problems, solving the set of unsteady, nonlinear governing equations, using both explicit and implicit finite

difference methods. Viskanta (1985) has surveyed the literature (up to the mid-1980s) related to investigations of natural convection in melting and solidification problems. Two main categories of models are used in numerical predictions of heat transfer in solidliquid phase-change problems: enthalpy models and temperature models. In enthalpy models, the specific enthalpy of the PCM is used as a dependent variable along with the temperature, and the position of the solid-liquid interface is determined by an examination of the enthalpy distribution. In temperature models, the energy equations for the solid and liquid phases are solved separately, and the conditions of continuity of temperature and heat flux at the solid-liquid interface are used to match the solutions. When temperature models are used, the time-varying solid-liquid interface must be tracked, and numerical methods based on adaptive grids are deemed desirable. A thorough discussion of the fundamental aspects of both enthalpy and temperature models, and their pros and cons, was provided by Crank (1988). A thorough review of experiments and numerical simulations of water-ice phase-change phenomena is available in the PhD thesis by Elkouh (1996). His steady-state experiments on natural convection in pure water and water-ice systems in open domains (without porous metal foams) were used as test problems to check the numerical methods and computer codes used in this work. Details of these tests will be provided in Chapter 4 of this thesis.

Kazmierczak et al. (1986) conducted a computational investigation of solid-liquid phase-change in a porous medium, with an embedded heated flat plate in both vertical and horizontal positions. Their main focus was on the effect of natural convection on the melting rate and the shape of the melting front. Beckermann and Viskanta (1988) undertook complementary numerical and experimental investigations of solid-liquid phase-change in a vertical square enclosure, with gallium as the PCM (fusion point of 29.8°C) and close-packed glass beads as the porous medium. Their volume-averaged model gave good predictions of the temperature profile and melting front location, and the results appeared to be strongly influenced by natural convection and the thermal conductivity of the solid, but not significantly by the thermal conductivity of the fluid. Their results were later used as benchmark data in several papers, including the numerical study of solid-liquid phase-change in porous metal foams by Krishnan et al. (2005).

Solid-liquid phase-change phenomena in metal foams have been the subject of several studies over the last decade, mostly because of the possibilities they offer for latent-heat TES systems. Mesalhy et al. (2004) numerically investigated melting of a PCM embedded in a porous metal foam, solving the volume-averaged conservation equations. They included the Darcy, Brinkman, and Forchheimer effects in the volume-averaged momentum equations, and used a two-temperature model for heat transfer. The domain they considered was the space between two concentric cylinders, akin to the annular space in a double-pipe heat exchanger. Their computer code could also be used for predictions of PCM melting in open domains (without porous media). The results showed that the addition of a porous matrix had significant influence on the rates of melting and heat transfer. Their results also demonstrated that decreasing the porosity of the matrix increases the melting rate, but it also dampens the convective fluid flow.

Krishnan et al. (2005) conducted a numerical study of solid-liquid phase-change phenomena in a two-dimensional rectangular domain filled with metal foams and PCMs. They used a finite-volume method with fixed grids to solve a model based on the extended Darcy-Brinkman-Forchheimer momentum and two-temperature energy equations. They validated their model and method by comparing the results to those of the melting-solidification experiments conducted by Beckermann and Viskanta (1988). The emphasis in their study was on the influence of the Rayleigh, Stefan, and interfacial Nusselt numbers. Their results showed that if the interfacial Nusselt number based on the pore diameter was greater than 5.9, a single-temperature model was sufficient. The value of this Nusselt number in porous metal foams filled with water was not determined, but a review of some of the available correlations that could serve as required inputs to their model was provided. However, none of these correlations appeared to accurately deal with interfacial heat transfer in the pure-conduction limit (very low values of the pore-scale Reynolds number).

Yang and Garimella (2010) extended the work of Krishnan et al. (2005) to include the effects of volume change in the PCM during melting. Their numerical results showed that

the melting rates were changed by about 10% by the inclusion of the volume-change effects.

Lafdi et al. (2006) used the mathematical model, numerical method, and results of Mesalhy et al. (2004) to investigate applications of PCM-foam composites to space and terrestrial latent-heat TES systems. Their simulations were carried out using the properties of commercially available paraffins, and a carbon-matrix porous foam. They averaged the results for several melting-solidification cycles and found that with the foam, the rates of heat transfer increased by eight and five times (compared to those without the foam) for space and terrestrial applications, respectively.

With respect to the reviewed investigations of fluid flow and heat transfer in porous metal foams, with and without solid-liquid phase-change, some of the key results and comments pertinent to the work reported in this thesis are summarized here:

- The usefulness of porous metal foams for heat transfer enhancement in latentheat TES systems (for both heat and cold) has been demonstrated experimentally in multiple investigations, but the mathematical modeling of the related thermofluid phenomena still presents multiple difficulties.
- The two-temperature model is necessary to treat porous metal foams filled with air or water, both for both forced and natural convection.
- There does not seem to be a consensus on the recommended correlation for estimation of the interfacial Nusselt number in the liquid-PCM-foam regions, especially for cases involving low values of the pore-level Reynolds number, and also for frozen-PCM-foam heat exchange.
- In most of the published investigations, thermal dispersion is modelled using classical isotropic dispersion correlations, but the thermal dispersion coefficient has not been determined precisely. The effect of thermal dispersion does not seem negligible in general.

- Several semi-empirical effective conductivity models were developed over the last decade but, to the best knowledge of the author, their adaptation to or incorporation in two-temperature models has not been critically assessed.
- To the best knowledge of the author, no experimental or numerical study on fluid flow and heat transfer in metal foams filled with water in the vicinity of its density inversion temperature is available in the literature.

#### 1.2.3 Key textbooks and handbooks

Dinçer and Rosen (2002) have written a very useful textbook on thermal energy storage (TES) systems, in which they describe the principles, types, and applications of such systems. Mehling and Cabeza (2008) have focused on solid-liquid latent-heat TES systems, and provided overviews of the related thermofluid phenomena and practical aspects, from the classical Stefan melting problem to the potential applications, especially in buildings.

Several excellent textbooks on the general field of heat transfer, for both teaching and research purposes, are available. An example is the textbook by Incropera and Dewitt (2002).

The physics of fluid flow and heat transfer phenomena in porous media, mathematical models of these phenomena, and some experimental investigations and results have been discussed in textbooks by Bear (1988), Kaviany (1999), and Nield and Bejan (2006). Comprehensive discussions of volume averaging, as applied to modeling of thermofluid phenomena in porous media, are presented in a book by Whitaker (1999). Review and discussions of various aspects of fluid flow and heat transfer in porous media are available in a handbook edited by Vafai (2000). Ashby et al. (2000) have provided a design guide to metal foams.

Patankar (1980) has presented and discussed numerical methods for heat transfer and fluid flow, with an emphasis on finite volume methods for predicting incompressible fluid flow. Comprehensive review articles on mathematical models and numerical

solution methods for predictions of a wide range of thermofluid phenomena are available in a handbook edited by Minkowycz et al. (2006).

#### 1.3 Specific objectives

The work reported in this thesis involved cost-effective volume-averaged mathematical models of conduction and laminar natural convection in ice-liquid-water-porous-metal-foam systems, and their numerical solution in the context of computationally convenient state-state, planar two-dimensional problems. This work was undertaken in two main parts. In the first part, the objectives were the following:

- Develop a novel expression for the interfacial heat transfer coefficient in the pure conduction limit, using models and numerical solutions for metal foams with periodic two-dimensional structures.
- Critically assess several existing semi-empirical expressions for effective conductivity of porous metals foams with their void spaces filled with another substance (liquid or solid), and suitably adapt the chosen expressions to ensure consistency of the one-temperature and two-temperature models of heat transfer in such systems.

In the second part of this work, the specific objectives were the following:

- Take an in-house two-dimensional, co-located, equal-order finite volume method and the corresponding computer program for fluid flow and heat transfer in open domains, without embedded solid obstructions or porous foam, and adapt it for predicting fluid flow and heat transfer in pure water-ice systems in open domains and domains containing porous metal foams.
- Benchmark the above-mentioned adapted finite volume method by applying
  it to conduction and natural convection phenomena in pure ice-water systems
  in open domains (without porous foams), and comparing the results to those
  of the experimental and numerical investigations performed by Elkouh
  (1996).

- Quantify the error resulting in the assumption of constant fluid properties in simulations of natural convection in pure water, contained in rectangular enclosures and with temperatures spanning the density inversion point, and recommend a suitable average (reference) temperature for the calculation of the values of these properties.
- Compute and compare the fluid flow, temperature, and heat transfer rates
  when a representative porous metal foam (Aluminum; 10 PPI, or pores per
  inch; 0.95 porosity) is added to six pure liquid-water and two pure ice-water
  configurations (without porous metal foam) studied earlier by Elkouh (1996).
- Compare the steady, two-dimensional natural convection heat transfer rates obtained in square enclosures (akin to the one illustrated schematically in Fig. 1.2) filled with pure liquid water and five different porous metal foams to those obtained in the same systems but without the porous metal foams, for a wide range of Rayleigh numbers. Assess the sensitivity of the results to changes in the conduction interfacial heat transfer coefficient.
- Discuss the impact of thermal dispersion and of the Forchheimer drag term, as well as the division of the heat transfer rates between the foam (10 PPI, 0.95 porosity) and the pure liquid water, for natural convection in enclosures akin to that shown schematically in Fig. 1.2, with the same two sets of wall temperatures and Rayleigh number ranges as in the previous section.
- Investigate a demonstration problem involving steady, two-dimensional, conduction and natural convection in ice-water-porous-metal-foam systems akin to that shown schematically in Fig. 1.2, with  $H_x = 10 \, \mathrm{cm}$ ,  $10 < H_y < 50 \, \mathrm{cm}$ ,  $T_C = -20 \, \mathrm{^{\circ}C}$ , and  $T_H = 20 \, \mathrm{^{\circ}C}$ , discuss the influence of the aspect ratio of the enclosure, and compare the results with those obtained with an open domain (no porous metal foam).

### Chapter 2: Mathematical Models

The numerical simulations undertaken in this work were performed with rectangular enclosures as the calculation domain, akin to that illustrated schematically in Fig. 1.2. Only steady-state, laminar, two-dimensional, fluid flow and heat transfer problems were considered in this work.

In this chapter, first, the equations that govern conduction and natural convection in ice-water systems in open domains (without foam) are presented, taking into account the variation of the thermophysical properties of liquid water and ice with temperature (the variation of these properties with pressure are negligibly small for the problems considered in this thesis). Following that, the governing equations for conduction and natural convection in ice-water-metal-foam systems and related issues are presented and discussed, with the assumption that the thermophysical properties of the liquid water, ice, and metal foams may be treated as essentially constant at values calculated at appropriate reference (or average) temperatures. Finally, the dimensionless parameters in the problems of interest are presented.

In this thesis, the subscript w is be used to indicate dependent variables, properties, and quantities pertaining to water. When a distinction between liquid water and ice is necessary, the subscripts l and i are used, respectively. Dependent variables, properties, and quantities associated with the embedded metal foam (referred to as the solid) are indicated by the subscript s. Regarding the properties, the subscript  $\theta$  is added to denote values calculated at a suitable reference (or average) temperature and assumed to remain constant (in the context of the Boussinesq assumption for the mass density of liquid water). Thus, for example, the temperature-dependent dynamic viscosity of liquid water is denoted by  $\mu_l = \mu_l(T_w)$ , and  $\mu_{l_0}$  denotes the value of dynamic viscosity of water calculated at a suitable reference (or average) temperature and is assumed to remain constant.

# 2.1 Conduction and natural convection in ice-water systems in open domains

The governing equations in open domains (no foam) are well-established, and they were directly taken from previous publications. So they are presented here in a very compact manner (mainly for the sake of completeness of this document). The reader requiring access to a derivation of these equations and related references is requested to refer to the Ph.D. thesis of Elkouh (1996).

With respect to the Cartesian coordinate system, calculation domain (without the foam), and boundary conditions schematically illustrated in Fig. 1.2, the continuity, x- and y-momentum, and energy equations that govern the fluid flow and heat transfer in the liquid-water region are cast in the following forms:

Continuity equation:

$$\frac{\partial}{\partial x}(\rho_l u) + \frac{\partial}{\partial y}(\rho_l v) = 0$$
 2.1

*x*-momentum equation:

$$\frac{\partial}{\partial x} (\rho_l u u) + \frac{\partial}{\partial y} (\rho_l v u) = -\frac{\partial P}{\partial x} + \frac{\partial}{\partial x} (\mu_l \frac{\partial u}{\partial x}) + \frac{\partial}{\partial y} (\mu_l \frac{\partial u}{\partial y}) + S_u$$
 2.2

*y*-momentum equation:

$$\frac{\partial}{\partial x}(\rho_l u v) + \frac{\partial}{\partial y}(\rho_l v v) = -\frac{\partial P}{\partial y} + \frac{\partial}{\partial x}\left(\mu_l \frac{\partial v}{\partial x}\right) + \frac{\partial}{\partial y}\left(\mu_l \frac{\partial v}{\partial y}\right) + S_v$$
 2.3

In equations 2.2 and 2.3,  $S_u$  and  $S_v$  denote volumetric (per unit volume) source terms that are necessary to account for the temperature-dependence of the thermophysical properties of liquid water and the buoyancy force:

$$S_{u} = \frac{\partial}{\partial x} \left( \mu_{l} \frac{\partial u}{\partial x} \right) + \frac{\partial}{\partial y} \left( \mu_{l} \frac{\partial v}{\partial x} \right) + \frac{\partial}{\partial x} \left[ \lambda_{l} \left( \frac{\partial u}{\partial x} + \frac{\partial v}{\partial y} \right) \right] + \left( \rho_{l} - \rho_{l_{0}} \right) g_{x}$$
 2.4

$$S_{v} = \frac{\partial}{\partial y} \left( \mu_{l} \frac{\partial v}{\partial y} \right) + \frac{\partial}{\partial x} \left( \mu_{l} \frac{\partial u}{\partial y} \right) + \frac{\partial}{\partial y} \left[ \lambda_{l} \left( \frac{\partial u}{\partial x} + \frac{\partial v}{\partial y} \right) \right] + \left( \rho_{l} - \rho_{l_{0}} \right) g_{y}$$
 2.5

In these equations,  $g_x = g \sin \theta$  and  $g_y = -g \cos \theta$  are components of the gravitational acceleration vector in the positive x and y directions shown in Fig. 1.2. The term  $\lambda_l$  is the second coefficient of viscosity. It is calculated by invoking the Stokes hypothesis, in which the bulk viscosity of the liquid water is set equal to zero:

$$\lambda_l + \frac{2}{3}\mu_l = 0 \tag{2.6}$$

P is the reduced pressure, which is related to the static pressure as follows:

$$P = p - \rho_{l_0}(xg_x + yg_y)$$
 2.7

The absolute pressure has no significance if the thermophysical properties of water can be considered to be essentially independent of pressure (an assumption that applies in the problems of interest in this work). Thus, for convenience, the value of the reduce pressure, P, was arbitrarily set to zero at the top-right-hand corner of the rectangular enclosure shown in Fig. 1.2 (in all of the numerical simulations). It should be noted here that if the constant-properties assumption is invoked in the context of the Boussinesq approximation (density is constant in all terms except those related to the buoyancy), then the volumetric source terms are given by:  $S_u = (\rho_l - \rho_{l_0})g_x$  and  $S_v = (\rho_l - \rho_{l_0})g_y$ .

The energy equation is the following [Elkouh (1996)]:

$$\frac{\partial}{\partial x} \left( \rho_l u T_w \right) + \frac{\partial}{\partial y} \left( \rho_l v T_w \right) = \frac{\partial}{\partial x} \left( \frac{k_l}{c_{p_{l0}}} \frac{\partial T_w}{\partial x} \right) + \frac{\partial}{\partial y} \left( \frac{k_l}{c_{p_{l0}}} \frac{\partial T_w}{\partial y} \right) + S_E$$
 2.8

$$S_{E} = -\left(\frac{\partial}{\partial x} \left[\rho_{l} u F\left(T_{w}\right)\right] + \frac{\partial}{\partial y} \left[\rho_{l} v F\left(T_{w}\right)\right]\right)$$
 2.9

The volumetric source term in this equation arises due to the variation of specific heat with temperature: the term F(T) is related to the variations of  $c_{p_l}$  with temperature, and is defined as follows:

$$c_{p_i} = c_{p_{i0}}(1 + f(T))$$
 and  $F(T) = \int f(T')dT'$  2.10

In the ice region, the only governing equation is the heat conduction equation:

$$\frac{\partial}{\partial x} \left( k_i \frac{\partial T_w}{\partial x} \right) + \frac{\partial}{\partial y} \left( k_i \frac{\partial T_w}{\partial y} \right) = 0$$
 2.11

The water-ice interface is at the freezing temperature at any point on it:

$$T_{w_{\text{interface}}} = T_{\text{melt}} = 0$$
°C 2.12

In addition, under steady-state conditions, the heat fluxes normal to the water-ice interface are related by the following equation:

$$\left(k_i \frac{\partial T_w}{\partial n}\right)_{ice} = \left(k_l \frac{\partial T_w}{\partial n}\right)_{water}$$
 2.13

The expression for the variation of the density of liquid water with temperature was taken from the works of Kukulka et al. (1987) and Elkouh (1996):

$$\rho_l = \rho_m \left( 1 - \alpha \left| T_w - T_m \right|^q \right) \tag{2.14}$$

In this equation,  $\rho_m = 1000 \text{ kg.m}^{-3}$  is the maximum density of liquid water; this maximum occurs at  $T_m = 4.029325 \,^{\circ}\text{C}$ ;  $\alpha = 9.297173 \times 10^{-6} \,(^{\circ}\text{C})^{-q}$ ; and q = 1.894816. This relationship is valid between 0°C and 20°C: a graphical representation is shown in Fig.

2.1. For the other thermophysical properties of the liquid water, the following expressions proposed by Elkouh (1996) were used (with  $T_w$  expressed in  ${}^{\circ}$ C):

$$\mu_t(\text{kg/m.s}) = 1.7910 \times 10^{-3} - (6.144 \times 10^{-5})T_w + (1.4510 \times 10^{-6})T_w^2 - (1.6826 \times 10^{-8})T_w^3 - 2.15$$

$$c_{p_l}(J/kg.^{\circ}C) = 4.2074 \times 10^3 - (1.3610)T_w + (1.5916 \times 10^{-6})T_w^2$$
 2.16

$$k_t (\text{W/m.}^{\circ}\text{C}) = 0.5654 + (1.700 \times 10^{-3})T_w - (5.944 \times 10^{-6})T_w^2$$
 2.17

$$k_i (W/m.°C) = 2.22 - (1.00 \times 10^{-2})T_w + (3.45 \times 10^{-5})T_w^2$$
 2.18

It should be noted here that between 0°C and 20°C, the mass density of liquid water changes by only 0.18%, but its dynamic viscosity decreases by 43.7%, its conductivity increases by 5.6%, its specific heat decreases by 0.50%, and the resulting Prandtl number decreases by 47%, going from 13.3 to 7.0. In the context of these observations, it is imperative to carefully examine the errors caused if a constant-property assumption are invoked, and determine a suitable reference (or average) temperature for the evaluation of the values of the properties in the corresponding model (one that minimizes the errors caused by the constant-property assumption). Such an investigation was undertaken in this work for natural convection in liquid water with no ice, in open media (no foam). The results are provided in Section 4.1. The expression for the thermal conductivity of ice is valid between -173°C and 0°C. In the problems considered in this work, the temperature of ice was varied between 0°C to -20°C, and in this range, the thermal conductivity of ice decreases by 8.8%.

It should also be noted that at the ice-liquid-water interface, for the steady-state problems considered in this work, the liquid water velocity is zero, and the influence of surface tension is negligible.

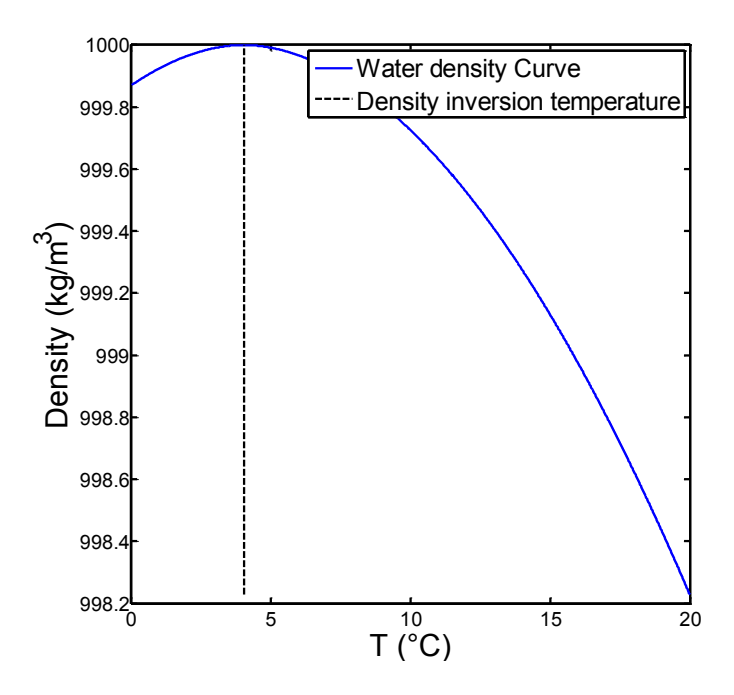


Figure 2.1: Variation of mass density of liquid water with temperature [Kukulka et al. (1987)].

With respect to the calculation domain illustrated in Fig. 1.2 (with no foam), the no-slip conditions applies at all four walls (u = v = 0 at x = 0, y = 0,  $x = H_x$  and  $y = H_y$ ), and the temperatures of the cold and hot side walls are maintained constant:

$$\begin{cases} T_w = T_C & \text{at} \quad x = 0 \\ T_w = T_H & \text{at} \quad x = H_x \end{cases}$$
 2.19

At the top and bottom walls, adiabatic conditions are imposed:

$$\frac{\partial T_{w}}{\partial y}_{|y=0} = \frac{\partial T_{w}}{\partial y}_{|y=H_{y}} = 0$$
2.20

#### 2.2 Conduction and natural convection in ice-water-metal-foam systems

The equations that govern steady-state fluid flow and heat transfer in rectangular enclosures (see Fig. 1.2) containing ice-water-metal-foam systems are presented in this section. The properties of the liquid water, ice, and porous metal foam are evaluated at suitable reference (average) temperatures, for each of the cases considered in this work,

and assumed to remain constant. Recommendations for these temperatures are presented and discussed in Chapter 4.

#### 2.2.1 Some definitions

As was pointed out in the literature review, the volume-averaging technique is the most common method that is used to obtain cost-effective (practical) mathematical models of fluid flow and heat transfer in porous media. Derivations of the volume-averaged governing equations are available in the works of Whitaker (1999) and Nield and Bejan (2006). These derivations start with equations that govern fluid flow and heat transfer in the pores of the porous medium, and heat conduction in the solid portion of the porous medium, and then apply suitable volume-averaging techniques to these equations. The volume-averaging is done over representative elementary volumes (r.e.v.), such as the one shown schematically in Fig. 2.2.

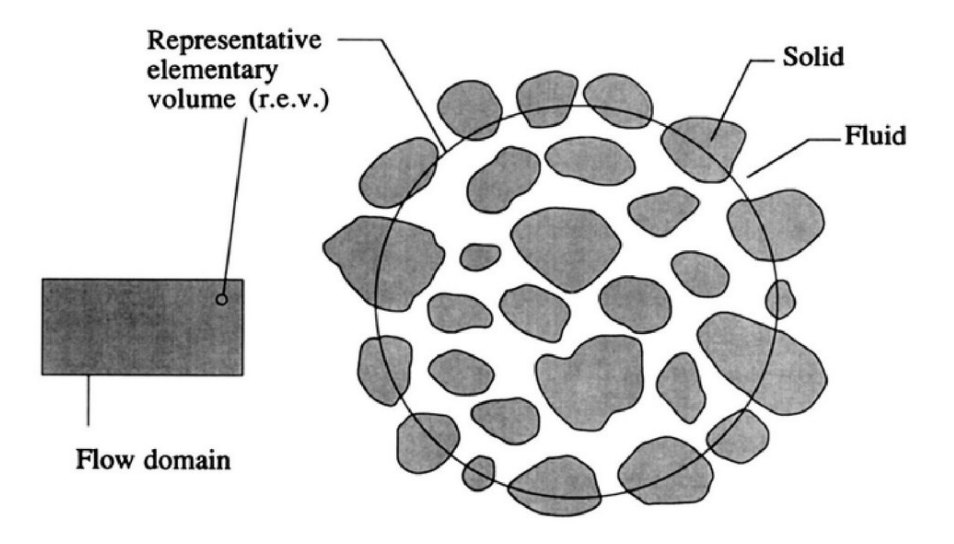


Figure 2.2: A representative elementary volume [Nield and Bejan (2006)].

The size of the representative elementary volume is chosen to be as small as possible with respect to the overall dimensions of the problems of interest, but still large enough to yield statistically meaningful local average quantities [Whitaker (1999)].

The porosity is defined as the ratio of volume of water (liquid or ice) to the total volume:

$$\varepsilon = \frac{V_w}{V_w + V_s} = \frac{V_w}{V}$$
 2.21

The volume average of a given quantity  $\Phi$  is defined as:

$$\left\langle \Phi \right\rangle = \frac{1}{V} \int_{V} \Phi dV \tag{2.22}$$

The intrinsic phase average of this quantity represents its volume average over a given phase, water (liquid or ice) and solid (material of the porous medium):

$$\langle \Phi \rangle^w = \frac{1}{V_w} \int_{V_w} \Phi dV \quad \text{and} \quad \langle \Phi \rangle^s = \frac{1}{V_s} \int_{V_s} \Phi dV$$
 2.23

$$\langle \Phi \rangle = \varepsilon \langle \Phi \rangle^{w} + (1 - \varepsilon) \langle \Phi \rangle^{s}$$
 2.24

For quantities defined only in the water (liquid or ice), the volume-average value is related to the intrinsic-phase-average value by the following equation:

$$\langle \Phi_{w} \rangle = \varepsilon \langle \Phi_{w} \rangle^{w}$$
 2.25

The volume-average velocity vector,  $\langle \mathbf{u}_w \rangle = \varepsilon \langle \mathbf{u}_w \rangle^w$ , is commonly referred to as the Darcy or superficial velocity vector. For convenience in this presentation, the following simplified notation is used for this Darcy or superficial velocity:  $\mathbf{u} = \langle \mathbf{u}_w \rangle = \varepsilon \langle \mathbf{u}_w \rangle^w$ . The following expressions apply to volume-averaging of the gradient and divergence operators [Whitaker (1999)]:

$$\langle \nabla \Phi \rangle = \nabla \langle \Phi \rangle + \frac{1}{V} \int_{Asf} \Phi dA$$
 2.26

$$\langle \nabla . \mathbf{b} \rangle = \nabla . \langle \mathbf{b} \rangle + \frac{1}{V} \int_{Asf} \mathbf{b} . \mathbf{dA}$$
 2.27

#### 2.2.2 Governing equations

In the available literature, the volume-averaged governing equations for fluid flow and heat transfer in porous media are usually derived for essentially constant thermophysical properties or for cases where the variations of these properties are negligible over the representative elementary volume [Whitaker (1999)]. However, the volume-averaged expressions for the source terms associated with non-constant fluid properties are, to the best knowledge of the author, not available in the literature. The derivation of such expressions would be, in itself, an interesting and challenging task, but it is not within the scope of this thesis. In this work, the constant-property assumption (in the context of the Boussinesq approximation) was invoked in the derivation and use of the volume-averaged governing equations for fluid flow and heat transfer in porous metal foams. The resulting errors (compared to predictions with variable-property models) were assessed for natural convection with pure water in open domains (no-foam). With a suitable reference (average) temperature for the evaluation of the values of the constant properties, the aforementioned errors were found to be quite small. These results are presented and discussed in Chapter 4.

### Volume-averaged continuity and momentum equations in the liquid-water-metalfoam regions

These equations are presented here for steady-state conditions and the constant-property assumption (in the context of the Boussinesq approximation). The continuity equation for the liquid in the pores of the porous medium is the following:

$$\nabla . \mathbf{u}_t = 0 \tag{2.28}$$

Here,  $\mathbf{u}_l$  is the water velocity vector in the pores. Volume-averaging of this equation is done over the representative elementary volume illustrated in Fig. 2.2, using equation 2.27 and the no-slip condition at the water-metal-foam interface. The resulting volume-averaged continuity equation in terms of the Darcy or superficial velocity is:

$$\nabla .\mathbf{u} = 0 \tag{2.29}$$

The steady-state momentum equation (Navier-Stokes equations) for the liquid water in the pores of the porous medium is the following:

$$\rho_{l_0} \nabla . \mathbf{u}_l \mathbf{u}_l = -\nabla P + \mu_{l_0} \nabla (\nabla \mathbf{u}_l) + (\rho_l - \rho_{l_0}) \mathbf{g}$$
 2.30

The volume-averaged form of this equation is the following (adaptation of the expression put forward by Hsu (1990)):

$$\rho_{l_0} \frac{\nabla .\mathbf{u}\mathbf{u}}{\varepsilon^2} = -\nabla \langle P \rangle^{w} + \frac{\mu_{l_0}}{\varepsilon} (\nabla^2 \mathbf{u}) + \mathbf{S}$$
 2.31

In this equation, the source term **S** is the sum of two drag terms and a buoyancy term associated with natural convection:

$$\mathbf{S} = \mathbf{r} + \left( \left\langle \rho_l \right\rangle^w - \rho_{l_0} \right) \mathbf{g}$$
 2.32

Here, **r** is the total drag term per unit volume, applied on the water by the solid phase:

$$\mathbf{r} = -\frac{1}{V} \int_{Asf} P \mathbf{dA} + \frac{\mu}{V} \int_{Asf} (\nabla \mathbf{u}_l) . d\mathbf{A}$$
 2.33

It cannot be evaluated analytically, unless the structure of the porous medium and the fluid flow within it are known exactly. At low values of Reynolds number, the pressure drop is related to the velocity and permeability K by the Darcy law:

$$-\nabla \langle P \rangle^{w} = \frac{\mu_{l_0} \mathbf{u}}{K} + o\left(\|\mathbf{u}\|^{2}\right)$$
 2.34

However, a second-order term is often introduced, since inertial (or form drag) effects cannot be neglected when the Reynolds number increases. It is quantified by a form-drag or Forchheimer coefficient, f, which is a function of the geometry of the metal foams [Calmidi (1998)]. With this modification,  $\mathbf{r}$  is expressed as follows:

$$\mathbf{r} = -\frac{\mu_{l_0} \mathbf{u}}{K} - \frac{\rho_{l_0} f}{\sqrt{K}} \|\mathbf{u}\| \mathbf{u}$$
 2.35

In this study, the following correlations proposed by Calmidi (1998) were adopted, as they show excellent agreement with available experimental data:

$$K = d_p^2 \times 0.00073 \times (1 - \varepsilon)^{-0.224} \left(\frac{d_f}{d_p}\right)^{-1.11}$$
 2.36

$$f = 0.00212 \times (1 - \varepsilon)^{-0.132} \left(\frac{d_f}{d_p}\right)^{-1.63}$$
 2.37

The volume-averaged buoyancy term is:

$$\left(\left\langle \rho_{l}\right\rangle^{w} - \rho_{l_{0}}\right)\mathbf{g} = \left[\rho_{m}\left(1 - \alpha\left\langle \left|T_{w} - T_{m}\right|^{q}\right\rangle^{w}\right) - \rho_{l_{0}}\right]\mathbf{g}$$
2.38

It is difficult to rigorously determine this term in the computer simulations, because of the non-linear variation of the liquid water density with temperature. In this work, it was assumed that the pore-scale variations of the fluid temperature are small enough to justify the following approximation:

$$\left(\left\langle \rho_{l}\right\rangle^{w} - \rho_{l_{0}}\right)\mathbf{g} = \left[\rho_{m}\left(1 - \alpha\left|\left\langle T_{w}\right\rangle^{w} - T_{m}\right|^{q}\right) - \rho_{l_{0}}\right]\mathbf{g}$$
2.39

The final form of the momentum equation is the following:

$$\rho_{l_0} \frac{\nabla .\mathbf{u}\mathbf{u}}{\varepsilon^2} = -\nabla \left\langle P \right\rangle^{w} + \frac{\mu_{l_0}}{\varepsilon} \left( \nabla^2 \mathbf{u} \right) - \frac{\mu_{l_0} \mathbf{u}}{K} - \frac{\rho_{l_0} f}{\sqrt{K}} \|\mathbf{u}\| \mathbf{u} + \left[ \rho_m \left( 1 - \alpha \left| \left\langle T_w \right\rangle^{w} - T_m \right|^q \right) - \rho_{l_0} \right] \mathbf{g} \quad 2.40$$

The boundary condition for the velocity field, with and without the porous metal foam, is the following:  $\mathbf{u} = 0$  at all boundaries (x = 0, y = 0,  $x = H_x$ ,  $y = H_y$ ).

#### **Energy Equations**

Full details of the derivation of the energy equations are presented and discussed in Whitaker (1999). Heat transfer in porous media can be studied with the assumption of local thermal equilibrium between the two phases (fluid and solid), when certain conditions or criteria are satisfied. For a discussion of these criteria, the reader is referred to the works of Whitaker (1999) and Nield and Bejan (2006). With this assumption, a single energy equation is used to describe the evolution of the intrinsic-phase-average temperatures,  $\langle T_s \rangle^s = \langle T_w \rangle^w = \langle T \rangle$ .

In the liquid-water-metal-foam region of the calculation domain, the one-temperature model of the energy equation is:

$$\rho_{l_0} c_{pl_0} \nabla \cdot (\mathbf{u} \langle T \rangle) = \nabla \cdot ((k_{eff_l} + \varepsilon k_D) \nabla \langle T \rangle)$$
 2.41

In the ice-metal-foam region of the calculation domain, the one-temperature model yields the following form of the energy equation:

$$0 = \nabla \cdot \left( k_{eff_i} \nabla \langle T \rangle \right)$$
 2.42

In these equations,  $k_{\it eff_i}$  and  $k_{\it eff_i}$  are the effective thermal conductivities when the porous metal foam is filled with liquid water and ice, respectively. In general, the effective thermal conductivity has to be expressed as a second-order tensor, but in the case of essentially isotropic porous media (over a representative elementary volume), such as the porous metal foams considered in this work, it can be approximated as a scalar. As was mentioned before, the liquid-water, ice, and porous metal properties were assumed to be essentially constant at suitable reference (average) temperatures in each of the cases considered in this work. The expressions for the effective thermal conductivities invoke this constant-property assumption. Strictly, the subscript  $\theta$  is necessary to indicate these constant properties, however, for convenience and simplicity in the presentations, this subscript will be dropped in the following discussions.

The thermal dispersion conductivity,  $\varepsilon k_D$ , is included to account for heat transfer enhancements due to hydrodynamic mixing of the fluid phase in the pores of the porous medium. A pore-level study of such flows could give an estimate of this coefficient, but there only are few studies of this type available in the literature, an example is the work of Pedras and De Lemos (2008). In general, thermal dispersion is non-isotropic. However, while the thermal dispersion in directions normal to the local (in the volume-averaged sense) superficial velocity vector can be significant, it is usually negligible in the direction of this velocity vector, compared to the corresponding advection transport. Thus, often, it is adequate (and simple) to assume that an expression for thermal dispersion transverse to the local superficial velocity vector is also applicable in all directions.

In natural convection problems involving liquid-water-porous-metal-foam systems, the fluid velocity is usually quite low, so the thermal dispersion can be assumed to be negligible. In this work, the applicability of this assumption was checked by using a relatively simple and adequate (in the context of the discussions given at the end of the previous paragraph) isotropic thermal dispersion model proposed by Hunt and Tien (1988)]:  $k_D = C_D \rho_{l_0} c_{pl_0} \sqrt{K} \|\langle \mathbf{u}_w \rangle^w \|$ . Thus:

$$\varepsilon k_D = C_D \rho_f c_{pf} \sqrt{K} \| \mathbf{u} \|$$
 2.43

Calmidi and Mahajan (2000) empirically estimated  $C_D = 0.06$ . Their  $C_D$  value was used in this work.

In the problems considered in this work, because of the large differences between the values of thermal conductivity of the metals (used to make the porous foam) and water (liquid and ice), the one-temperature model may not be valid, even under steady-state conditions [Whitaker (1999)]. A two-temperature model was therefore adopted. As was stated earlier, in the two-temperature model, the intrinsic-phase-average temperatures of the water (liquid or ice) and the solid (porous metal foam),  $\langle T_w \rangle^w$  and  $\langle T_s \rangle^s$ , respectively, as not assumed to be locally equal, and two different energy equations are used for these

temperatures, in both the liquid-water-metal-foam and ice-metal-foam regions of the calculation domain.

The energy equations in the two-temperature model of the liquid-water-metal-foam region are the following:

$$\rho_{l_0} c_{pl_0} \mathbf{u} \cdot \nabla \langle T_w \rangle^w = \nabla \cdot \left( \left( k_{ll} + k_{sl} + \varepsilon k_D \right) \nabla \langle T_w \rangle^w \right) - a_{sf} h_l \left( \langle T_w \rangle^w - \langle T_s \rangle^s \right)$$

$$0 = \nabla \cdot \left( \left( k_{ss} + k_{sl} \right) \nabla \langle T_s \rangle^s \right) + a_{sf} h_l \left( \langle T_w \rangle^w - \langle T_s \rangle^s \right)$$
2.44

In the ice-metal-foam region, the energy equations in the two-temperature model are the following:

$$0 = \nabla \cdot \left( \left( k_{ii} + k_{si} \right) \nabla \left\langle T_{w} \right\rangle^{w} \right) - a_{sf} h_{i} \left( \left\langle T_{w} \right\rangle^{w} - \left\langle T_{s} \right\rangle^{s} \right)$$

$$0 = \nabla \cdot \left( \left( k_{ss} + k_{si} \right) \nabla \left\langle T_{s} \right\rangle^{s} \right) + a_{sf} h_{i} \left( \left\langle T_{w} \right\rangle^{w} - \left\langle T_{s} \right\rangle^{s} \right)$$

$$2.45$$

In these equations,  $k_{ss}$  is the solid (metal foam) effective thermal conductivity;  $k_{ll}$  and  $k_{ii}$  refer to the effective thermal conductivities of the liquid water and ice, respectively; and  $k_{si}$  and  $k_{si}$  are the so-called coupling thermal conductivities, which arise from volume-averaging of the heat conduction terms in the energy equations. Strictly, the term  $\left(k_{ii}+k_{si}\right)\nabla\langle T_w\rangle^w$  should be replaced by  $\left(k_{ii}\nabla\langle T_w\rangle^w+k_{si}\nabla\langle T_s\rangle^s\right)$  in equation 2.45, but in this work, the local gradient equilibrium hypothesis validated by Quintard and Whitaker (1995) is used. Thus,  $\nabla\langle T_w\rangle^w$  and  $\nabla\langle T_s\rangle^s$  are assumed to be close enough for the coupled thermal conductivities to be used as simple additional effective conductivities in both the solid (metal foam) and the water (liquid or ice) regions. A close look at their definition shows that  $k_{sl}=k_{ls}$  and  $k_{si}=k_{ls}$ . With the effective conductivity model used in this work, these coupled contributions represented only 1% to 3% of the effective thermal conductivities.

The terms  $h_i$  and  $h_i$  are the interfacial heat transfer coefficients at the liquid-water-metal-foam and ice-metal-foam interfaces, respectively. They are used to model the rate of heat

transfer between the water (liquid or ice) and the metal foam, caused by differences in their intrinsic-phase-average temperature:

$$h = \frac{\overline{q}_{\text{water to solid}}^{"}}{\langle T_{w} \rangle^{w} - \langle T_{s} \rangle^{s}}$$
 2.46

The coefficient  $h_i$  quantifies the interfacial heat transfer by pure conduction between the ice and the metal foam. However, at the interface between the liquid-water and the metal foam, the heat transfer is also influenced by convection around the foam fibers. Novel expressions for these coefficients are proposed in Section 2.2.5. The term  $a_{sf}$  is the specific (per unit volume) interfacial area over which the aforementioned heat exchanges occurs, and it is a purely geometrical parameter.

If local thermal equilibrium is achieved  $(\langle T \rangle = \langle T_w \rangle^w = \langle T_s \rangle^s)$ , the summation of the two equations in each set of equations 2.44 or equations 2.45 should yield the single-temperature equations 2.41 and 2.42, respectively. The necessary conditions for achieving these consistency requirements are the followings:

$$k_{eff_i} = k_{ll} + 2k_{sl} + k_{ss}$$
 and  $k_{eff_i} = k_{ii} + 2k_{si} + k_{ss}$  2.47

These consistency issues, as well as the choice of the best available effective thermal conductivity expressions, will be tackled in Section 2.2.4.

The boundary conditions of the problem numerically studied in this work are reported in Fig. 1.2; the temperatures of the cold and hot side walls are again maintained constant:

$$\begin{cases} \langle T_w \rangle^w = \langle T_s \rangle^s = T_C & \text{at} \quad x = 0 \\ \langle T_w \rangle^w = \langle T_s \rangle^s = T_H & \text{at} \quad x = H_x \end{cases}$$

At the top and bottom walls, the adiabatic conditions impose:

$$\frac{\partial \langle T_w \rangle^w}{\partial y}\Big|_{y=0} = \frac{\partial \langle T_w \rangle^w}{\partial y}\Big|_{y=H_y} = \frac{\partial \langle T_s \rangle^s}{\partial y}\Big|_{y=0} = \frac{\partial \langle T_s \rangle^s}{\partial y}\Big|_{y=H_y} = 0$$
2.49

In addition, under steady-state conditions, the heat fluxes normal to the water-ice interface are related by the following equations:

$$\begin{cases}
\left(k_{ii} + k_{si}\right) \left(\frac{\partial \langle T_w \rangle^w}{\partial n}\right)_{ice} = \left(k_{ll} + k_{sl}\right) \left(\frac{\partial \langle T_w \rangle^w}{\partial n}\right)_{water} \\
\left(k_{ss} + k_{si}\right) \left(\frac{\partial \langle T_s \rangle^s}{\partial n}\right)_{ice} = \left(k_{ss} + k_{sl}\right) \left(\frac{\partial \langle T_s \rangle^s}{\partial n}\right)_{water}
\end{cases}$$
2.50

#### 2.2.3 Geometrical characteristics of porous metal foams

A close look at the structure of open-cell metal foams (akin to that shown in Fig. 1.1, in Chapter 1) reveals that at the pore-level, it is highly anisotropic, and its full geometric characterization is complex and requires numerous parameters. However, foam manufacturing processes (for example, air bubbling and particle decomposition) give random orientations to the cells within the foam. Thus, over a representative elementary volume, metal foams can be assumed to be essentially isotropic.

Most manufacturers of porous metal foams only provide their clients with values of a parameter called pores-per-inch (PPI) and the porosity. From this data, it is necessary to estimate the pore diameter, ligament diameter, and specific area. Calmidi (1998) modelled the foam as a periodic hexagonal structure with cylindrical ligaments, and used a geometrical analysis to conclude that the pore and ligament diameters could be linked by the following relationship:

$$\frac{d_f}{d_p} = 1.18\sqrt{\frac{1-\varepsilon}{3\pi}} \frac{1}{G(\varepsilon)}$$
 2.51

A typical value of 
$$(d_f/d_p)$$
 is 0.1  $\left(\text{note } \frac{d_f}{d_p} = 0.1205 \text{ at } \epsilon = 0.95\right)$ .  $G(\epsilon)$  is a shape

function determined experimentally, and it quantifies the deformation of the fiber cross-section as the porosity increases. Indeed, observations show that the fiber cross-section goes from a circle to a triangle as the porosity of metal foams is increased.

$$G(\varepsilon) = 1 - e^{\frac{-(1-\varepsilon)}{0.04}}$$
 2.52

This relationship was validated on foams with porosities ranging from 0.9 to 0.98.

Knowing any two of the aforementioned parameters (porosity, pore diameter, and fiber diameter), the third one can be determined. The PPI value of a foam is supposedly linked to the pore diameter by the relationship  $d_p(inch) = \frac{1}{PPI}$ . But experimental data show that this relationship does not apply, especially at high values of pore density. It is, however, reasonable to assume that each PPI value corresponds to a single average pore diameter, as is shown by the data displayed in Fig. 2.3. This data also shows that there is no clear dependence of the pore diameter on porosity. For the data shown graphically in Fig. 2.3, the assumption of a constant average pore diameter for a given value of the PPI parameter, leads to an average quadratic (rms) error of only 4.82%, and all the errors are below 10%. The values adopted for these metal foams (the ones for which the data in Fig. 2.3 applies) are listed in Table 2.1.

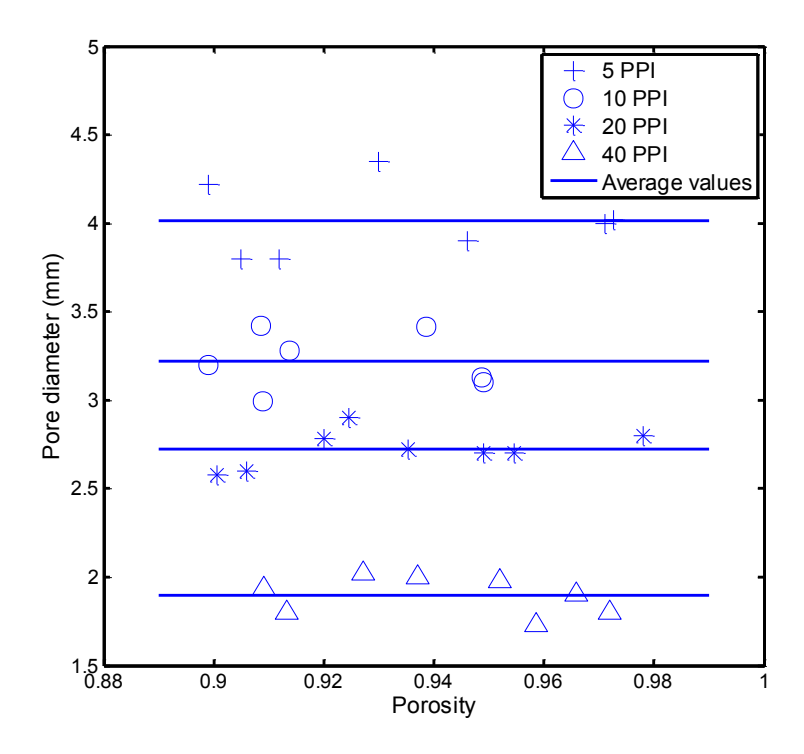


Figure 2.3: Pore diameter as a function of porosity for 22 different metal foams: experimental data from Bhattacharya et al. (2002).

Foam Type	$d_p$ (mm)	$d_f$ (mm), for $\varepsilon = 0.95$
5 PPI	4.01	0.48
10 PPI	3.22	0.39
20 PPI	2.72	0.33
40 PPI	1.90	0.23

Table 2.1: Average values of pore diameter for porous metal foams with PPI values of 5, 10, 20, and 40, and corresponding values of ligament diameter for porosity of 0.95.

Using equation 2.51 and the values of  $d_p$  from Table 2.1, the predicted values of  $d_f$ , with  $0.9 < \varepsilon < 0.98$  show an average quadratic (rms) difference of 7.2% and a maximum difference of 21.1% compared to available experimental data, the highest difference occurring for the most porous foam. These results validate the analytical model leading to equation 2.51 (it was adopted in this work). For the metal foams considered in this work, the chosen values of pore diameter and the corresponding ligament diameter are summarized in Table 2.1 for  $\varepsilon = 0.95$ .

The corresponding expression for the specific (per unit volume) interfacial area for the metal foams considered in this work is the following [Calmidi (1998)]:

$$a_{sf} = \frac{A_{sf}}{V} = \frac{3\pi d_f}{\left(0.59 \times d_p\right)^2} G(\varepsilon)$$
 2.53

#### 2.2.4 Comparison and adaptation of effective thermal conductivity models

The effective thermal conductivity of low porosity media, such as rock beds, saturated with water can be reasonably well-approximated by the parallel-conduction model:  $k_{\it eff} = (\varepsilon k_{\it w} + (1-\varepsilon)k_{\it s})$  . However, experimental measurements of the effective thermal conductivity of highly-porous metal foams saturated with water show that the parallelconduction model leads to significant overestimations [Calmidi (1998); Bhattacharya et al. (2002)]. The predictions yielded by the semi-empirical models of effective thermal conductivity proposed by Calmidi and Mahajan (1999), Boomsma and Poulikakos (2001), Bhattacharya et al. (2002), and Jagjiwanram and Singh (2004) are presented graphically in Fig. 2.4, for aluminum foams saturated with liquid water. Corresponding experimental data from Bhattacharya et al. (2002), for 11 water-saturated aluminum foams with porosity in the range 0.906 to 0.978, are also presented in this figure. The differences between the predictions provided by the aforementioned correlations and the experimental measurements of Bhattacharya et al. (2002) are presented in Table 2.2. All of these models are suitable for use in the volume-averaged one-temperature model of the energy equation. The modifications needed for using or extending these models for use with volume-averaged two-temperature models of the energy equation are presented later in the section.

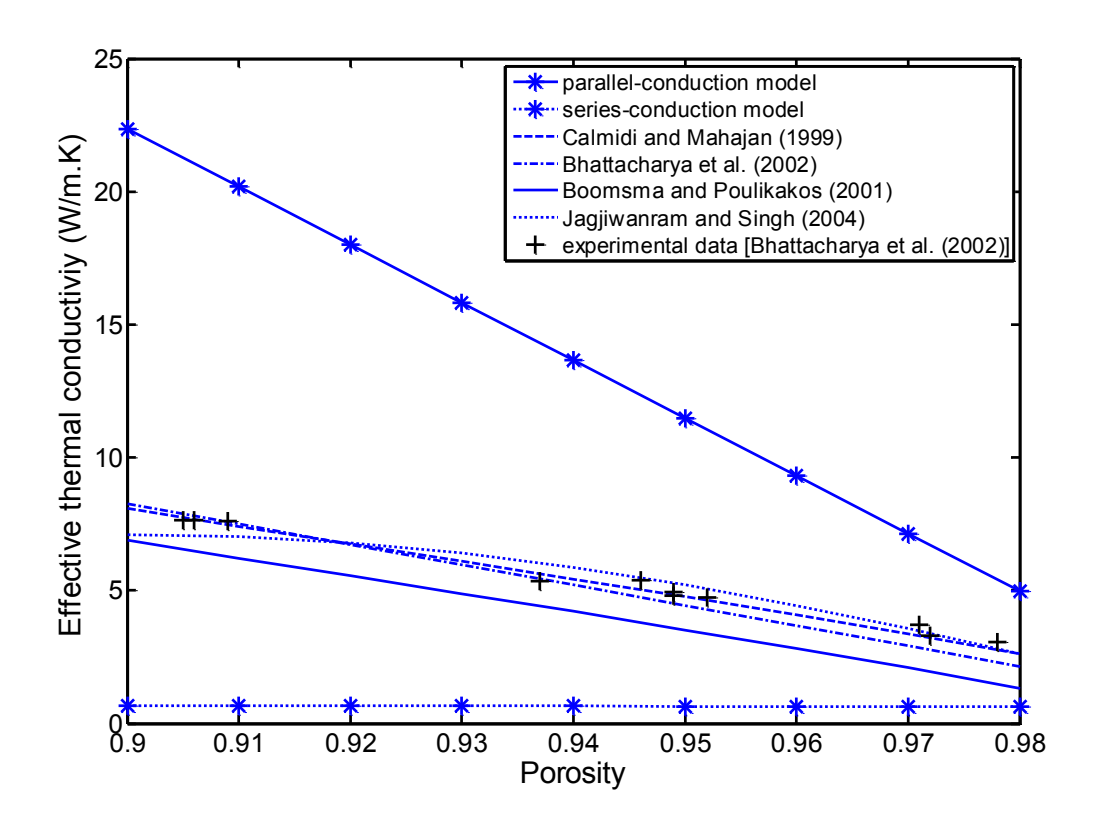


Figure 2.4: Effective thermal conductivity of aluminum foams saturated with liquid water: predictions obtained with several models, and experimental data of Bhattacharya et al. (2002).

Model	Quadratic (rms)	Maximum absolute	
Model	difference (%)	difference (%)	
Parallel-conduction	140.2	180.0	
Series-conduction	86.6	91.1	
Calmidi and Mahajan (1999)	5.3	11.0	
Bhattacharya et al. (2002)	12.8	24.7	
Boomsma and Poulikakos (2001)	31.0	51.2	
Jagjiwanram and Singh (2004)	7.5	12.9	

Table 2.2: Differences between the predictions yielded by several thermal conductivity models and the experimental measurements of Bhattacharya et al. (2002).

As can be seen from the results presented in Fig. 2.4, the parallel-conduction model overpredicts the effective thermal conductivity of metal foams saturated with water, and the series-conduction model leads to underestimations of this property over the entire porosity range considered, 0.906 to 0.978. In the derivations of the models of Calmidi and Mahajan (1999) and Boomsma and Poulikakos (2001), the effective thermal conductivity is estimated by analytically modelling the foams as regular periodic structures and adjusting a geometrical parameter, for example, fiber-to-bulb-radius ratio in the work of Calmidi and Mahajan (1999), to fit the experimental data. In the derivations of the models of Bhattacharya et al. (2001) and Jagjiwanram and Singh (2004), it was assumed that the effective thermal conductivity can be expressed as a suitable combination of the parallel and series contributions, and the related coefficients were determined empirically. All of the aforementioned models respect the limit  $k_{eff} \xrightarrow[s \to t]{} k_w$ . It should be noted that the model of Boomsma and Poulikakos (2001) cannot be used for open (non-porous) media, since it does not respect the requirement  $k_{eff} \xrightarrow[s \to t]{} k_w$ .

An analysis of the results presented in Fig. 2.4 shows that for aluminums foams saturated with water, the best predictions of effective thermal conductivity are obtained with the model proposed by Calmidi and Mahajan (1999), with a quadratic (rms) error of 5.3% and a maximum error of 11.0%. Therefore, their model was adopted for the work reported in this thesis. This model is also the most consistent of the aforementioned models when transposed to the two-temperature model (additional discussions presented later in this section).

For predicting the effective thermal conductivity of water-saturated aluminum foams, the model proposed by Calmidi and Mahajan (1999) can be cast in the following form:

$$k_{eff} = \frac{1}{\left(\frac{2}{\sqrt{3}}\right)\left(\frac{r\left(\frac{b}{L}\right)}{k_{w} + \left(1 + \frac{b}{L}\right)\frac{k_{s} - k_{w}}{3}} + \frac{(1 - r)\left(\frac{b}{L}\right)}{k_{w} + \frac{2}{3}\frac{b}{L}(k_{s} - k_{w})} + \frac{\frac{\sqrt{3}}{2} - \frac{b}{L}}{k_{w} + \frac{4r}{3\sqrt{3}}\frac{b}{L}(k_{s} - k_{w})}\right)}$$
 2.54

In this equation,  $\frac{b}{L}$  is the bulb-radius-to-fiber-length ratio. It can be expressed as a function of porosity [Calmidi and Mahajan (1999)]:

$$\frac{b}{L} = \frac{-r + \sqrt{r^2 + 4(1-\epsilon)\frac{\sqrt{3}}{6}\left(2 - r\left(1 + \frac{4}{\sqrt{3}}\right)\right)}}{\frac{2}{3}\left(2 - r\left(1 + \frac{4}{\sqrt{3}}\right)\right)}$$
2.55

The fiber-radius-to-bulb-radius ratio, r=t/b, was determined experimentally by Calmidi and Mahajan (1999) and validated for aluminum foams with porosity values between 0.9 and 0.98, saturated with air or water. The best fit was obtained with the value r=0.09. In this thesis, when the aluminum foam is filled with liquid water,  $k_w=k_{l_0}$ , and the effective thermal conductivity is denoted as  $k_{eff_l}$ ; and when it is filled with ice,  $k_w=k_{l_0}$  and  $k_{eff}=k_{eff_l}$ .

In the two-temperature model of the volume-averaged energy equations (equations 2.44 and 2.45), five thermal conductivities are required: the effective thermal conductivities of the solid (aluminum foam), liquid water, ice, and two coupling thermal conductivities.

The effective thermal conductivities of the solid (aluminum foam), liquid water, and ice  $(k_{ss}, k_{ll} \text{ and } k_{ii})$  needed in the two-temperature model of the energy equations are calculated using the following substitutions in equation 2.54, which was originally derived for use in the single-temperature model of the energy equation [Calmidi and Mahajan (1999)]: for obtaining  $k_{ss}$  from the expression for  $k_{eff}$ , set  $k_s = k_{Al_0}$  and  $k_w = 0$ ; for obtaining  $k_{ll}$  from the expression for  $k_{eff}$ , set  $k_s = 0$  and  $k_w = k_{l_0}$ ; and for obtaining  $k_{il}$  from the expression for  $k_{eff}$ , set  $k_s = 0$  and  $k_w = k_{l_0}$ . It should also be noted that this approach cannot be used with the purely empirical correlations of Bhattacharya et al. (2002) and Jagjiwanram and Singh (2004), because  $k_{ss}$  would tend to infinity when the porosity approaches 1. Their correlations were designed only for use with one-temperature models, and they cannot be transposed to two-temperature models.

In most publications on the two-temperature model of convective heat transfer in porous metal foams, the coupling thermal conductivities,  $k_{sl}$  and  $k_{si}$ , are ignored or assumed to

be negligible. Without the coupling thermal conductivities, the consistency conditions expressed in equations 2.47 reduce to the following forms:  $k_{eff_i} = k_{il} + k_{ss}$  and  $k_{eff_i} = k_{ii} + k_{ss}$ . These reduced conditions are met only by the parallel-conduction model, and not by any of the other above-mentioned models. When the consistency conditions are not met, the rates of heat transfer obtained with the single-temperature and two-temperature models are not the same even in the limit where  $\langle T_w \rangle^w - \langle T_s \rangle^s \rightarrow 0$  (this limit is approximated at small values of the Rayleigh number in natural convection problems, for example, as will be shown in Chapter 4). Therefore, the coupling thermal conductivities are not ignored in this work. In addition, a simple, but effective, formulation is proposed to ensure that the aforementioned consistency is respected.

In this work, the following equations are used to represent the coupling thermal conductivities:

$$k_{sl} = \frac{k_{eff_i} - k_{ss} - k_{ll}}{2}$$
 and  $k_{si} = \frac{k_{eff_i} - k_{ss} - k_{ii}}{2}$  2.56

This proposed formulation for representing the coupling thermal conductivities ensures that the conditions given in equation 2.47 are satisfied. The contributions of  $k_{ll}$ ,  $k_{ss}$ , and  $k_{sl}$  to the effective thermal conductivity  $k_{eff_l}$  for foams saturated with liquid water and porosity values in the range 0.9 to 0.98 are shown graphically in Fig. 2.5. For the results shown in this figure, the Calmidi an Mahajan (1999) model was used for calculations of  $k_{ll}$ ,  $k_{ss}$ , and  $k_{eff_l}$ , and the first of equations 2.53 was used for calculating  $k_{sl}$ . These results show that the coupled thermal conductivity contributes to the effective thermal conductivity by only 1.8% (average value over the considered porosity range); but on the average, it is 17.3% of the effective thermal conductivity of the liquid water. Thus, the coupled thermal conductivity has a significant influence on the volume-averaged energy equation for the liquid water in the two-temperature model.

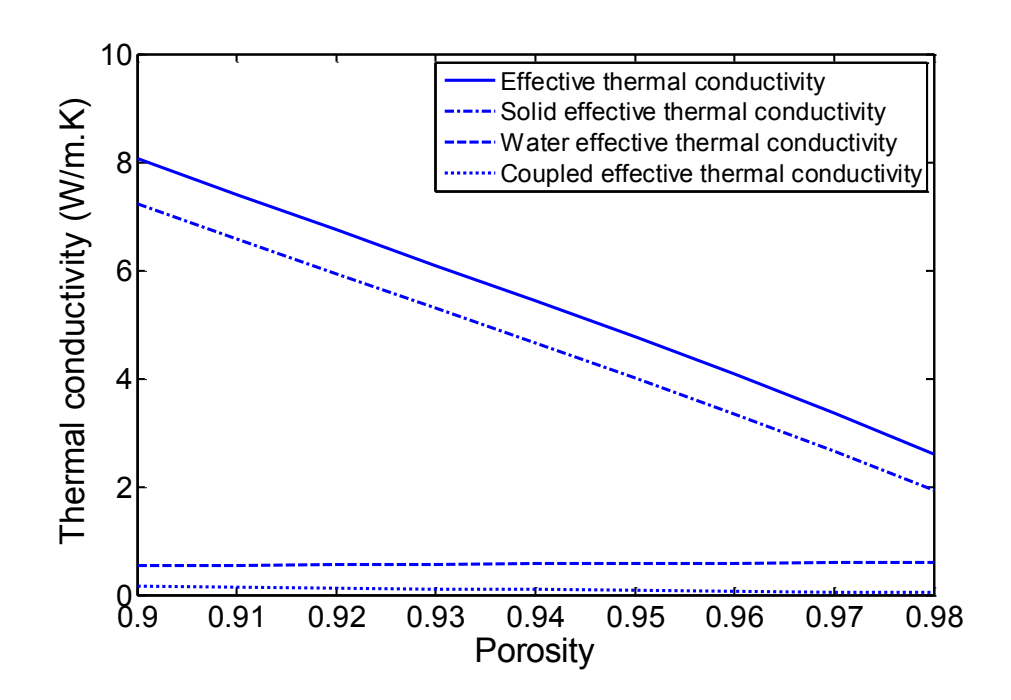


Figure 2.5: Contributions of the solid, liquid water, and coupled effective thermal conductivities to the overall effective thermal conductivity of porous aluminum foam saturated with liquid water at 10°C: predictions obtained with the model of Calmidi and Mahajan (1999).

# 2.2.5 Interfacial heat transfer coefficients for pore-scale heat exchange in the metal-foam-liquid-water and metal-foam-ice regions

In the metal-foam-liquid-water region, the interfacial heat transfer at the surface of the foam ligaments can be due to local natural convection, forced convection, or mixed convection. An adaptation of correlations for mixed convection from cylinders was used to determine the corresponding interfacial heat transfer coefficient,  $h_l$ . In the metal-foam-ice region, the heat transfer at the surface of the foam ligaments is due to pure conduction at the pore level, and proper correlations for the corresponding interfacial heat transfer coefficient  $h_i$  are not provided (or ignored) in the literature. In this section, novel expressions for both the interfacial heat transfer coefficient in the metal-foam-liquid-water region and the metal-foam-ice region are proposed and discussed.

#### Interfacial convection heat transfer in the metal-foam-liquid-water region

The relative importance of forced, natural, and mixed convection to the interfacial heat transfer in the metal-foam-liquid-water region was assessed using the following criterion [Incropera and DeWitt (2002)]: if  $Gr_{d_f}/(\mathrm{Re}_{d_f})^2 << 1$ , natural convection is negligible and forced-convection dominates; if  $Gr_{d_f}/(\mathrm{Re}_{d_f})^2 >> 1$ , the local heat transfer is natural-convection; and if  $0.1 \le Gr_{d_f}/(\mathrm{Re}_{d_f})^2 \le 10$ , mixed convection prevails. Here,  $Gr_{d_f}$  is the local Grashof number based on the ligament diameter. In the problems of interest, the temperature difference responsible for pore-scale natural convection in the metal-foam-liquid-water region is  $\langle T_w \rangle^w - \langle T_s \rangle^s$ , and it involves temperatures that span the density inversion point for water. Thus, the following adapted definition of a modified Grashof number [Elkouh (1996)] was used for  $Gr_{d_f}$ :

$$Gr_{d_f} = \frac{g\rho_m \rho_0 d_f^3 \alpha \left| \left\langle T_w \right\rangle^w - \left\langle T_s \right\rangle^s \right|^q}{\mu_0^2}$$
 2.57

 $Re_{d_f}$  is the local Reynolds number based on the ligament diameter:

$$\operatorname{Re}_{d_f} = \frac{\rho_{l_0} \left\| \left\langle \mathbf{u}_w \right\rangle^w \right\| d_f}{\mu_{l_0}} = \frac{\rho_{l_0} \left\| \mathbf{u} \right\| d_f}{\varepsilon \mu_{l_0}}$$
 2.58

The interfacial Nusselt number is based on the fiber diameter and a suitable average thermal conductivity:  $Nu_{\text{convection}} = \overline{h}_{\text{convection}} d_f / k_{l_0}$ . In this work, the criterion for assessing the importance of forced, natural, and mixed convection to the interfacial heat transfer in the metal-foam-liquid-water region was recast as follows:

$$\begin{cases} \text{if} & \frac{Gr_{d_f}}{\left(\text{Re}_{d_f}\right)^2} < 0.1 \quad , \qquad Nu_{\text{convection}} = Nu_{\text{forced convection}} \\ \text{if} & \frac{Gr_{d_f}}{\left(\text{Re}_{d_f}\right)^2} > 10 \quad , \qquad Nu_{\text{convection}} = Nu_{\text{natural convection}} \end{cases}$$

$$\text{if} & 0.1 \le \frac{Gr_{d_f}}{\left(\text{Re}_{d_f}\right)^2} \le 10 \quad , \qquad Nu_{\text{convection}} = Nu_{\text{mixed convection}} \end{cases}$$

A summary of many of the empirical correlations for forced convection around cylinders can be found in Incropera and DeWitt (2002). They have the following general form:

$$\overline{Nu} = \frac{\overline{h}D}{k_f} = C \operatorname{Re}_D^m \operatorname{Pr}^n$$
 2.60

D id the cylinder diameter C, n and m are determined using experimental data, and depend on the range of Reynolds number. For water-saturated metal foams, Calmidi and Mahajan (2000) developed a correlation similar to one proposed by Zukauskas (1971): they assumed m = 0.5 and n = 0.37 and correlated experimental data obtained with seven different metal foams to equation 2.60. Their final result is the following:

$$Nu_{\text{forced convection}} = 0.52 \,\text{Re}_{d_f}^{0.5} \,\text{Pr}_{l_0}^{0.37}$$
 2.61

This result is not purely experimental, since the local (pore-level) heat transfer coefficient cannot be directly measured. Thus, Calmidi and Mahajan (2000) used a two-temperature model to predict the total heat transfer from a metal foam subjected to forced convection, and determined the values of the interfacial heat transfer coefficient which gave the best agreement with their experimental data. Their results and correlations must therefore be adopted with some caution, since they are influenced by the uncertainties in various other parameters of the two-temperature model, such as effective thermal conductivities and thermal dispersion conductivity, for example.

For the pore-scale natural convection, an equation proposed by Zhao et al. (2005) was adopted (it was inspired by a correlation proposed by Churchill and Chu (1975) for natural convection around cylinders):

$$Nu_{\text{natural convection}} = 0.36 + 0.518 \left( \frac{Ra_{d_f}}{1 + (0.559 / Pr_{l_0})^{9/16}} \right)^{1/4}$$
 2.62

In this equation,  $Ra_{d_f}$  is the fiber-diameter-based local Rayleigh number,  $Ra_{d_f} = Gr_{d_f}/Pr_{l_0}$ .

When pore-scale mixed-convection prevails in the metal-foam-liquid-water region, the following relation based on a combination of heat transfer coefficients for transverse forced and natural convection around cylinders [Incropera and DeWitt (2002)] was used:

$$Nu_{\text{mixed convection}} = \left(Nu_{\text{forced convection}}^4 + Nu_{\text{natural convection}}^4\right)^{\frac{1}{4}}$$
 2.63

#### Interfacial conduction heat transfer in the metal-foam-ice region

In the metal-foam-ice region, there is no fluid flow, and the interfacial heat transfer is due to pure conduction. The corresponding interfacial conduction heat transfer coefficient in this region has not been studied with care in the published literature, to the best knowledge of the author. It is convenient to estimate the conduction-limit Nusselt number in this region by simply setting the Reynolds and Rayleigh numbers to zero, as has been done in several recent publications, but this approach in inaccurate and inapplicable. Furthermore, the forced-convection Nusselt number goes to zero when the value of zero is substituted for the Reynolds number in the corresponding correlations (see expression in the previous section, for example). Thus, a novel approach is needed for prescribing a suitable interfacial conduction heat transfer coefficient.

A full three-dimensional model of conduction heat transfer in a representative module of the porous-metal-foam-ice region, akin to that used by Boomsma and Poulikakos (2001), could be used to obtain insights and data for prescribing a correlation for the conduction heat transfer coefficient. However, as was discussed in the previous section, Nusselt number correlations for steady, two-dimensional, forced and natural convection from cylinders have been adapted with considerable success to estimate the interfacial convection heat transfer coefficient. Drawing inspiration from that success, in this work, relatively simple models of steady-state, two-dimensional, heat conduction in a constant-property substance occupying the interstices of regular arrays of in-line and staggered rods were solved numerically, and the results were used to formulate a correlation for an interfacial conduction Nusselt number ( $Nu_{conduction}$ ) as a function of porosity in the porous-metal-foam-ice region.

Experimental observations of the fibers (or ligaments) of porous metal foams show that their cross-section is not perfectly circular, but has a shape somewhere between a triangle and a circle, especially at high values of porosity [Calmidi (1998)]. Therefore, rods of circular, square, and triangular cross-sections were considered in this study. The in-line and staggered arrays of such rods that were used in the above-mentioned models of steady-state, two-dimensional, heat conduction are illustrated in Figures 2.6 to 2.9. For each of these arrays, the distance between the centers of the rods is denoted by L. Other geometrical features of the arrays and related notation are indicated in the figures.

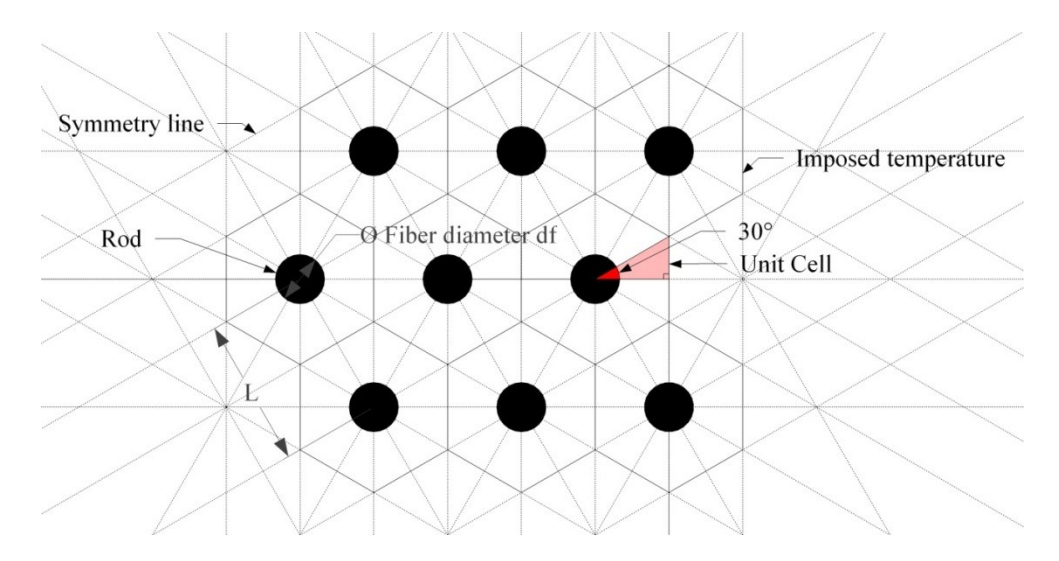


Figure 2.6: Regular array of staggered rods of circular cross-section used in computations of an interfacial conduction Nusselt number: Case 1.

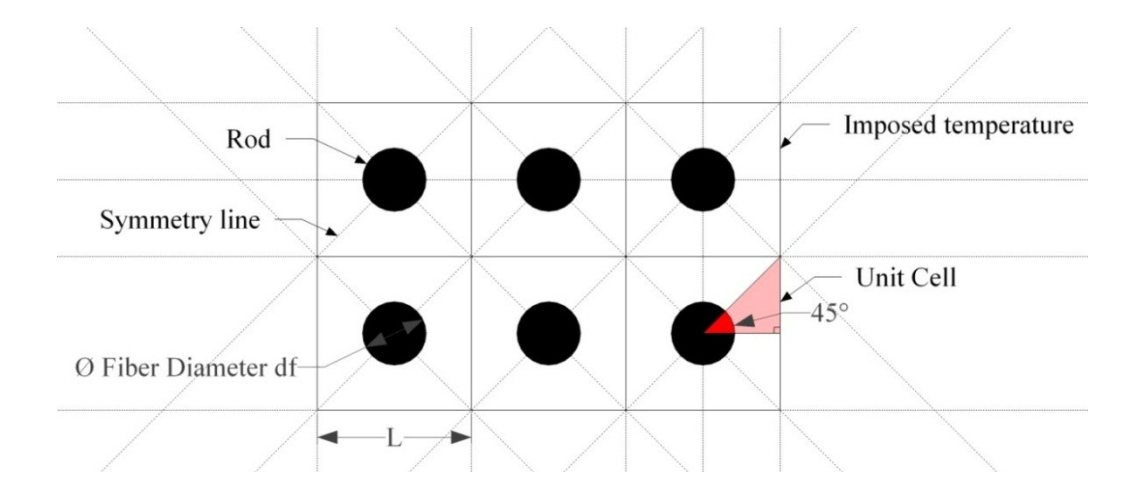


Figure 2.7: Regular array of in-line rods of circular cross-section used in computations of an interfacial conduction Nusselt number: Case 2.

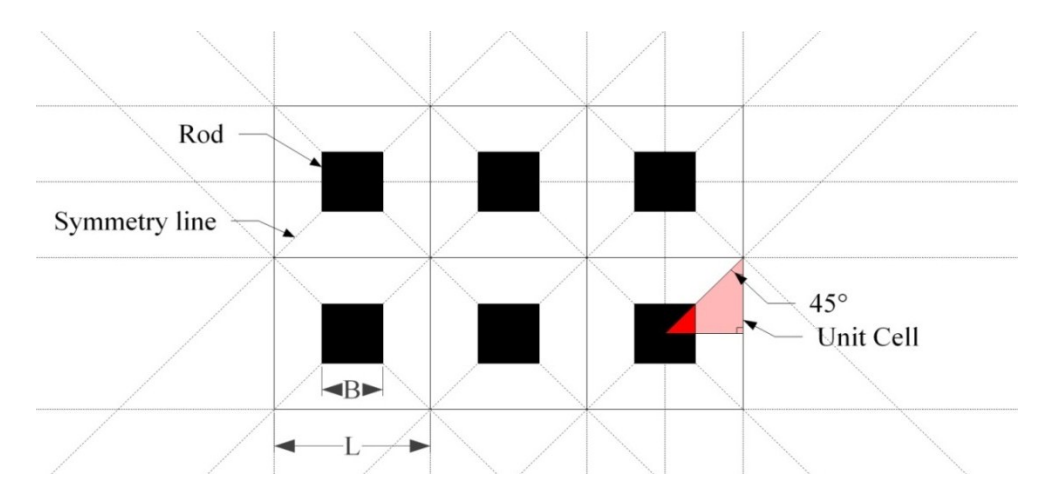


Figure 2.8: Regular array of in-line rods of square cross-section used in computations of an interfacial conduction Nusselt number: Case 3.

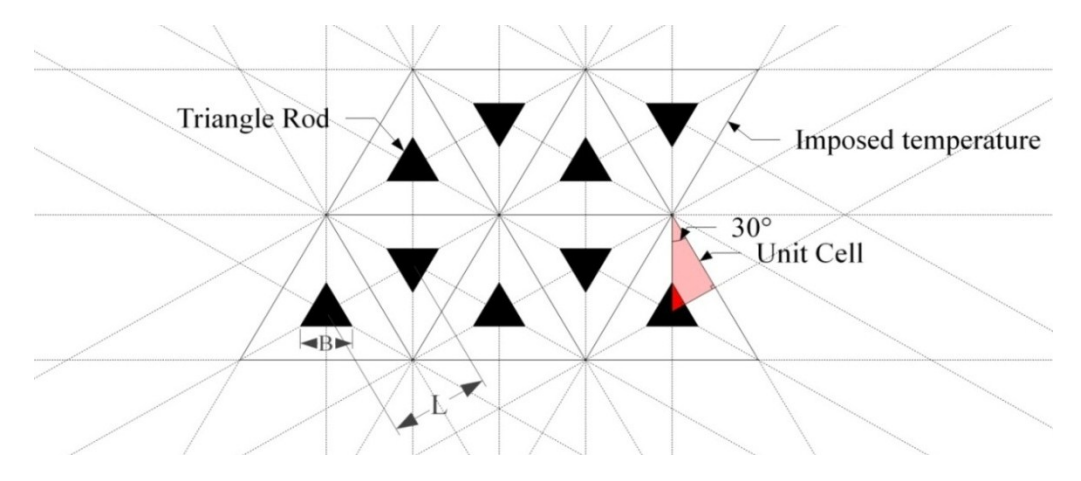


Figure 2.9: Regular array of in-line rods of triangle cross-section used in computations of an interfacial conduction Nusselt number: Case 4.

Each of the rod arrays illustrated in Figures 2.6 to 2.9 has numerous symmetry surfaces (shown by dotted lines in these figures) that allow delineation of representative periodic modules or unit cells. Examples of these unit cells for the four cases considered (Cases 1 – 4) are shown shaded in Figures 2.6 to 2.9. Detailed illustrations of individual unit cells for each of these four cases are provided in Fig. 2.10. The thermal boundary conditions for each cell are the following (also illustrated for Case 1 in Fig. 2.10):  $T = T_C$  at the right (vertical) boundary;  $T = T_H$  at the left boundary (rod surface); and the no-normal-flux condition is imposed on the symmetry surfaces. The rods were considered to have a uniform temperature ( $T_H$ ), since the thermal conductivity of aluminum (solid material of the foam) is much greater than that of ice and also liquid water:  $(k_s/k_{i_0}) \simeq -\infty$  and  $(k_s/k_{i_0}) \simeq -\infty$ .

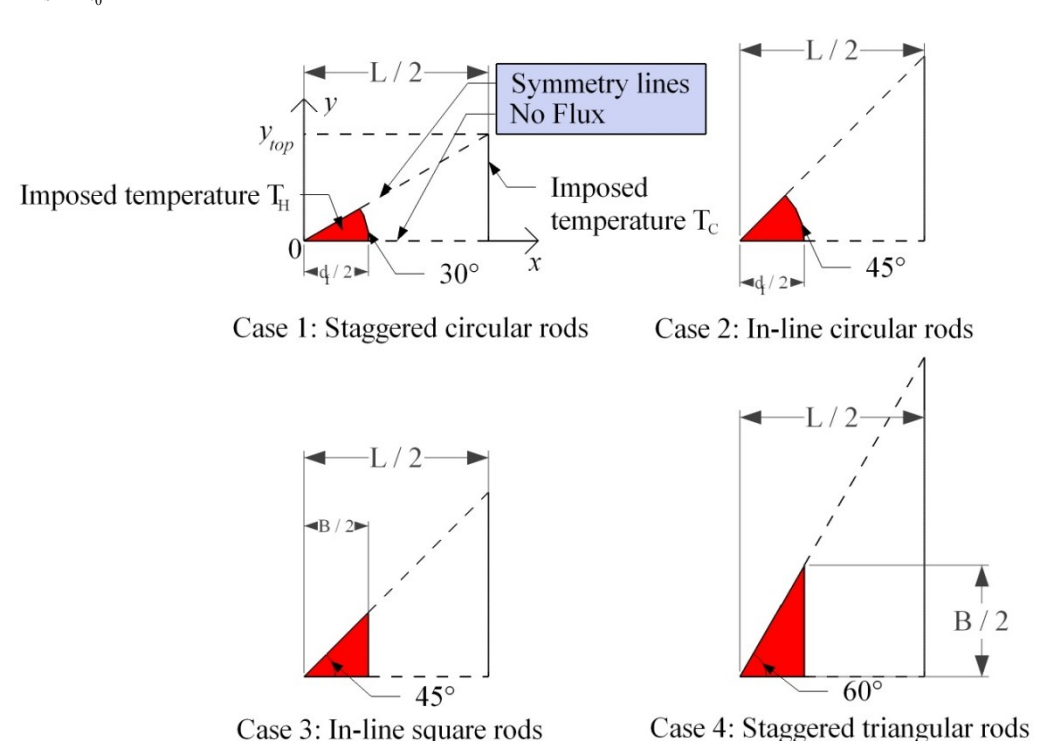


Figure 2.10: Unit cells in the four configurations, Cases 1-4.

Steady-state heat conduction in a constant-property substance (ice in this case) occupying the space between the rod surface and the other boundary surfaces of each unit cell shown in Fig. 2.10 is governed by the following equation:  $\nabla \cdot (k_{i_0} \nabla T) = 0$ . This equation,

subjected to the thermal boundary conditions discussed in the previous paragraph, were solved using an in-house computer code based on a control-volume finite element method (CVFEM) described fully in Baliga and Atabaki (2006). In each case of interest, the CVFEM code was used to compute the temperature distribution and also the rate of heat transfer per unit depth (q') from the rod surface to the ice in the unit cell. Then, the average interfacial conduction heat transfer coefficient and the corresponding average interfacial Nusselt number at the surface of the rod were calculated using the following equations:  $\bar{h} = q'/[l \times (T_H - T_C)]$  and  $Nu_{sf} = \bar{h}l_c/k_{i_0}$ , where l is the rod surface per unit depth in the unit cell, and  $l_c$  is a suitable characteristic length. This characteristic length is defined as follows:

$$l_c = (\text{Area of longitudinal surface of fiber per unit length})/\pi$$
 2.64

A summary of the geometrical properties of the unit cell for all four cases illustrated in Fig. 2.10 is provided in Table 2.3.

	Case 1:	Case 2:	Case 3:	Case 4:
	staggered	in-line circular	in-line square	Staggered
	circular rods	rods	rods	triangular rods
Unit cell base angle	30°	45°	45°	60°
Porosity	$\varepsilon = 1 - \frac{\pi d_f^2}{2\sqrt{3}L^2}$	$\varepsilon = 1 - \frac{\pi d_f^2}{4L^2}$	$\varepsilon = 1 - \frac{B^2}{L^2}$	$\varepsilon = 1 - \frac{B^2}{3L^2}$
Characteristic length in the Nusselt number definition	$l_c = d_f$	$l_c = d_f$	$l_c = \frac{4B}{\pi}$	$l_c = \frac{3B}{\pi}$
Unit cell rod surface area per unit depth	$l = \frac{\pi d_f}{12}$	$l = \frac{\pi d_f}{8}$	$l = \frac{B}{2}$	$l = \frac{B}{2}$
Unit cell right boundary height	$y_{top} = \frac{L}{2\sqrt{3}}$	$y_{top} = \frac{L}{2}$	$y_{top} = \frac{L}{2}$	$y_{top} = \frac{L}{2}\sqrt{3}$

Table 2.3: Geometrical properties of the unit cells for the four cases considered in the study for determining the interfacial conduction Nusselt number.

In Cases 1-4 for which the unit cells are depicted in Fig. 2.10, the heat flux cannot be determined analytically, so numerical solutions were obtained using a CVFEM [Baliga

and Atabaki (2006)]. However, in Case 1, the unit cells can be combined to yield a domain that is quite similar to the annular region in between two concentric cylinders (see Fig. 2.11) with specified temperatures of the inside and outside surfaces, and in which the heat conduction is one-dimensional radial.

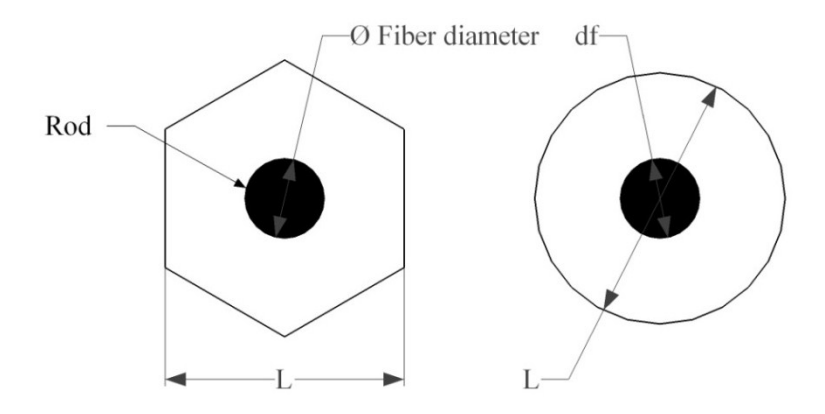


Figure 2.11: Domain created by combining 12 unit cells for Case 1 and the annular region in between two concentric cylinders.

The thermal resistance per unit depth for steady-state one-dimensional radial heat conduction through the annular region in between two concentric cylinders (with constant thermal conductivity,  $k_{i_0}$ , and the domain shown in Fig. 2.11) can be obtained analytically [Incropera and DeWitt (2002)]:

$$R_{\text{th, hollow cylinder}} = \ln\left(\frac{L}{d_f}\right) / 2\pi k_{i_0}$$
 2.65

Using this equation, the corresponding conduction heat transfer coefficient and Nusselt number are given by:

$$h = 1/(R_{\text{th, hollow cylinder}} \pi d_f) = (2k_{i_0}/d_f)/\ln(L/d_f) \quad \text{and} \quad Nu_{\text{hollow cylinder}} = 2/\ln(L/d_f) \quad 2.66$$

For the annular region between two concentric cylinders, the porosity can be defined as the ratio of the fluid surface to total surface:  $\varepsilon = 1 - (d_f^2/L^2)$ . In terms on this porosity, the Nusselt number given in the previous equation can be expressed as follows:

$$Nu_{\text{hollow cylinder}} = \frac{-4}{\ln(1-\varepsilon)}$$
 2.67

As was stated earlier, predictions of steady-state two-dimensional heat conduction in the unit cells for Cases 1-4 illustrated in Fig. 2.10 were obtained using a CVFEM [Baliga and Atabaki (2006)]. In each case, grids of 81 x 81 nodes were used, as grid-independence checks showed that the corresponding results differed by less than  $\pm$  1% from the essentially grid-independent values obtained using a modified Richardson extrapolation technique [Baliga and Atabaki (2006)]. These predictions were used to compute values of the conduction Nusselt number for porosity values in the range 0.9-0.98. The variation in porosity for each of the cases was achieved by keeping the distance L between the centers of adjacent rods constant and adjusting the fiber diameter,  $d_f$ , or the base length, B. As was expected, the conduction Nusselt number did not depend on the thermal conductivity ( $k_{i_0}$ ), the imposed temperatures ( $T_H$  and  $T_C$ ), or L. Examples of the resulting temperature fields for  $\epsilon = 0.9$  for Cases 1-4 are shown in Fig. 2.12.

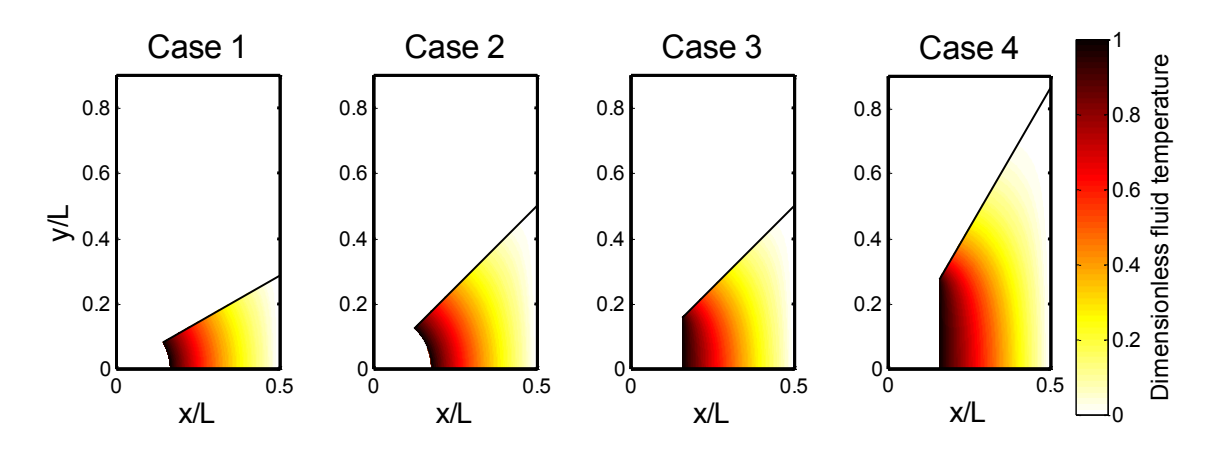


Figure 2.12: Pictorial representation of the dimensionless temperature field,  $T^* = (T - T_C)/(T_H - T_C)$  in the unit cells for Cases 1 – 4 and  $\varepsilon = 0.90$ .

The difference between the highest and lowest predicted values of the conduction Nusselt number ranged from 28% at  $\varepsilon = 0.9$  to 18% at  $\varepsilon = 0.98$ . Case 4 (the one with rods of triangular cross-section) always yielded the highest value of the conduction Nusselt number, while Case 1 (the one with staggered rods of circular cross-section) always

yielded the lowest value of this Nusselt number. At was pointed out earlier, the inputs to the computer simulations were taken from experimental data for rods of essential circular cross-section. Therefore, more trust was put in predictions obtained for Cases 1 and 2, and the following correlation was obtained using the corresponding results:

$$Nu_{\text{conduction}} = \frac{-4.1}{\ln(1-\varepsilon)}$$
 2.68

The values of the conduction Nusselt number calculated using the CVFEM predictions, the analytical solution for the annular region in between concentric cylinders, and the correlation given in equation 2.68 are presented graphically in Fig. 2.13. These results show that the proposed correlation yields results that are in very good agreement with those yielded by the CVFEM predictions for Cases 1 and 2, and reasonably good agreement with the predictions for Case 3.

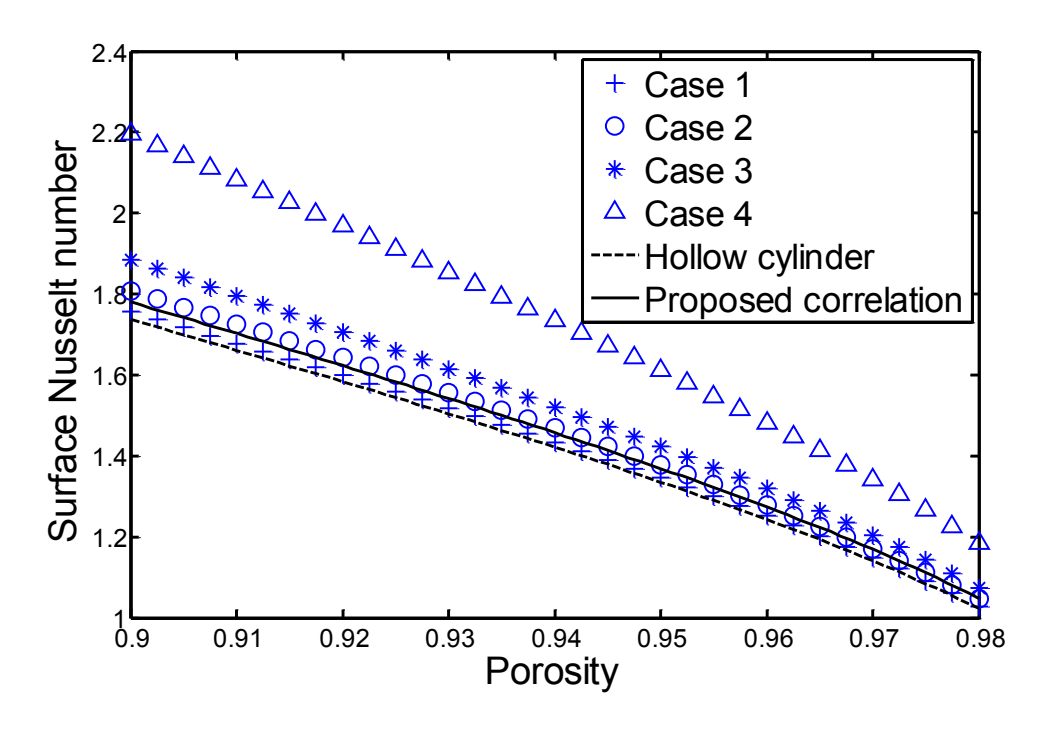


Figure 2.13: Conduction Nusselt number calculated using the CVFEM predictions, the analytical solution for the annular region in between concentric cylinders, and the proposed correlation.

It is acknowledged here that using Cases 1-4 to approximate the conduction heat transfer in the metal-foam-ice region, and also situations in which the fluid flow in the metal-foam-liquid-water region is very low, is somewhat ad hoc. Therefore, the predictions yielded by the proposed correlation in equation 2.68 must be treated as only somewhat rough estimates of the actual values of  $Nu_{sf}$  in conduction-dominated situations. In addition, it would be useful to conduct studies to assess the sensitivity (to the values of the conduction Nusselt number) of the simulations of conduction and natural convection in ice-liquid-water-porous-metal-foam systems. Such sensitivity checks were undertaken in this work, by first using equation 2.68 for calculating the values of the conduction Nusselt number and then doing the same calculations with these values multiplied first by 0.5 and then by 2. The results are presented in Chapter 4.

## Transition between the conduction and convection regimes in the interfacial heat transfer

In the metal-foam-ice region, the conduction Nusselt number was calculated using the correlation given in equation 2.68:

$$Nu_{sf_i} = \frac{h_i d_f}{k_{i_0}} = \frac{-4.1}{\ln(1-\epsilon)}$$
 2.69

In the metal-foam-liquid-water region, it must be ensured that the interfacial values of  $Nu_{sf_i}$  is not be less than the corresponding value of  $Nu_{conduction}$ , and this requirement was ensured by using the following equation:

$$Nu_{sf_l} = \frac{h_l d_f}{k_{l_0}} = \max\left(\frac{-4.1}{\ln(1-\epsilon)}, Nu_{convection}\right)$$
 2.70

#### 2.3 Dimensionless parameters

For natural convection in open rectangular enclosures (no foam) akin to that shown in Fig. 1.2, with only liquid water (no ice;  $T_C \ge 0$ °C) and temperatures spanning the density inversion point, the following five independent dimensionless parameters apply:

$$Ra = \frac{g\rho_{m}\rho_{l_{0}}H_{x}^{3}\alpha |T_{H} - T_{C}|^{q}c_{p_{l_{0}}}}{\mu_{l_{0}}k_{l_{0}}}, \quad T_{m}^{*} = \frac{T_{m} - T_{C}}{T_{H} - T_{C}}, \quad Pr = \frac{\mu_{l_{0}}c_{p_{l_{0}}}}{k_{l_{0}}}, \quad AR = \frac{H_{y}}{H_{x}} \quad \text{and} \quad \theta \quad 2.71$$

The modified Rayleigh number, Ra, is an adaptation of the classical Rayleigh number [Elkouh (1996)], and accounts for the particular nonlinear variation of the density of water with temperature. The parameter  $\theta$  (in radians) quantifies the inclination of the enclosure from the vertical.  $T_m^*$  is the density inversion parameter, which quantifies the relative position of the density inversion temperature with respect to the wall temperatures. If  $T_m^* \geq 1$ , then  $T_m \geq T_H$  and the water behaves as a fluid with a negative value of the classical thermal volumetric expansion coefficient,  $\beta \triangleq 0$ , then  $T_m \leq T_C$  and the water behaves as a fluid with a positive value of  $\beta$ . The value of the density inversion parameter has a strong influence on the fluid flow pattern inside the cavity and the heat transfer rates, as will be shown by the results presented in Chapter 4. For ice-water systems in open (no foam) rectangular enclosures,  $T_C$  is replaced by 0°C in the definitions of the Rayleigh number, Ra, and the density inversion parameter,  $T_m^*$ .

When porous metal foam is included in the rectangular enclosure, and ice-liquid-water-metal-foam systems are considered, four additional independent dimensionless parameters are involved: the porosity of the metal foam; the water-to-foam thermal conductivity ratio, which is  $k_{i_0}/k_s$  in the ice-metal-foam region and  $k_{l_0}/k_s$  in the liquid-water-metal-foam region, and the Darcy number. The Darcy number is the normalized permeability [Nield and Bejan (2006)]:

$$Da = \frac{\sqrt{K}}{H_x}$$
 2.72

All the other commonly used dimensionless parameters involved in ice-liquid-water-metal-foam systems can be expressed as functions of the above-mentioned independent dimensionless parameters: the dimensionless pore diameter,  $D_p = d_p/H_x$  can be calculated from the porosity and Darcy number, thanks to equations 2.36, 2.51, 2.52, and 2.72; the dimensionless fiber diameter can be calculated using the porosity, the dimensionless pore diameter and equations 2.51 and 2.52; and the Forchheimer coefficient can be calculated using equation 2.37. The specific area,  $a_{sf}$ , and the interfacial Nusselt number,  $Nu_{sf_t}$ , needed in the two-temperature models, can be calculated using equations 2.53 and 2.70, respectively.

The predicted values of the average rates of heat transfer on the left or right wall will be presented (in Chapter 4) in dimensionless forms as wall-average Nusselt number:

$$\overline{Nu}_{wall} = \overline{h}_{wall} H_{x} / k_{L}$$
 2.73

In this equation,  $\overline{h}_{wall}$  is the average heat transfer coefficient on the left or right wall, defined as follows:

$$\bar{h}_{wall} = \frac{q'_{wall}}{H_{y}(T_{H} - T_{C})}$$
 2.74

In open domains (no foam), the total rate of heat transfer per unit depth,  $q'_{\text{wall}}$ , into the enclosure at the heated wall and out of the enclosure at the cooled wall, is calculated as follows:

$$q'_{wall \text{ (no foam)}} = k_{w_0} \int_0^{H_y} \left(\frac{\partial T}{\partial x}\right)_{wall} dy$$
 2.75

In this equation,  $k_{w_0}$  is the suitably averaged thermal conductivity along the wall, equal to  $k_{l_0}$  if the wall temperature is greater than  $T_{melt}$ , and equal to  $k_{i_0}$  if the wall temperature is less than  $T_{melt}$ .

When the metal foam is included in the domain, the wall Nusselt number can be written, for both the cold and hot walls, as the sum of a fluid (ice or liquid water) Nusselt number and foam Nusselt number:

$$\overline{Nu}_{wall} = Nu_{\text{foam left}} + Nu_{\text{fluid left}} = Nu_{\text{foam right}} + Nu_{\text{fluid right}}$$
 2.76

$$\begin{cases} Nu_{\text{foam left}} = \frac{(1/AR)}{k_{l_0} (T_H - T_C)} \int_0^{H_y} \left( (k_{ss} + k_{sw}) \frac{\partial T_s}{\partial x} \right) dy \\ Nu_{\text{fluid left}} = \frac{(1/AR)}{k_{l_0} (T_H - T_C)} \int_0^{H_y} \left( (k_{ww} + k_{sw}) \frac{\partial T_f}{\partial x} \right) dy \\ Nu_{\text{foam right}} = \frac{(1/AR)}{k_{l_0} (T_H - T_C)} \int_0^{H_y} \left( (k_{ss} + k_{sw}) \frac{\partial T_s}{\partial x} \right) dy \\ Nu_{\text{fluid right}} = \frac{(1/AR)}{k_{l_0} (T_H - T_C)} \int_0^{H_y} \left( (k_{ww} + k_{sw}) \frac{\partial T_f}{\partial x} \right) dy \end{cases}$$

The equality of equation 2.76 always holds under steady-state conditions, but the repartition of the rates of heat transfer between the metal foam and the fluid (ice or liquid water) can be different on the two walls: thus, for example  $Nu_{\text{foam right}}$  can be significantly different from  $Nu_{\text{foam right}}$ .

### Chapter 3: Numerical Method

This chapter is organized as follows: first, a synopsis of a finite volume method (FVM) described by Baliga and Atabaki (2006) for the solution of steady, two-dimensional (Cartesian), Newtonian fluid flow and heat transfer problems in open domains (without porous media) is provided; then, modifications needed to adapt this FVM for solving the mathematical models of the water-ice-metal-foam systems of interest (described in Chapter 2) are summarized. A control-volume finite element method (CVFEM) was used for the determination of a correlation for the interfacial conduction Nusselt number, using a formulation and procedures described in Section 2.2.5. For full details and discussions of this CVFEM, the interested reader is referred to the work of Baliga and Atabaki (2006). The CVFEM described in their work was used here without any modifications.

# 3.1 Synopsis of a Finite Volume Method for steady, two-dimensional, fluid flow and heat transfer in open domains

A detailed description of this finite volume method (FVM) is available in Baliga and Atabaki (2006). Thus, only a synopsis is provided here.

#### 3.1.1 Governing equations

As was mentioned above, this FVM is designed for solving steady, two-dimensional (Cartesian), Newtonian fluid flow and heat transfer problems in open domains. In the Cartesian coordinate system, and the equations that govern these problems can be cast in the following forms:

Continuity equation:

$$\frac{\partial}{\partial x}(\rho_l u) + \frac{\partial}{\partial y}(\rho_l v) = 0$$
3.1

*x*-momentum equation :

$$\frac{\partial}{\partial x} \left( \rho_l u u \right) + \frac{\partial}{\partial y} \left( \rho_l v u \right) = -\frac{\partial P}{\partial x} + \frac{\partial}{\partial x} \left( \mu_l \frac{\partial u}{\partial x} \right) + \frac{\partial}{\partial y} \left( \mu_l \frac{\partial u}{\partial y} \right) + S_u$$
 3.2

y-momentum equation:

$$\frac{\partial}{\partial x}(\rho_l u v) + \frac{\partial}{\partial y}(\rho_l v v) = -\frac{\partial P}{\partial y} + \frac{\partial}{\partial x}\left(\mu_l \frac{\partial v}{\partial x}\right) + \frac{\partial}{\partial y}\left(\mu_l \frac{\partial v}{\partial y}\right) + S_v$$
 3.3

Energy equation:

$$\frac{\partial}{\partial x} \left( \rho_l u T_w \right) + \frac{\partial}{\partial y} \left( \rho_l v T_w \right) = \frac{\partial}{\partial x} \left( \frac{k_l}{c_{pl_0}} \frac{\partial T_w}{\partial x} \right) + \frac{\partial}{\partial y} \left( \frac{k_l}{c_{pl_0}} \frac{\partial T_w}{\partial y} \right) + S_T$$
 3.4

In equations 3.1–3.4,  $S_u$ ,  $S_v$ , and  $S_T = S_E/c_{pl_0}$  are volumetric source terms, which can be used to model actual physical sources of *x*-momentum, *y*-momentum, and thermal energy, respectively, and also include all terms that are not explicitly shown in these equations [Patankar (1980); Baliga and Atabaki (2006)]. Following Patankar (1980), it is noted that equations 3.1-3.4 are all specialized versions of a general form of these governing equations. This general equation is given below:

$$\frac{\partial}{\partial x} \left( \rho_l u \phi \right) + \frac{\partial}{\partial y} \left( \rho_l v \phi \right) = \frac{\partial}{\partial x} \left( \Gamma_\phi \frac{\partial \phi}{\partial x} \right) + \frac{\partial}{\partial y} \left( \Gamma_\phi \frac{\partial \phi}{\partial y} \right) + S_\phi$$
 3.5

In this equation,  $\phi$  denotes a general specific (per unit mass) scalar dependent variable,  $\Gamma_{\phi}$  a diffusion coefficient associated with  $\phi$ , and  $S_{\phi}$  the corresponding volumetric (per unit volume) source term. If needed, all of the source terms are linearized and cast in the following form [Patankar (1980)]:

$$S_{\phi} = S_C^{\phi} + S_P^{\phi} \phi \tag{3.6}$$

#### 3.1.2 Domain discretization

The domains of interest are first discretized into contiguous rectangular control volumes that fill the domain exactly. Then, the nodes or grid points are located at the geometric centers of the control volumes, the centers of the control volume faces that coincide with the boundaries of the domain, and the corners of rectangular domain. The grid points or nodes lie on lines that are parallel to the grid axes, and these grid lines could be non-uniformly spaced. This domain discretization scheme is illustrated in Fig. 3.1. All dependent variables are located (stored) at the same set of nodes (co-located formulation). The same set of nodes also serve as storag locations for  $\rho_l$ ,  $\mu_l$ ,  $k_l$ ,  $c_{pl}$ ,  $S_u$ ,  $S_v$ ,  $S_T$ ,  $\Gamma_\phi$ , and  $S_\phi$ .

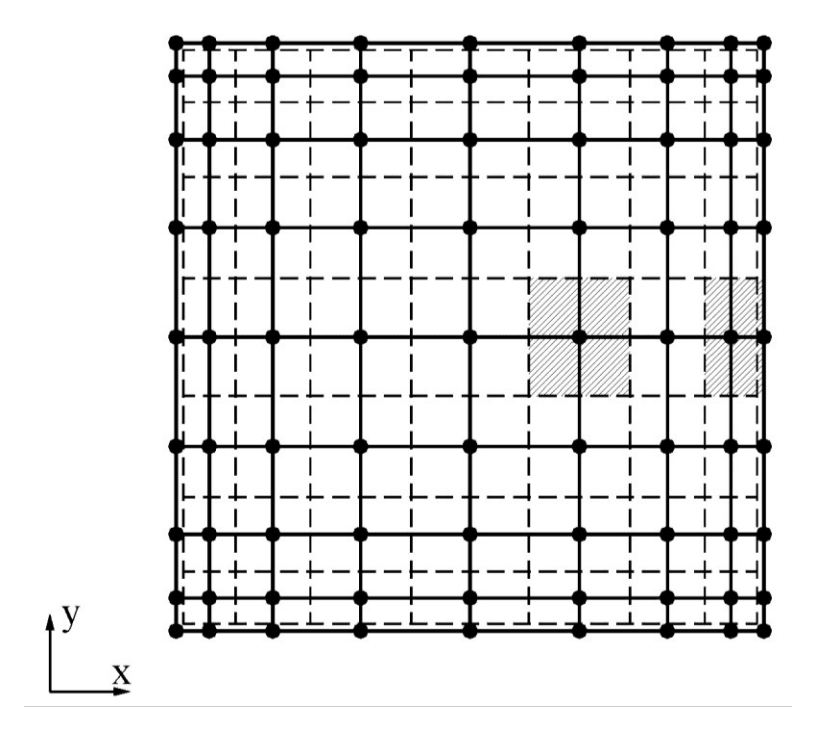


Figure 3.1: Discretization of a rectangular calculation domain: dashed lines indicate control volume faces; solid dots indicate nodes or grid points; and solid lines denote grid lines.

The notations that are used to denote grid details for interior and boundary nodes are provided in Figures 3.2 (a) and (b), respectively.

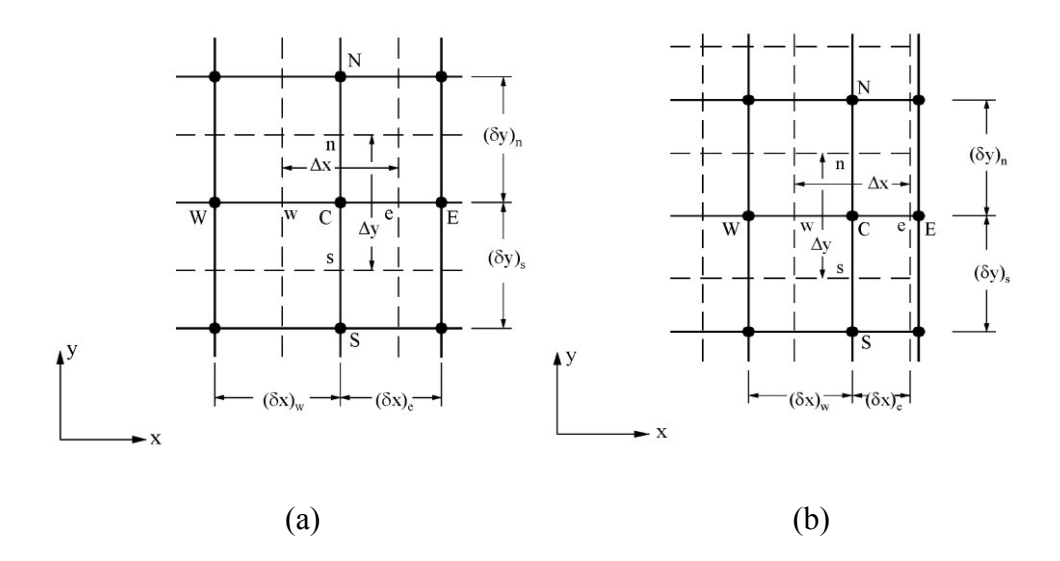


Figure 3.2: Notations associated with (a) interior nodes and (b) boundary nodes.

#### 3.1.3 Discretized equations

The governing differential equations are first integrated over the control volumes shown in Figures 3.1 and 3.2, and algebraic approximations to the integral conservation equations are then derived. These algebraic approximations are called the discretized equations. In the derivation of these discretized equations, the advection and diffusion (or viscous and conduction) terms are discretized using the hybrid scheme [Patankar (1980); Baliga and Atabaki (2006)], which is second-order accurate at low velocities (strictly, at grid Peclet number values less than 2) and uniform grids. Quadratic interpolation is used at the boundaries, appropriately adjusted to incorporate the specified boundary conditions and designed to ensure second-order accuracy [Baliga and Atabaki (2006)]. The reduced pressure is interpolated using piecewise-linear functions between the nodes. In the mass flow rate terms, the velocity components are interpolated using the so-called momentum interpolation scheme [Rhie and Chow (1983); Baliga and Atabaki (2006)], to avoid undesirable checkerboard pressure and velocity distributions that would otherwise afflict this equal-order co-located FVM [Patankar (1980)]. The values of thermophysical properties stored at the nodes are interpolated to locations where the grid lines intersect the control-volume faces using a resistance analogy (which reduces to the harmonic mean on uniform grids), as described in Patankar (1980) and Baliga and Atabaki (2006). The

resulting discretized equations for u, v, P, T, and  $\phi$  can be cast in the following forms [Baliga and Atabaki (2006)].

Discretized *u* equations:

$$a_C^u u_C = \sum_{nb=E.N.W.S} a_{nb}^u u_{nb} + b_C^u - \left(\overline{\partial P / \partial x}\right) Vol_C$$
 3.7

Discretized *v* equations:

$$a_C^{\nu} v_C = \sum_{nb=E.N.W.S} a_{nb}^{\nu} v_{nb} + b_C^{\nu} - \left( \overline{\partial P / \partial y} \right) Vol_C$$
 3.8

Discretized *P* equations:

$$a_C^P P_C = \sum_{nb=E.N.W.S} a_{nb}^P P_{nb} + b_C^P$$
 3.9

Discretized *T* equations:

$$a_C^T T_C = \sum_{nb=E.N.W.S} a_{nb}^T T_{nb} + b_C^T$$
 3.10

Discretized  $\phi$  equations:

$$a_C^{\phi} \phi_C = \sum_{nb=E,N,W,S} a_{nb}^{\phi} \phi_{nb} + b_C^{\phi}$$
 3.11

In equations 3.7 and 3.8,  $(\overline{\partial P/\partial x})$  and  $(\overline{\partial P/\partial y})$  are the reduced pressure gradients in the x and y directions, respectively, averaged over the control volume,  $Vol_C$ , associated with the node C.

#### 3.1.4 Solution of the discretized equations

The sets of discretized equations, represented by equations 3.7 to 3.11, were solved using a sequential iterative variable adjustment (SIVA) procedure. In each overall (or outer) iteration of this procedure, linearized (if required) and decoupled sets of the discretized

equations for u, v, P, and other dependent variables, as needed, are solved sequentially; and in this sequence, each linearized and decoupled set of discretized equations for each dependent variable is solved using an iterative line-Gauss-Seidel scheme (inner iterations), which involves a line-by-line application of the tri-diagonal-matrix-algorithm (TDMA). The overall iterations of the SIVA procedure are repeated until a suitable convergence criterion is met. Full details of the SIVA procedure are available in Baliga and Atabaki (2006), so they are not repeated here.

To ensure convergence of the SIVA procedure, it is essential to under-relax the discretized equations. The implicit under-relaxation procedure of Patankar (1980) was used in this work. Thus, for example, the set of discretized equations for the general variable,  $\phi$ , is first under-relaxed and rewritten as follows, and then solved:

$$\left(\frac{a_C^{\phi}}{\alpha_{\phi}}\right)\phi_C = \sum_{nb=E,N,W,S} a_{nb}^{\phi}\phi_{nb} + \left\{b^{\phi} + \left(\frac{1-\alpha_{\phi}}{\alpha_{\phi}}\right)a_C^{\phi}\phi_C^*\right\}$$
3.12

In this equation,  $\alpha_{\phi}$  is the under-relaxation parameter associated with the dependent variable  $\phi$ , and  $\phi_{C}^{*}$  is the latest available value (or guess value at the start of the overall iterations) of  $\phi$  at the node under consideration. The following values of the under-relaxation parameters are recommended by Baliga and Atabaki (2006) and were found to work well in this work:  $\alpha_{u} = \alpha_{v} = 0.5$ ;  $\alpha_{P} = 1.0$ . The temperature under-relaxation parameter was set to  $\alpha_{T} = 0.9$ .

The iterations of the SIVA procedure were assumed to have converged when the maximum values of suitably normalized absolute residues of the sets of discretized equations of all dependent variables had all fallen below  $10^{-6}$ .

# 3.2 Finite Volume Method for simulation of steady, two-dimensional, fluid flow and heat transfer in Water-Ice-Metal-Foam systems

The modifications that were necessary to adapt the FVM (described in Section 3.2) for solving the mathematical models of fluid flow and heat transfer in the water-ice-metal-foam systems of interest are summarized in this section.

### 3.2.1 Recasting of the governing equations

First, equations 2.29 and 2.40 were recast in the following forms:

$$\nabla \cdot (\rho_{l_0} \mathbf{u}) = 0 \tag{3.13}$$

$$\nabla \cdot \left[ \left( \rho_{l_0} \mathbf{u} \right) \mathbf{u} \right] = -\varepsilon^2 \nabla \langle P \rangle^w + \varepsilon \mu_{l_0} \left( \nabla^2 \mathbf{u} \right) - \left[ \varepsilon^2 \frac{\mu_{l_0}}{K} + \varepsilon^2 \frac{\rho_{l_0} f}{\sqrt{K}} \| \mathbf{u} \| \right] \mathbf{u}$$

$$+ \varepsilon^2 \left[ \rho_m \left( 1 - \alpha \left| \langle T_w \rangle^w - T_m \right|^q \right) - \rho_{l_0} \right] \mathbf{g}$$
3.14

The energy equations for the intrinsic-phase-average temperatures of the solid (metal foam) and water (ice or liquid), equations 2.44 and 2.45, were also recast as follows:

In the liquid-water-metal-foam region:

$$\begin{cases}
\nabla \cdot \left(\rho_{l_0} \mathbf{u} \left\langle T_w \right\rangle^w\right) = \nabla \cdot \left(\frac{k_{ll} + k_{sl} + \varepsilon k_D}{c_{pl_0}} \nabla \left\langle T_w \right\rangle^w\right) - \frac{a_{sf} h_l}{c_{pl_0}} \left(\left\langle T_w \right\rangle^w - \left\langle T_s \right\rangle^s\right) \\
0 = \nabla \cdot \left(\frac{k_{ss} + k_{sl}}{c_{ps_0}} \nabla \left\langle T_s \right\rangle^s\right) + \frac{a_{sf} h_l}{c_{ps_0}} \left(\left\langle T_w \right\rangle^w - \left\langle T_s \right\rangle^s\right)
\end{cases}$$
3.15

In the ice-metal-foam region:

$$\begin{cases}
0 = \nabla \cdot \left(\frac{k_{ii} + k_{si}}{c_{pi_0}} \nabla \langle T_w \rangle^w\right) - \frac{a_{sf} h_i}{c_{pi_0}} \left(\langle T_w \rangle^w - \langle T_s \rangle^s\right) \\
0 = \nabla \cdot \left(\frac{k_{ss} + k_{si}}{c_{ps_0}} \nabla \langle T_s \rangle^s\right) + \frac{a_{sf} h_i}{c_{ps_0}} \left(\langle T_w \rangle^w - \langle T_s \rangle^s\right)
\end{cases}$$
3.16

Under steady-state conditions, the values of the ice and foam specific heat at constant pressure,  $c_{pi_0}$  and  $c_{ps_0}$ , do not influence the solution of the governing equations, but they were included for consistency and also potential extensions to unsteady simulations.

### 3.2.2 Modifications implemented for computing fluid flow and pressure

In the liquid-water-metal-foam region, the steady-state FVM described in Section 3.1 was adapted for solving the set of equations that govern the superficial (or Darcy) velocity,  $\mathbf{u}$ , and the intrinsic-phase-average reduced pressure,  $\langle P \rangle^w$  (equations 3.13 and 3.14) using the following minor modifications: 1) the term  $Vol_C$  in equations 3.7 and 3.8 is replaced by  $\varepsilon^2 Vol_C$ ; and 2) the dynamic viscosity,  $\mu_{l_0}$ , is replaced by  $\varepsilon \mu_{l_0}$ . In addition, the source terms in the x and y momentum equations were set equal to the following values:

$$S_{C}^{u} = \varepsilon^{2} \left[ \rho_{m} \left( 1 - \alpha \left| \left\langle T_{w} \right\rangle^{w} - T_{m} \right|^{q} \right) - \rho_{l_{0}} \right] g_{x}$$

$$S_{C}^{v} = \varepsilon^{2} \left[ \rho_{m} \left( 1 - \alpha \left| \left\langle T_{w} \right\rangle^{w} - T_{m} \right|^{q} \right) - \rho_{l_{0}} \right] g_{y}$$

$$S_{P}^{u} = S_{P}^{v} = - \left[ \frac{\varepsilon^{2} \mu_{l_{0}}}{K} + \frac{\varepsilon^{2} f \rho_{f} \|\mathbf{u}\|}{\sqrt{K}} \right]$$
3.17

Here,  $g_x$  and  $g_y$  are components of the gravitational acceleration vector in the positive x and y directions, respectively.

At the nodes associated with control volumes in the ice-metal-foam region, the velocity was set to zero. This was done by modifying the coefficients in the discretized momentum equations as follows:

$$a_P^{u,v} = 1$$
 ;  $a_{nb}^{u,v} = 0$  ;  $b^{u,v} = 0$  3.18

The treatment of the coefficients in the discretized pressure equation was similar, but done in the context of additional modifications. The reduced pressure values at nodes inside the ice-metal-foam region were totally decoupled from the rest of the fluid domain,

by imposing zero values of the interpolated pseudo-velocities u and  $\hat{}$ , and also zero values of  $d_u$  and  $d_y$ , using the definitions and procedures proposed by Baliga and Atabaki (2006). After that, the reduced pressure in the ice-porous-metal region was fixed to the convenient value of zero, using the following modifications of the coefficients in the corresponding discretized equation:

$$a_P^p = 1$$
 ;  $a_{nb}^p = 0$  ;  $b^p = 0$  3.19

At any solid boundary, the mass flow rates that are used to approximate advection at the control-volume faces were also set equal to zero. Furthermore, the volume-averaged gradients of the reduced pressure,  $(\overline{\partial P/\partial x})$  and  $(\overline{\partial P/\partial y})$ , were calculated in a modified manner for control volumes in the liquid-water-porous-foam region, but immediately adjacent to (one or more faces on) the ice-porous-foam region: the terms  $(\overline{\partial P/\partial x})$  and  $(\overline{\partial P/\partial y})$  were computed using only the values of reduced pressure at nodes in the liquid-water-porous-foam region, since the zero values of the reduced pressure imposed at the nodes inside the ice-porous-foam region have no physical relevance in the context of this FVM.

## 3.2.3 Modifications implemented for computing intrinsic-phase-average temperatures

Modifications of the FVM (described in Section 3.1) to enable solutions of equations 3.15 and 3.16 that govern the intrinsic-phase-average temperatures of the solid (metal foam) and water (ice or liquid water),  $\langle T_s \rangle^s$  and  $\langle T_w \rangle^w$ , respectively, in the liquid-water-porous-metal-foam and ice-porous-metal-foam regions are summarized in this subsection. First, the relevant diffusion coefficients and source terms were set as follows:

In the liquid-water-metal-foam region:

$$\begin{cases}
\Gamma_{\langle T_{w}\rangle^{w}} = \frac{k_{ll} + k_{sl} + \varepsilon k_{D}}{c_{pl_{0}}} ; \quad (S_{C})_{\langle T_{w}\rangle^{w}} = \left(\frac{h_{l}a_{sf}}{c_{pl_{0}}}\right) \langle T_{s}\rangle^{s} ; \quad (S_{P})_{\langle T_{w}\rangle^{w}} = -\left(\frac{h_{l}a_{sf}}{c_{pl_{0}}}\right) \\
\Gamma_{\langle T_{s}\rangle^{s}} = \frac{k_{ss} + k_{sl}}{c_{ps_{0}}} ; \quad (S_{C})_{\langle T_{s}\rangle^{s}} = \left(\frac{h_{l}a_{sf}}{c_{ps_{0}}}\right) \langle T_{w}\rangle^{w} ; \quad (S_{P})_{\langle T_{s}\rangle^{s}} = -\left(\frac{h_{l}a_{sf}}{c_{ps_{0}}}\right)
\end{cases}$$
3.20

In the ice-metal-foam region:

$$\begin{cases}
\Gamma_{\langle T_{w} \rangle^{w}} = \frac{k_{ii} + k_{si}}{c_{pi_{0}}} ; \quad (S_{C})_{\langle T_{w} \rangle^{w}} = \left(\frac{h_{i}a_{sf}}{c_{pi_{0}}}\right) \langle T_{s} \rangle^{s} ; \quad (S_{P})_{\langle T_{w} \rangle^{w}} = -\left(\frac{h_{i}a_{sf}}{c_{pi_{0}}}\right) \\
\Gamma_{\langle T_{s} \rangle^{s}} = \frac{k_{ss} + k_{si}}{c_{ps_{0}}} ; \quad (S_{C})_{\langle T_{s} \rangle^{s}} = \left(\frac{h_{i}a_{sf}}{c_{ps_{0}}}\right) \langle T_{w} \rangle^{w} ; \quad (S_{P})_{\langle T_{s} \rangle^{s}} = -\left(\frac{h_{i}a_{sf}}{c_{ps_{0}}}\right)
\end{cases}$$
3.21

An additional binary integer variable called the solid-liquid indicator ISL was used in the computations to indicate and determine whether a node was located in the ice-metal-foam region or the liquid-water-metal-foam region. Its value was set equal to one (1) at nodes (grid points) in the liquid-water-metal-foam region, and to zero (0) at the grid points in the ice-metal-foam region. In addition, to avoid uncontrollable oscillations of the waterice interface and potential divergence of the FVM solution, prescription of a melting temperature tolerance,  $\Delta T_{\it melt}$  , was found to be necessary. If the conditions at a node corresponded to the ice-metal-foam region in a particular overall iteration of the FVM, then in the next iteration, these conditions were change to those corresponding to the liquid-water-metal-foam region only if the computed value of  $\langle T_w \rangle^w$  was greater than  $T_{melt} + \Delta T_{melt}$ . Similarly, in successive overall iterations of the FVM, the conditions of liquid-water-metal-foam at a node were changed to those of ice-metal-foam only if the computed temperature of value of  $\left\langle T_{_W} \right\rangle^{_W}$  was smaller than  $T_{_{melt}} - \Delta T_{_{melt}}$  . In the final simulations, each case of interest was started with a relatively large value of  $\Delta T_{\it melt}$  (of the order of 1 or 2  $^{\rm o}$ C, or as need to get convergence), and then the value of  $\Delta T_{\rm melt}$  was gradually reduced until its influence on the final results for this case became negligible.

#### 3.3 Continuation method

A so-called continuation method was used to facilitate convergence of the FVM in the final simulations. In a series of runs, after a converged solution (values of the dependent variables  $\mathbf{u}$ ,  $\langle P \rangle^w$ ,  $\langle T_s \rangle^s$ , and  $\langle T_w \rangle^w$ , and also  $\mathit{ISL}$ ), was obtained for a case of interest (with a given set of input parameters  $H_x$ ,  $H_y$ ,  $\theta$ ,  $T_H$ ,  $T_C$ ,  $\varepsilon$ ,  $d_p$  and  $\Delta T_{melt}$ ), this solution was used as the initial guess for the next case of interest. This method saved a considerable amount of computational time in the final simulations. It also provided another very important advantage: converged solutions could be obtained for difficult cases (for example, cases in which the density inversion parameter was close to 0.5, or the value of Rayleigh number was quite high), by starting with a fully converged solution to a less difficult case, and then slowly changing the set of inputs towards those of the difficult case, using the continuation method to obtain fully-converged intermediate and final solutions. Examples of results yielded by continuation method are presented in Chapter 4.

### Chapter 4: Results and Discussions

Applications of the mathematical models and the finite volume method (FVM) proposed in Chapters 2 and 3 to test and demonstration problems, and the results obtained, are presented and discussed in this chapter. As was mentioned and discussed in Chapters 1 and 2, attention was limited in this work to steady-state, two-dimensional planar, conduction and laminar natural convection heat transfer in ice-liquid-water systems contained in rectangular enclosures, with and without porous metal (aluminum) foams.

In this chapter, first, results for laminar natural convection in liquid water in open square enclosures (no ice; no porous metal foam), with temperatures spanning the density inversion point, are presented and compared to the experimental and numerical results of Elkouh (1996). This problem was first solved using a variable-property model (VPM) and then a constant-property model (CPM), with the constant fluid properties evaluated at several different reference (or average) temperatures, and the reference (or average) temperature that yields the lowest differences between the results computed with the VPM and CPM was determined. These results are also presented and discussed.

Next, results for conduction and laminar natural convection in ice-liquid-water systems in open square enclosures (no porous metal foam) are presented and compared to some experimental and numerical results presented by Elkouh (1996). Particular attention is given to the influence of the Rayleigh number on the streamlines and ice-liquid-water interface position.

Following that, results obtained for conduction and laminar natural convection in liquid-water-porous-metal-foam systems contained in square enclosures are presented and discussed. The effects of adding five different porous metal foams to the liquid water problems considered by Elkouh (1996) are discussed first, and then simulations and results that were used to assess the influence of Rayleigh number, thermal dispersion, and Forchheimer drag on the streamlines and values of average Nusselt number are presented.

Finally, simulations of a demonstration problem involving conduction and laminar natural convection heat transfer in ice-liquid-water-metal-foam systems contained in

rectangular enclosures are presented, for enclosure dimensions and wall temperatures that are relevant to cold-storage situations. Results obtained with and without the foam are compared and the effect of aspect ratio is quantified.

# 4.1 Natural convection in liquid water contained in open square enclosures (no foam), with temperatures spanning the density inversion point

This problem was used to validate the proposed mathematical models and FVM. The calculation domain is the rectangular enclosure illustrated schematically in Fig. 1.2, but with no ice and no foam (in this test problem). First, the results obtained for 12 different cases simulated using the variable-property model (VPM) described in Chapter 2 are presented and compared to the experimental and numerical results of Elkouh (1996). These cases were also simulated using the constant-property model (CPM) discussed in Chapter 2, with the constant fluid properties evaluated at several reference (or average) temperatures. Then, the reference (or average) temperature that yields the lowest differences between the results computed with the VPM and CPM was determined. These results are also presented and discussed in this section.

In the experiments of Elkouh (1996) for this problem, the dimensions of the square enclosure were kept constant at  $H_x = H_y = H = 6.012 \text{cm}$ , its left-wall temperature was maintained as close as possible to 0°C, and its right-wall temperature was maintained at different values between the density inversion temperature of water and 20°C. The inclination angle,  $\theta$ , was 0° in the first six runs, and 45° in the next six runs. The conditions for the 12 cases (Runs # 1 – 12) of this problem investigated experimentally by Elkouh (1996) are summarized in Table 4.1. Also provided in this table are values of the Rayleigh and Prandtl numbers calculated using the definitions given in Chapter 2, and with water properties based on a zonal temperature that is defined later in this section. Elkouh (1996) used a dye-injection technique to obtain photographs of the streamline patterns for the aforementioned 12 runs, but he did not present any quantitative data related to the natural convection heat transfer. Thus, only qualitative comparisons were possible between his experimental results and the numerical predictions obtained in this work.

Run number	Cavity angle $\theta$	$T_C$ (°C)	$T_H$ (°C)	Density inversion parameter $T_m^*$	Rayleigh number	Prandtl number
1	0°	0.00	4.01	1.006	$1.22 \times 10^6$	12.4
2	0°	0.01	6.02	0.669	$2.63 \times 10^6$	12.4
3	0°	0.00	8.04	0.501	4.56×10 <sup>6</sup>	12.4
4	0°	0.03	10.00	0.401	$7.91 \times 10^6$	10.4
5	0°	0.04	14.98	0.267	$1.82 \times 10^7$	9.56
6	0°	0.00	20.00	0.202	$3.37 \times 10^7$	8.84
7	45°	0.00	4.04	1.001	$1.24 \times 10^6$	12.4
8	45°	0.00	6.01	0.670	2.63×10 <sup>6</sup>	12.4
9	45°	0.01	8.02	0.502	4.53×10 <sup>6</sup>	12.4
10	45°	0.01	10.00	0.402	$7.95 \times 10^6$	10.4
11	45°	0.03	15.00	0.267	$1.83 \times 10^6$	9.56
12	45°	0.03	19.99	0.201	$3.36 \times 10^6$	8.84

Table 4.1: Laminar natural convection in liquid water contained in an open square enclosure: summary of parameters for the 12 cases investigated experimentally by Elkouh (1996).

As was mentioned in Chapter 2, in the published literature [Whitaker (1999); Nield and Bejan (2006)], the derivations of volume-averaged governing equations for fluid flow and heat transfer in fluid-saturated porous media are done assuming that the properties of the fluid are essentially constant (no terms that arise due to variable density, viscosity, specific heat at constant pressure, and thermal conductivity of the fluid are considered in these derivations). Thus, the models of conduction and laminar natural convection in iceliquid-water-porous-metal-foam systems discussed in Chapter 2 must be used with the assumption that the properties of the water (ice and liquid) calculated at a suitable reference (or average) temperature remain essentially constant for each case considered. This requirement brings up the question of the best reference (or average) temperature for basing the constant fluid properties in each of the cases of interest. This question was answered by simulating each of the 12 cases of this test problem (see related parameters in Table 4.1) using the variable-property model (VPM) and the constant-property model (CPM), with the constant fluid properties in the CPM evaluated at several different

reference (or average) temperatures. Then, the reference (or average) temperature that yields the lowest differences between the results computed using the VPM and CPM was determined. This reference (or average) temperature was used for calculating the constant fluid properties used in the constant-property models (CPMs) of conduction and laminar natural convection in the liquid-water-porous-metal-foam and ice-liquid-water-porous-metal-foam systems investigated in this work.

For the problems considered in this work, the most intuitive choice of the reference (or average) temperature on which to base the values of the constant fluid properties is the arithmetic-average of the cold- and hot-wall temperatures:  $T_{av} = (T_C + T_H)/2$ . Some authors have used the cold-wall temperature as the reference (or average) temperature,  $T_{av} = T_C$ ; and others have used the density inversion temperature of water, at which the density achieves its maximum value, as the reference (or average) temperature,  $T_{av} = T_m = 4.029325$ °C. Elkouh suggested that a zonal temperature be used as the reference (or average) temperature:  $T_{av} = T_{zonal}$ . This zonal temperature is defined as follows, with reference to values of the density inversion parameter,  $T_{\scriptscriptstyle m}^*$ , defined in Section 2.3: if  $0.5 < T_m^* \le 1$ , then  $T_{zonal} = (T_C + T_m)/2$ ; if  $0 \le T_m^* < 0.5$ , then  $T_{zonal}=(T_m+T_H)/2$ ; if  $T_m^*=0.5$ , then  $T_{zonal}=T_m$ ; and if  $T_m^*<0$  or  $T_m^*>1$ , then  $T_{zonal} = (T_C + T_H)/2$ . The logic underlying the choice of the zonal temperature is that if  $0 \le T_m^* \le 1$ , then fluid flow and heat transfer phenomena are dominated by the larger of the two main counter-rotating recirculation cells within the enclosure for any given value of  $T_m^*$ , except at  $T_m^* = 0.5$  for  $\theta = 0^\circ$ , where both these cells exert almost the same influence [Elkouh (1996)]. It should also be noted that in cases involving ice and liquid water within the enclosure, with or without the porous metal foam,  $T_{melting} = 0$ °C is used in place of  $T_C$  in the definition of  $T_{zonal}$ , since the cold-boundary of the liquid-water region inside calculation domain is the ice-liquid-water interface and its temperature is the melting temperature of water (ice).

The values of the average Nusselt number on the hot wall of the square enclosure (note that  $\overline{Nu}_{hotwall} = \overline{Nu}_{cold\,wall} = \overline{Nu}_{wall}$  in this problem, for fully converged solutions) obtained using the VPM and the CPM were compared to assess the suitability of the aforementioned four candidates for the reference (or average) temperature. To ensure consistency in this particular series of comparisons, the value of thermal conductivity used in the definition of this Nusselt number, in all cases, was based on the zonal temperature. Thus,

$$\overline{Nu}_{wall} = (\overline{h}_{wall} H_x) / k_{l_0} = \{ (q'_{lowater at hot wall} / H_y) / (T_H - T_C) \} H_x / k_{l_0}$$
 4.1

$$k_{l_0} = 0.5654 + (1.700 \times 10^{-3}) T_{zonal} - (5.944 \times 10^{-6}) T_{zonal}^2$$
 4.2

Here,  $T_{zonal}$  is in °C, and the thermal conductivity of the liquid water at this temperature,  $k_{l_0}$ , is expressed in W/m.°C.

The results of grid-independence checks for Run # 6, for which the Rayleigh number value was the highest, so the normal gradients of the temperature and velocity fields at the hot and cold walls were also the highest, are presented in Table 4.2. Seven different uniform grids (Grids # 1-7) were used, and the simulations were carried out using the CPM, with the constant fluid properties based on the zonal temperature. The results in Table 4.2 show that the difference in the value of the average Nusselt number on the hot wall (see equations 4.1 and 4.2) yielded by any particular grid and the extrapolated grid-independent value, obtained using Richardson extrapolation [Baliga and Atabaki (2006)] of values yielded by Grids # 6 and 7 (the finest two grids), decreases monotonically as the grid is refined. With a grid of  $105 \times 105$  nodes, this difference was 1.49%, which was considered acceptable for the purposes of this study. It should be noted here that in similar grid checks done for Runs # 1-5 and 7-12, this level of precision was achieved with grids of  $75 \times 75$  nodes. Thus, all final simulations undertaken in this test problem were carried out with uniform grids of  $105 \times 105$  nodes.

			Difference with
Grid#	Number of nodes	$\overline{Nu}_{wall}$ (see	respect to extrapolated
Ond #	Number of nodes	equation 4.1)	grid-independent
		•	value (%)
1	55×55	22.8778	11.40
2	75×75	21.4759	4.57
3	95×95	20.9643	2.08
4	105×105	20.8434	1.49
5	115×115	20.7643	1.11
6	155×155	20.6307	0.46
7	205×205	20.5906	0.26
Extrapolated grid-	independent value (obtained		
using Richardson	extrapolation of results from	20.5371	-
Gr	ids # 6 and 7)		

Table 4.2: Results of grid-independence checks performed for Run # 6.

For Runs # 1 – 6 (specifications given in Table 4.1), Fig. 4.1 shows dye-injection photographs and computed streamline patterns obtained by Elkouh (1996), along with the computed streamline patterns obtained in this work with the variable-property model (VPM) and uniform grids of 105 x 105 nodes (in the last column of this figure). These results show very good agreement for all runs, except Run # 3, which corresponds to  $T_m^* = 0.5$ . At or in the vicinity of this value of the density inversion parameter, Elkouh (1996) has established (experimentally and numerically) that the results, especially streamline patterns, are extremely sensitive to even minute variations in the values of  $T_C$  and  $T_H$ : so the experimental results (with the associated uncertainties) are difficult to duplicate numerically; and the numerical results are very sensitive to the computational grids employed and the criteria used to check convergence of the overall iterative solution.

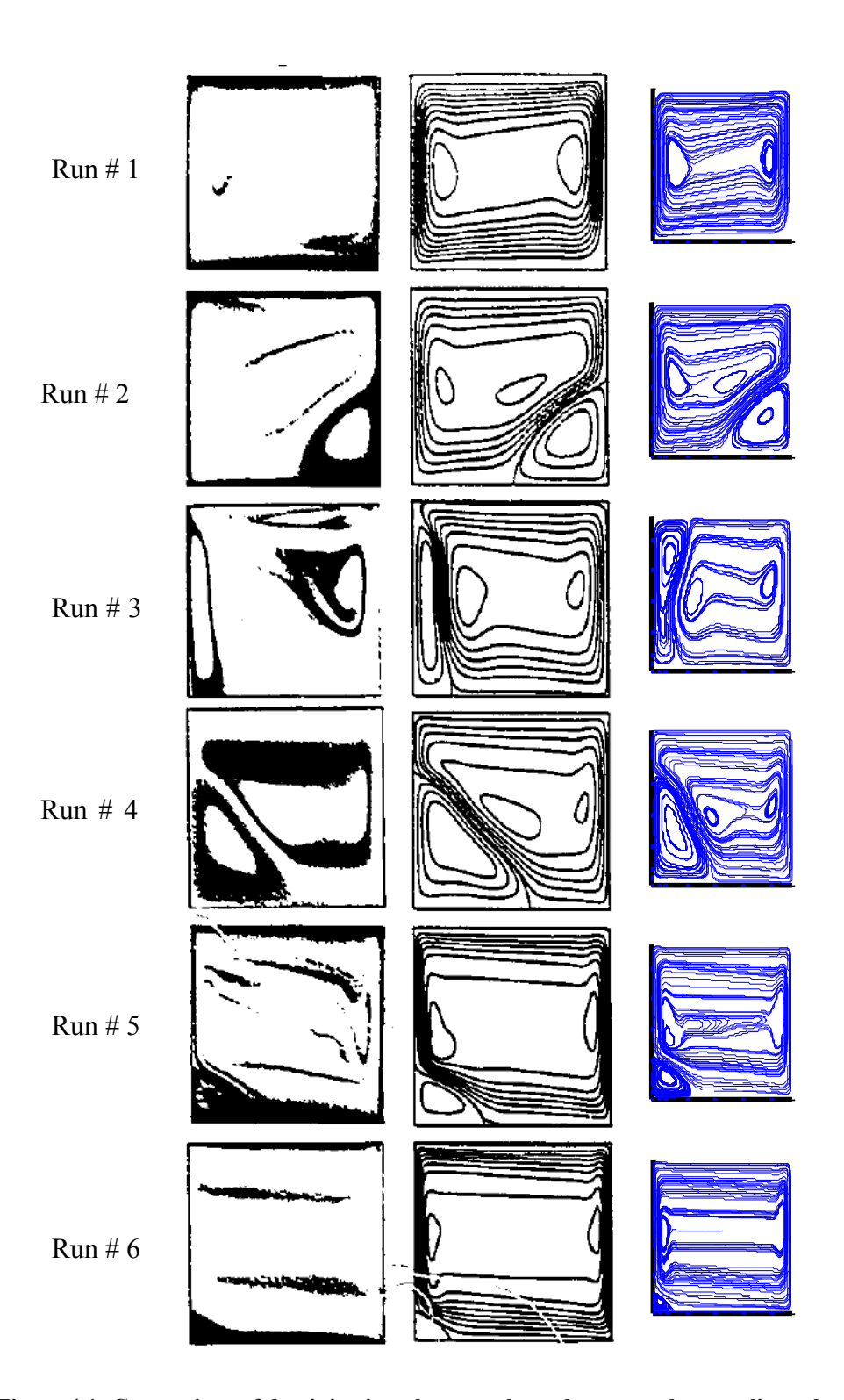


Figure 4.1: Comparison of dye-injection photographs and computed streamlines obtained by Elkouh (1996) to streamlines computed using the variable-property model (VPM), for Runs # 1 – 6.

	$\overline{Nu}_{wall}$					
		Results obtained using CPM, with four different $T_{av}$				
Run #	Results	(Percentage erro				
	obtained using VPM	$T_{av} = \frac{T_H + T_C}{2}$		$T_{av} = T_m$	$T_{av} = T_{zonal}$	
1	9.742	9.766 (+0.24%)	9.543 (-2.04%)	9.989 (+2.54%)	9.767 (+0.26%)	
2	8.651	8.756 (+1.21%)	8.461 (-2.21%)	8.855 (+2.35%)	8.658 (+0.08%)	
3	6.250	6.444 (+3.1%)	6.162 (-1.41%)	6.445 (+3.11%)	6.304 (+0.86%)	
4	10.27	10.05 (-2.13%)	9.506 (-7.46%)	9.947 (-3.17%)	10.27 (-0.04%)	
5	16.30	16.06 (-1.51%)	14.79 (-9.29%)	15.47 (-5.10%)	16.38 (+0.50%)	
6	20.82	20.56 (-1.26%)	18.45 (-11.38%)	19.31 (-7.24%)	20.84 (+0.11%)	
Average absolu	Average absolute error for		5.620/	3.92%	0.31%	
Runs # 1 – 6 (	Runs # 1 – 6 ( $\theta = 0^{\circ}$ )		5.63%			
7	2.977	2.980 (+0.10%)	2.936 (-1.39%)	3.024 (+1.56%)	2.980 (+0.10%)	
8	3.132	2.970 (-5.17%)	2.862 (-8.61%)	3.013 (-3.78%)	2.932 (-6.38%)	
9	6.895	6.688 (-3.00%)	6.426 (-6.80%)	6.689 (-2.99%)	6.559 (-4.88%)	
10	10.54	10.27 (-2.64%)	9.771 (-7.33%)	10.17 (-3.54%)	10.46 (-0.80%)	
11	16.16	15.95 (-1.33%)	14.80 (-8.45%)	15.42 (-4.60%)	16.24 (+0.50%)	
12	20.09	19.87 (-1.08%)	18.00 (-10.37%)	18.77 (-6.58%)	20.22 (+0.68%)	
	Average absolute error for Runs # $7 - 12 (\theta = 45^{\circ})$		7.16%	3.84%	2.22%	
Average absolute error for Runs # 1 – 12		1.90%	6.39%	3.89%	1.27%	

Table 4.3: Hot-wall Nusselt number values computed using the variable-property model (VPM) and constant-property model (CPM), the latter with four different reference (or average) temperatures.

Table 4.3 presents values of the average Nusselt number on the hot wall computed using the VPM and the CPM, the latter with values of the constant fluid properties based on the four above-mentioned reference (or average) temperatures, for Runs # 1 - 12

(specifications given in Table 4.1). The  $\overline{Nu_{wall}}$  values obtained with the VPM were regarded as benchmark results, so the differences between the various CPM results and the corresponding VPM results are referred to as errors. The zonal temperature gives the best results, with an average absolute error over Runs # 1 - 12 of only 1.27%. The comparative advantage of the zonal temperature is particularly evident for cases with  $\theta = 0^{\circ}$  (Runs # 1 – 6), for which all the errors are below 1%. When the cavity is inclined at  $\theta = 45^{\circ}$ , the dominant recirculation flow cell is determined by not just the value of the density inversion parameter,  $T_m^*$ , but also by the inclination of the enclosure with respect to the gravitational acceleration vector: thus, for Runs #7 - 12, the individual CPM errors associated with the zonal temperature are comparable to those associated to the classical arithmetic-average temperature. On the basis of these results, for all computations undertaken in this work with the CPM, the zonal temperature was chosen for calculating the properties of the fluid. It should also be noted that in all CPM simulations of ice-liquid-water-porous-metal-foam systems considered in this work, the thermal conductivity of ice,  $k_i$ , was based on  $T_{av} = T_{melting} = 0$ °C, as the cold-wall temperature in these systems was maintained in the range  $-20^{\rm o}{\rm C} \le T_{\rm C} < 0^{\rm o}{\rm C}$  , and the changes of  $k_i$  in this temperature range are negligibly small compared to its value at  $0^{\circ}$ C ; and the properties of the metal (aluminum) were based on  $T_{av} = (T_C + T_H)/2$ . For this test problem, additional computations, complementary to those discussed in the previous paragraph and with results summarized in Table 4.3, were undertaken with the VPM, but with only one of the liquid-water properties (  $\mu_l$  ,  $c_{pl}$  , or  $k_l$  ) maintained constant, individually, at the zonal temperature. It should be noted that the density of water was always assumed constant in all terms except those related to buoyancy term, in the context of the Boussinesq assumption, as was discussed in Chapter 2. These additional computations showed that the assumption of constant dynamic viscosity (  $\mu_l = \mu_{l_0} =$ constant) caused the biggest errors, relative to those caused by assuming  $c_{pl} = c_{pl_0} =$ constant and  $k_l = k_{l_0} = \text{constant}$ , individually. Since a volume-averaged approach to porous media is used in the thesis, it is assumed that the justification of the use of CPM and the determination of the best averaging method presented in this section can be reasonably extrapolated to simulations of fluid flow and heat transfer in metal foams filled with water.

# 4.2 Conduction and natural convection in ice-liquid-water systems contained in open square enclosures (no foam)

## 4.2.1 Validation of the proposed mathematical model, verification of the FVM, and illustration of the proposed continuation method

Validation of the proposed mathematical model (VPM) and verification of the FVM were done by undertaking simulations of two cases of this problem investigated experimentally and numerically by Elkouh (1996), and labelled Runs A and C by him, and using his results to check the numerical predictions. The dimensions of the square enclosure in these two runs were maintained constant at  $H_x = H_y = H = 6.012$  cm, as was done in the experiments of Elkouh (1999). The other pertinent conditions in the experiments of Elkouh (1996) and the corresponding values of the Rayleigh and Prandtl number in the liquid-water region (with the properties used to compute these parameters based on the above-mentioned zonal temperature) for these two runs are summarized in Table 4.4. The properties of the ice were maintained constant at values corresponding to  $T_{melt} = 0^{\circ}\text{C}$ .

Run	Cavity angle θ	$T_H$ (°C)	$T_C$ (°C)	Density inversion parameter $T_m^*$	Rayleigh number	Prandtl number
A	0°	10.00	-8.71	0.4029	$7.94 \times 10^6$	10.4
С	0°	5.98	-4.69	0.6738	$2.59 \times 10^6$	12.4

Table 4.4: Summary of conditions for two liquid-water-ice problems studied experimentally by Elkouh (1996), and used for validating the mathematical model and FVM proposed in this work.

Based on findings of grid-independence checks akin to those describe in Section 4.1, fixed uniform grids with 101×101 nodes were found to yield satisfactory results, and used to obtain the results reported in this section. It should also be noted that for both of the cases considered (Runs A and C), converged solutions could only be obtained using

the continuation method described in Chapter 3. For Run A, a 17-step continuation method (with the conditions for each step summarized in Table 4.5) was necessary to obtain a converged solution (criteria given earlier in Chapter 3): in the first six of these steps, the value of the cold-wall temperature,  $T_{\rm C}$ , was started at 0°C and then progressively decreased to the desired value of -8.71°C; and in Steps 7 – 17,  $\Delta T_{\rm melt}$  was started at a value of 1°C and then progressively decreased to a value of 0.02°C, which ensured essentially no influence of this parameter on the computed results. A similar continuation method was used to obtain a converged solution for Run C, but only five steps were necessary, as the value of Rayleigh number in Run C is not as high as that in Run A, and the left recirculating flow cell is in contact with the full water-ice interface, which is consequently smoother (as can be seen in the ice-liquid-water interface position and streamline patterns presented in Fig. 4.2). In the continuation method used for Run C, the value of  $\Delta T_{\rm melt}$  was started at 1°C and then progressively decreased to 0.025°C, which ensured essentially no influence of this parameter on the computed results.

Step number	$T_H$ (°C)	$T_C$ (°C)	$\Delta T_{melt}(^{\circ}\mathrm{C})$
1	10.00	0.00	-
2	10.00	-3.00	1.000
3	10.00	-5.00	1.000
4	10.00	-5.00	0.500
5	10.00	-7.00	1.000
6	10.00	-8.71	1.000
7	10.00	-8.71	0.700
8	10.00	-8.71	0.600
9	10.00	-8.71	0.400
10	10.00	-8.71	0.300
11	10.00	-8.71	0.200
12	10.00	-8.71	0.150
13	10.00	-8.71	0.100
14	10.00	-8.71	0.050
15	10.00	-8.71	0.030
16	10.00	-8.71	0.025
17	10.00	-8.71	0.020

Table 4.5: Summary of the conditions used in a 17-step continuation method that was necessary to obtain a fully-converged solution for Run A.

The fully-converged values of  $\overline{Nu}_{hotwall}$  obtained with the VPM for Runs A and C were 5.5190 and 5.2155, respectively.

In Fig. 4.2, the ice-liquid-water interface and streamlines in the liquid-water region for Runs A and C obtained experimentally and numerically by Elkouh (1996) are compared to the corresponding results obtained computationally in this work. The experimental results of Elkouh (1996) were obtained using laser shadowgraphy and dye injection. He computed the streamlines in the liquid-water region using a control-volume finite element method, with the left-boundary shape and conditions of this region specified using the ice-liquid-water interface profile (and  $T_{melting} = 0$ °C) determined in his experimental investigation. The agreement between these results of Elkouh (1996) and those obtained in this work is qualitatively excellent, with no noticeable differences.

The vertical dotted lines associated with the results of this investigation presented in Fig. 4.2 represent the ice-liquid-water interface in the pure-conduction limit (no natural convection in the liquid water region). In this pure-conduction limit, the problem becomes one-dimensional (the temperatures in the ice and the liquid-water regions vary only in the x direction); and at the ice-liquid-water interface, the temperature is  $T_{melting} = 0$ °C and the heat flux normal to the interface on the liquid-water side is equal to that away from the interface on the ice side. A CPM model of this one-dimensional problem was solved analytically. The values of the hot-wall Nusselt number (which is equal to the cold-wall Nusselt number under steady-state conditions) in this one-dimensional pure-conduction problem were determined to be 2.3946 and 2.3096 for boundary conditions corresponding to those in Runs A and C, respectively. Comparing these values of wall Nusselt number to those obtained for the actual Runs A and C (5.5190 and 5.2155, respectively), it can be deduced that natural convection in the liquid-water enhances the overall rates of heat transfer in these runs by about 130% and 126%, respectively.

In these runs, the shape and position of the interface are influenced by both the density inversion parameter and the Rayleigh number. As can be seen from the results presented

in Fig. 4.2, when the density inversion parameter is smaller than 0.5 (Run A), the right counter-clockwise flow recirculation cell dominates, and since it brings relatively hot water to the top of the enclosure, the upper portion of ice-water interface bends to the left; and when this parameter is greater than 0.5 (Run C), the left clockwise flow recirculation cell dominates and the interface is bent to the right. Run A is particularly interesting since the right flow recirculation cell is strong enough and large enough to reach the ice-liquid-water interface, causing its particular shape: the two flow recirculation cells meet at the rightmost point of this interface, and a strong jet of relatively cold water leaves the interface at this point and flows towards the right wall; above this point, the interface is bent to the left, while it is bent to the right below it.

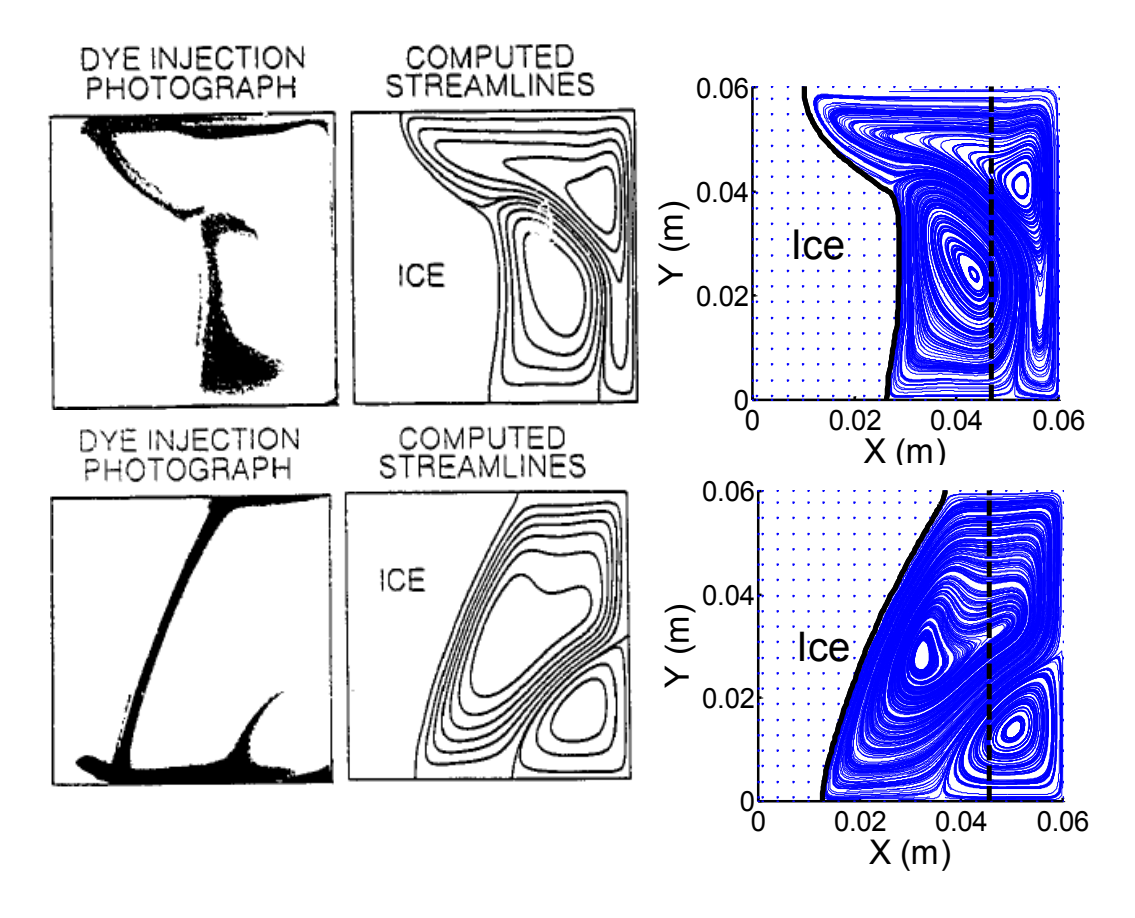


Figure 4.2: Ice-liquid-water interface and streamlines in the liquid-water region for Runs A (above) and C (below): comparison of the experimental and numerical results of Elkouh (1996) with the numerical results obtained in this work (rightmost figures).

Elkouh (1996) also investigated another case of this problem (he called it Run B), with the following conditions:  $T_C = -4.58^{\circ}\text{C}$ ,  $T_H = 8.01^{\circ}\text{C}$ , and  $T_m^* = 0.503$ . In this work, an

attempt was made to apply the proposed mathematical model (VPM) and FVM to this case, but without success. The closeness of the density inversion parameter  $(T_m^*)$  in this case to 0.5 and with  $\theta = 0^\circ$ , a converged solution was essentially impossible to obtain. Attempts were made to apply the continuation method to this case, starting with a solution for an inclined enclosure with  $\theta = 10^\circ$ , and then progressively reducing the value of  $\theta$  to the desired value of  $0^\circ$ . However, satisfactory convergence of the solutions could be achieved only for  $\theta \ge 4^\circ$ .

## 4.2.2 Flow patterns and ice-liquid-water interface shapes for high values of the Rayleigh number

After the completion of the simulations described in the previous subsection, the proposed VPM and FVM were used to investigate the influence of higher values of Rayleigh number on the natural convection flow patterns and ice-liquid-water interface shapes, in problems involving ice-liquid-water systems in open (no foam) square enclosures. In these simulations, the walls temperatures of Run C (see Table 4.4) were used throughout, and the values of Rayleigh number were increased by changing the dimensions of the square enclosure:  $H_x = H_y = H$ , with  $6.012 \text{cm} \le H \le 35 \text{cm}$ , which produce Rayleigh number values in the range  $2.59 \times 10^6 \le Ra \le 5.12 \times 10^8$ . The continuation method was used to progressively advance the values of H from 6.012 cm to 35 cm in eight runs. For each of these runs, 4 - 6 additional steps of the continuation method were used, starting with  $\Delta T_{melt} = 1$  °C and then progressively pushing this value down to  $\Delta T_{melt} = 0.05$  °C, at which its influence on the results was negligibly small. The values of the Rayleigh number explored experimentally by Elkouh (1996) were all less than or equal to  $3.37 \times 10^7$ . The computed streamline patterns and ice-liquid-water interface positions obtained in this work are shown in Fig. 4.3 for four different values of Rayleigh number,  $Ra = 2.59 \times 10^6$ , 6.11 x 10<sup>6</sup>, 2.06 x 10<sup>7</sup>, and 9.55 x 10<sup>7</sup>, obtained with H = 6.012 cm, 0.08 m, 12 cm, and 20 cm, respective. With H = 6.012 cm, this problem is identical to Run C discussed in the previous section.

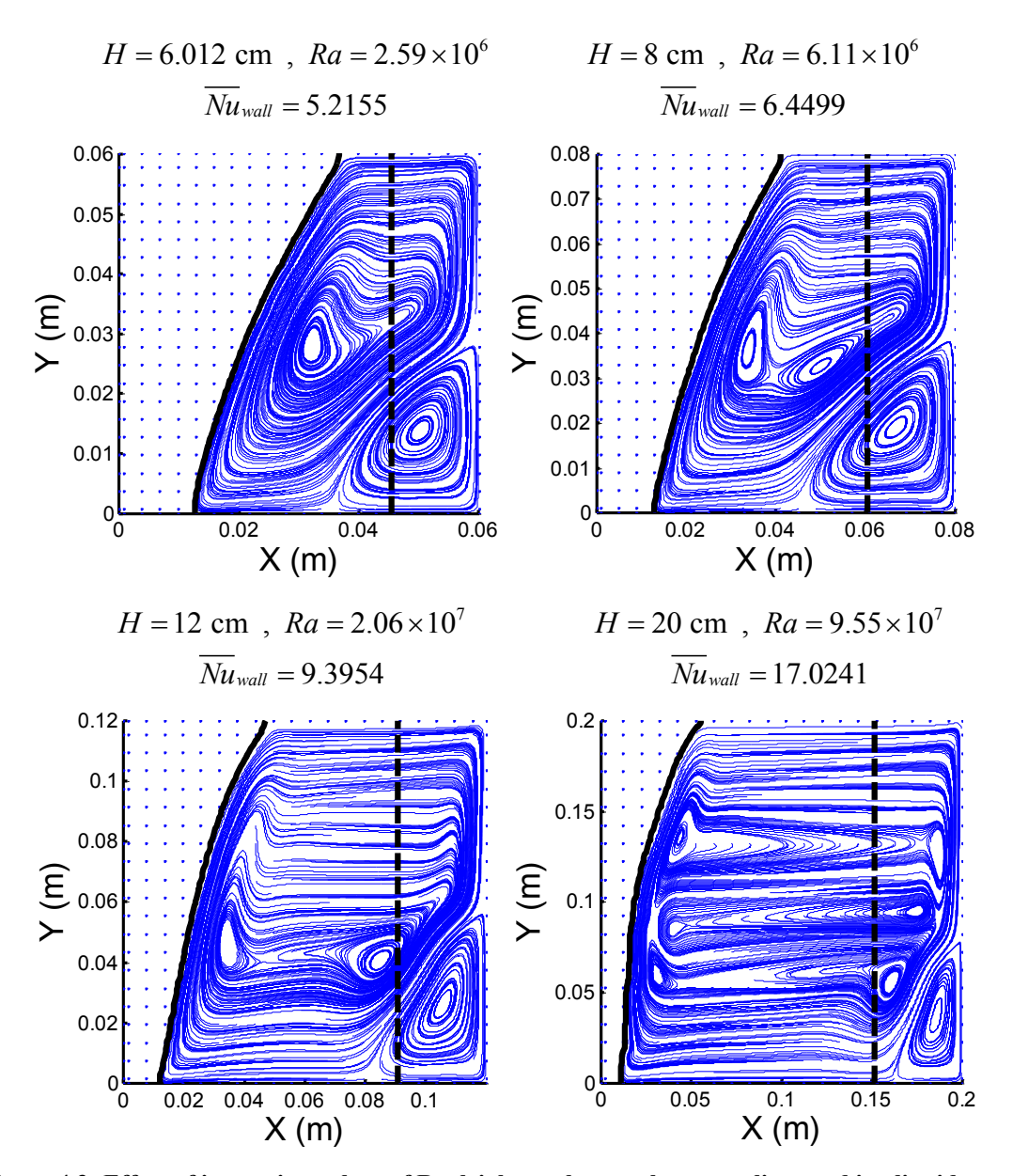


Figure 4.3: Effect of increasing values of Rayleigh number on the streamlines and ice-liquid-water interface position.

The results in Fig. 4.3 show that with increasing values of Rayleigh number, the ice-liquid-water interface shifts to the left, the dominant recirculation flow cell adjacent to this interface becomes larger, and the smaller recirculation flow cell (in the bottom right-hand corner of the enclosure) cell shrinks, mainly from the left side and eventually reaches approximately one-fifth of its original size. Two additional cells within the dominant cell start to appear around  $Ra = 5 \times 10^6$ , and multiple cells form for values of Rayleigh numbers greater than  $5 \times 10^7$ . At  $Ra = 5.12 \times 10^8$ , the ice-liquid-water interface

was nearly vertical and very close to the left (cold) wall, with multiple flow recirculation cells and the first signs of turbulence. Converged solutions for this problem could not be obtained for  $Ra > 5.12 \times 10^8$ .

# 4.3 Natural convection in liquid-water-porous-metal-foam systems contained in square enclosures

The results of simulations that were undertaken to determine the influence of the addition of porous metal foams on the conduction and natural convection in square enclosures filled with liquid water are presented and discussed in this section. The schematic illustration in Fig. 2.1 also applies to this problem, but with no ice and  $\theta = 0^{\circ}$ . In all cases considered in this portion of the present investigation, the temperature of the left (cold) wall of the square enclosure was kept constant at  $0^{\circ}$ C, to ensure relevance and similarity to the left (cold) boundary temperature of the liquid-water region in ice-liquid-water-porous-metal systems contained in similar enclosures. Using grid-independence checks akin to those discussed in Section 4.1, it was determined that for the highest value of the Rayleigh number (details presented in Section 4.3.2), the value of the hot-wall Nusselt number obtained with a uniform grid of 101 x 101 nodes was only about 0.576% different from an essentially grid-independent value obtained with Richardson extrapolation of results yielded by uniform grids of 151 x 151 and 201 x 201 nodes. Thus, all final simulations discussed in this section were done with uniform grids of 101 x 101 nodes.

### 4.3.1 Comparison of natural convection with and without porous metal foam

These simulations were done for the conditions for the first six runs (Runs # 1 – 6) listed in Table 4.1, with an open domain (cases already presented earlier in Section 4.1) and with a porous aluminum foam of PPI = 10 and  $\varepsilon$  = 0.95. This particular foam is referred to as the 'reference' foam in the rest of this section and also in the next section. As was mentioned above, all simulations were done with uniform grids of 101 x 101 nods. In the pure-conduction limit (no natural convection), the intrinsic-phase-average temperature fields of the foam and the liquid are both one-dimensional, varying only in the x

direction. For this pure-conduction limit, the governing equations were solved analytically and the following expressions were derived for the Nusselt numbers at the left (cold) and right walls:

$$Nu_{\text{foam left}} = Nu_{\text{foam right}} = \frac{k_{ss} + k_{ls}}{k_{l_0}} ; Nu_{\text{fluid left}} = Nu_{\text{fluid right}} = \frac{k_{ll} + k_{ls}}{k_{l_0}}$$

$$\overline{Nu}_{wall} = \frac{k_{eff_l}}{k_{l_0}}$$

$$4.3$$

These pure-conduction-limit Nusselt numbers on the left and right walls depend only on the thermal conductivity of the metal (aluminum; based on  $T_{av} = (T_C + T_H)/2$ ), foam porosity, and liquid-water thermal conductivity based on the zonal temperature (discussed in Section 4.1). With the reference foam, the computed value of the pure-conduction-limit wall Nusselt number was 8.6.

The Prandtl and Rayleigh numbers for the runs considered in this study were calculated using liquid-water properties based on the zonal temperature. Values of the wall Nusselt number computed for Runs # 1 – 6 (conditions given in Table 4.1) without and with the reference foam are presented in Table 4.6, along with the foam contributions to these values on both the left (cold) and right (hot) walls (related definitions were presented in Chapter 2). These results show that inclusion of the foam increases the values of the wall Nusselt number in Runs # 2, 3, and 6, compared to the values obtained for these runs without the reference foam; and lowers the values of the wall Nusselt number for Runs # 1, 4, and 5.

The results obtained for Runs # 1-6 also showed that the natural convection flow pattern for each case with the reference foam was similar to that obtained at a lower value of Rayleigh number for the same case without the foam. To illustrate this observation, sample streamline patterns for Run # 4 without and with the reference foam are shown in Fig. 4.4.

	$Nu_{wall}$ Open-Domain FVM Simulations (with CPM, $T_{av} = T_{zonal}$ )	With Reference Foam				
Run#		Pure-Conduction Limit (analytical results)		Results of FVM Simulations		
		Nu <sub>wall</sub>	Foam contributi on (%)	Nuwall (difference with respect to pureconduction limit)	Foam contribution on the left wall $\frac{Nu_{\text{foam left}}}{Nu_{\text{wall}}}$ (%)	Foam contribution on the right wall $\frac{Nu_{\text{foam right}}}{\overline{Nu}_{wall}}$ (%)
1	9.767	8.5871	87.80	<b>9.113</b> (+2.9%)	87.74	87.78
2	8.658	8.5871	87.80	<b>9.024</b> (+1.9%)	87.73	87.79
3	6.304	8.5871	87.80	<b>8.930</b> (+0.8%)	87.74	87.74
4	10.27	8.7480	87.65	<b>9.389</b> (+7.3%)	87.60	87.40
5	16.38	8.6963	87.57	15.69 (+80.4%)	87.47	86.31
6	20.84	8.6458	87.50	<b>25.56</b> (+195.6%)	86.18	84.35

Table 4.6: Values of wall Nusselt number for Runs # 1-6, without and with the reference foam (porous aluminum foam with 10 PPI and  $\mathcal{E}=0.95$ )

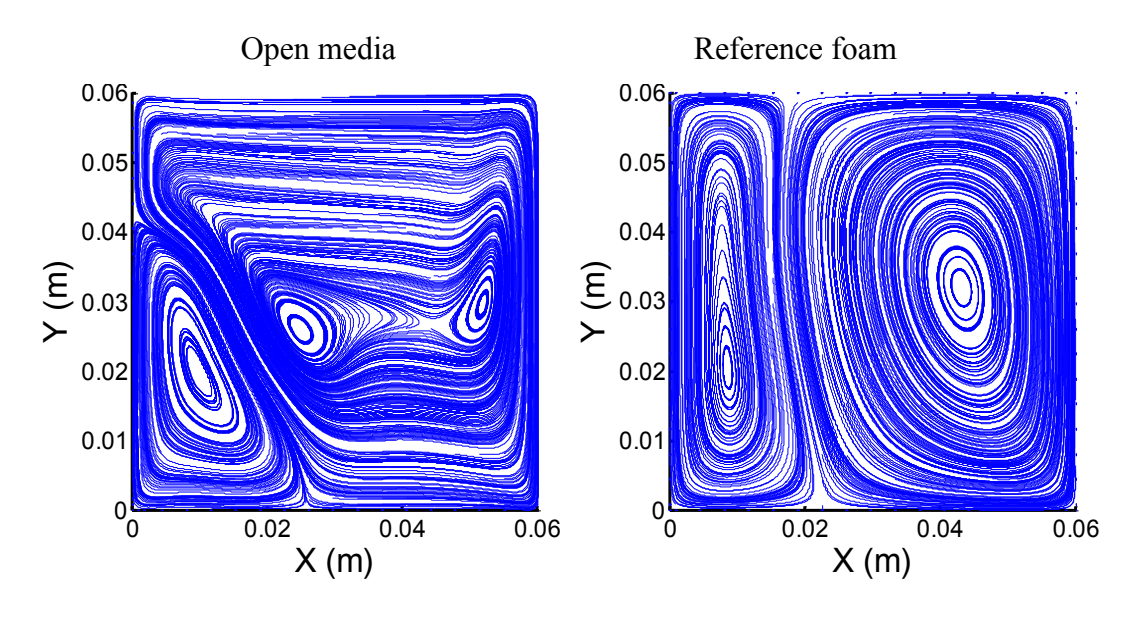


Figure 4.4: Streamline patterns for Run # 4, without and with the reference foam.

The results in Table 4.6 show that for Runs # 1-3, the values of the wall Nusselt number are very close to those for the pure-conduction limit, with all differences less than 3%, and the foam carries about 88% of the rates of heat transfer at both the left (cold) and right (hot) walls in these runs. For Runs # 4-6, the influence of natural convection is significant (values of wall Nusselt number considerably greater than the corresponding values for the pure-conduction limit), but the foam still roughly carries 88% of the rates of heat transfer at both the left (cold) and right (hot) walls, as the no-slip condition applies at the walls with the Darcy-Brinkman-Forchheimer momentum equation, and the superficial velocity of the fluid in the immediate vicinity of the walls is quite low.

### 4.3.2 Influence of Rayleigh number and five different foams

Results of simulations that were used to assess the influence of the Rayleigh number and five different porous aluminum foams are presented in this section. The temperature of the left (cold) and right (hot) walls were kept constant at 0°C and 20°C, respectively, conditions that correspond to Run # 6, investigated here without and with the five foams. These wall temperatures yield a value of the density inversion parameter of 0.202; this value is sufficiently far from 0.5, so this parameter did not cause any special convergence issues in the simulations (see related discussions in Section 4.1). A summary of the characteristics of the five foams considered in this study are provided in Table 4.7.

Foam Number	Porosity	Foam PPI
Foam 1 (the reference foam)	0.95	10
Foam 2	0.90	10
Foam 3	0.98	10
Foam 4	0.95	20
Foam 5	0.95	40

Table 4.7: Characteristics of the five porous aluminum foams considered in this work.

The continuation method was used to progressively change the enclosure dimensions from  $0.005 \text{ m} \times 0.005 \text{ m}$  to  $0.30 \text{ m} \times 0.30 \text{ m}$ , which produced Rayleigh number values in the range  $1.93 \times 10^4$  to  $4.18 \times 10^9$ . The corresponding values of Darcy number for the reference foam (see Table 4.7) ranged from  $1.3 \times 10^{-3}$  to  $7.9 \times 10^{-2}$ . The enclosure with

the smallest dimensions (0.005 m x 0.005 m) corresponds to approximately twice the pore diameter for the porous aluminum foams with 10 PPI: thus, the requirements of the volume-averaging procedure are not strictly met for this enclosure; so the results for the corresponding low values of the Rayleigh number should be accepted cautiously (with this limitation in mind). To ensure consistency in the comparison exercises, the CPM with fluid properties based on the zonal temperature was adopted for simulations, with and without the foams.

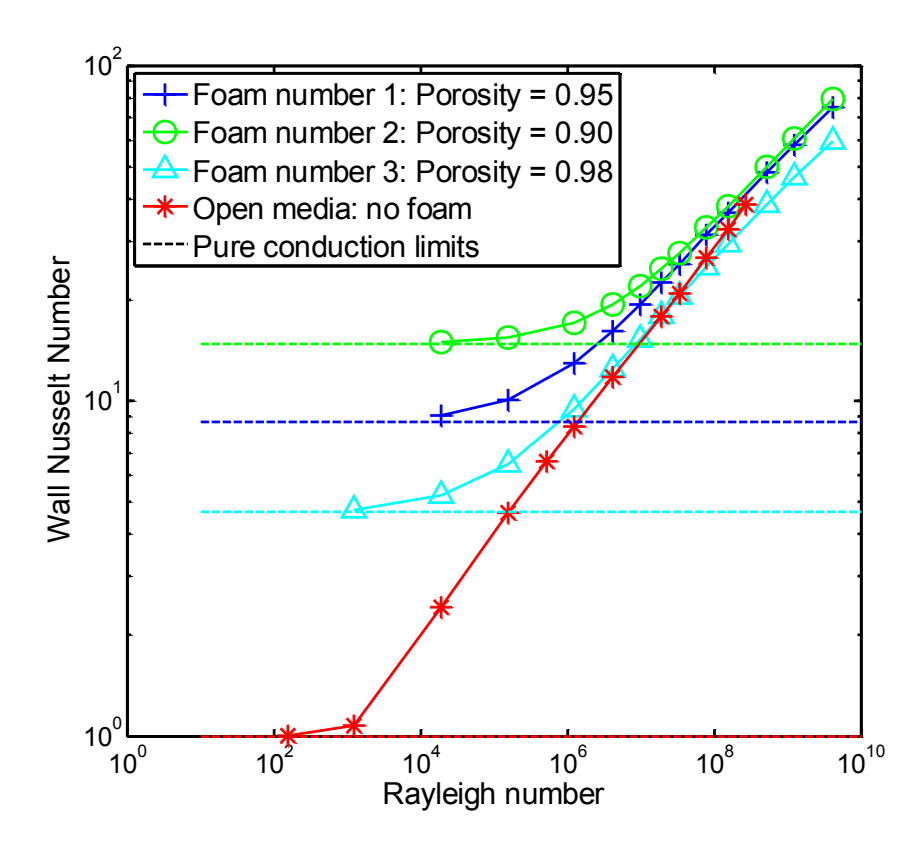


Figure 4.5: Influence of the Rayleigh number on wall Nusselt number for Foams # 1 - 3 and open domain (no foam); wall temperatures correspond to those for Run # 6 in all cases.

The influence of the Rayleigh number on the wall Nusselt number with Foams # 1, 2, and 3 (same PPI or pore diameter, but different porosities) and also with no foam (open domain) is illustrated by the results presented in Fig. 4.5 (here, and also in all other similar figures in this chapter, curves drawn through the symbols represent trend lines). In all cases, for low values of the Rayleigh number, the values of the wall Nusselt number are essentially equal to those of the pure-conduction limit (analytical solution given in equation 4.3 for the cases with foam; equal to one (10<sup>0</sup>) for the case with no foam or

open-domain). For high enough values of the Rayleigh number, for all cases (with and without foam), the log-log plots of wall Nusselt number versus Rayleigh number in Fig. 4.5 are essentially straight lines, indicating the suitability of the following power-law fit:

$$\overline{Nu_{wall}} = C \times Ra^n$$
 4.4

The best fit values of the exponent n in this equation was determined to be n = 0.22, n = 0.22, and n = 0.23 for Foams # 1, 2, and 3, respectively. The start of the power-law regime  $Ra_{power \, law}$  is defined in each case as the Rayleigh number of the first experiment presenting less than a 5% difference to the power-law regime (first defined on the five highest Rayleigh number experiments).

Porosity of the foam influences the value of the Rayleigh number at which natural convection becomes significant: lower the value of porosity, higher the value of the Rayleigh number necessary for the onset of significant natural convection. However, in the pure-conduction limit, Foam # 2 (the least porous) leads to 1.71 and 3.16 times higher rates of overall heat transfer than Foams # 1 and 3, respectively. When the power-law regime is reached for the three foams (for  $Ra > 10^8$ ), these ratios of the enhancement of the rates of heat transfer are only about 1.3 and 1.7, respectively, and remain approximately constant. Of the three foams considered in the study, Foam # 2 always yields the highest overall rate of heat transfer.

For Run # 6 with open domain (no foam), the influence of natural convection is significant (values of wall Nusselt number at least 5% higher than the value for the pure-conduction limit,  $\overline{Nu_{wall}} = 1$ ) for values of Rayleigh number as low as  $10^3$ . A power-law regime was also observed for this case (no foam), with an exponent of n = 0.29, which is higher than the exponent value of n = 0.22 obtained for the cases with foams. At the highest Rayleigh number for which converged solutions could be obtained, the no-foam value of wall Nusselt number falls in between those for Foams # 1 and 3.

The influence of the pore diameter was evaluated by comparing the results for foams of the same porosity but different pore diameters: Foams # 1, 4, and 5. The temperatures of

the left (cold) and right (hot) walls were fixed at  $T_C = 0^{\circ}$ C and  $T_H = 20^{\circ}$ C (conditions corresponding to Run # 6). Again, the enclosure dimensions were adjusted to obtain values of Rayleigh number in the range  $1.93 \times 10^4$  to  $4.18 \times 10^9$ . The variations of wall Nusselt number with the Rayleigh number for these cases are presented in Fig. 4.6. Since the effective thermal conductivity does not depend on the pore diameter (see definitions given in Chapter 2), the Foams # 1, 4, and 5 yield the same values of wall Nusselt number in the pure-conduction limit. With a foam of smaller pore diameter, the drag force is greater and the natural convection becomes significant at a higher value of the Rayleigh number. A power-law regime is exhibited by the plots for all three foams in Fig. 4.6, with the value of the exponent essentially independent of the PPI value. The values of wall Nusselt number for Foams # 4 and 5 (20 PPI and 40 PPI) are 1.2 and 1.9 times lower, respectively, than the values for Foam # 1 (10 PPI) in the power-law regime.

A quantitative presentation of some of the key results for the five foams (Foams # 1-5) and also the open domain (no foam), for wall temperatures corresponding to Run # 6, are presented in Table 4.8.

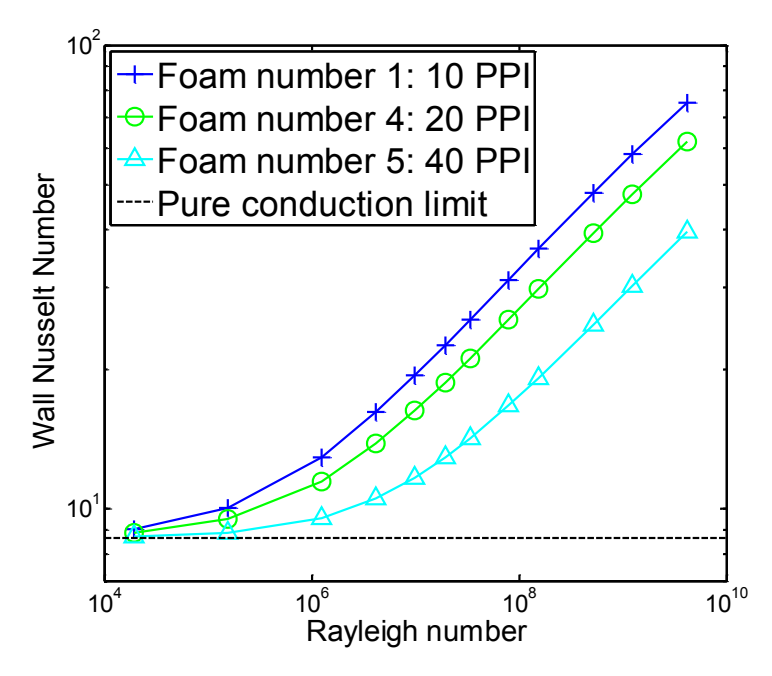


Figure 4.6: Influence of the Rayleigh number on the wall Nusselt number for Foams 1, 4, and 5, which have the same porosity but different pore diameters: wall temperatures correspond to those for Run # 6 in all cases.

Wall temperatures	Foam number and characteristics	Nu <sub>wall</sub> Pure- conduction limit	Start of the power-law regime $Ra_{power  law}$	Exponent in the power-law regime n
	1: $\varepsilon = 0.95$ , 10 PPI	8.65	$2\times10^6$	0.22
	2: $\varepsilon = 0.90, 10 \text{ PPI}$	14.75	$2\times10^7$	0.22
$T_{C} = 0.00^{\circ} \text{C}$ $T_{H} = 20.00^{\circ} \text{C}$	3: $\varepsilon = 0.98$ , 10 PPI	4.67	$2\times10^5$	0.23
	4: $\varepsilon = 0.95$ , 20 PPI	8.65	5×10 <sup>6</sup>	0.22
	5: $\varepsilon = 0.95, 40 \text{ PPI}$		4×10 <sup>7</sup>	0.21
	Open domain	1	$10^{3}$	0.29

Table 4.8: Summary of some key results for natural convection with liquid water and Foams # 1 - 5, and also in open domains (no foam); and wall temperatures corresponding to Run # 6.

As was pointed out in Chapter 2, the correlation for the interstitial interfacial heat transfer coefficient used in the two-temperature model of heat transfer in ice-porous-metal-foam and liquid-water-porous-metal-foam regions in the pure-conduction limit was obtained using numerical solutions of heat conduction in relatively simple two-dimensional unit-cell models of the porous metal foam. To assess the sensitivity of the results to this correlation, simulations with the reference foam (Foam # 1 in Table 4.7) and wall temperatures corresponding to Run # 6 were redone with the correlation for the interstitial interfacial conduction Nusselt number calculated using the following expressions:  $Nu_{\text{conduction}} = 2(-4.1/\ln(1-\varepsilon))$ ;  $Nu_{\text{conduction}} = 0.5(-4.1/\ln(1-\varepsilon))$ . The maximum differences between the results obtained with the proposed correlation and those with twice and one-half this correlation were 0.6% and 2.4%, respectively.

### 4.3.3 Influence of thermal dispersion and Forchheimer drag term

An examination of the Darcy-Brinkman-Forchheimer momentum equation and the fluid energy equation in the two-temperature model (discussed in Chapter 2) reveals that the relative importance of the thermal dispersion and Forchheimer drag terms is proportional locally to the permeability Reynolds number defined by  $\operatorname{Re}_K = \rho_{l_0} \sqrt{K} \|\mathbf{u}\| / \mu_0$ :

$$\frac{\left|\varepsilon k_{d}\right|}{\left|k_{eff}\right|} = \left(C_{D} \frac{k_{0}}{k_{eff}} \operatorname{Pr}_{0}\right) \operatorname{Re}_{K} \quad \text{and} \quad \frac{\operatorname{Forchheimer drag term}}{\operatorname{Darcy drag term}} = f \operatorname{Re}_{K} \quad 4.5$$

The variations of the maximum and spatial-average values of  $Re_K$  as a function of Ra, with the wall temperatures of Run 6, the reference foam, and  $1.93 \times 10^4 < Ra < 4.18 \times 10^9$  are presented in Fig. 4.7. As the Rayleigh number increases, natural convection is stronger and the maximum value of  $Re_K$  keeps increasing until it reaches its highest value,  $Re_K = 0.47$ , at the maximum Rayleigh number,  $Ra = 4.18 \times 10^9$ . This maximum value of  $Re_K$  always occurs in the dominant recirculation flow cell, in the boundary-layer-like flows in the vicinity of the walls. On the other hand, the spatial-average  $Re_K$  peaks at around 0.091 at  $Ra = 10^6$ , which corresponds to the following spatial-average values of the ratios of equation 4.5:  $\frac{|\mathcal{E}k_d|}{|k_{eff}|} = 0.56\%$  and  $\frac{\text{Forchheimer drag term}}{\text{Darcy drag term}} = 0.90\%$ ,

and then decreases. This seems to indicate that as the Rayleigh number increases, the area of the high-velocity boundary-layer region does not increase as fast as (proportionally to) the size of the cavity. To illustrate this phenomenon, the dimensionless area of a "high-velocity-zone" is also plotted in Fig. 4.7:

$$A_{\text{high-velocity}} = \frac{\text{Area of the high-velocity zone}}{H_x \times H_y}$$
 4.6

For each value of the Rayleigh number, the high-velocity zone is defined as the region in which the magnitude of the velocity is at least 30% of the magnitude of the maximum

velocity in the calculation domain. As is shown by the corresponding results plotted in Fig. 4.7,  $A_{\text{high-velocity}}$  decreases monotonically with increasing Rayleigh number, from 73% to 4.9%.

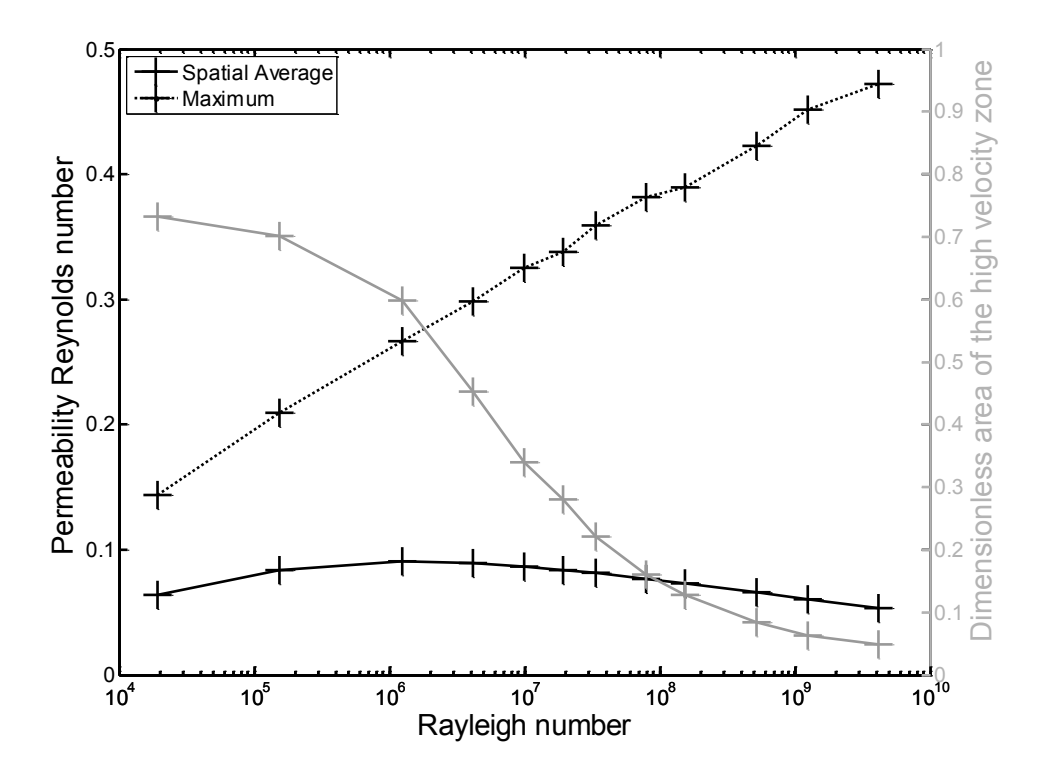


Figure 4.7: Variations of the maximum and spatial-average values of the permeability Reynolds with Rayleigh number, for the wall temperatures of Run # 6 and the reference foam. The evolution of the dimensionless area of the high-velocity zone is also presented.

Based on the results presented in Fig. 4.7, it can be concluded that the maximum relative effects of the thermal dispersion and the Forchheimer drag term increase as the Rayleigh number increases (as their influence gets stronger at points inside the high-velocity boundary-layer region), but their average effects may increase or decrease marginally.

### 4.4 Conduction and natural convection in ice-liquid-water-porous-metalfoam systems contained in rectangular enclosures

### 4.4.1 Comparison of results obtained with and without porous metal foam

Results obtained from simulations of conduction and natural convection in ice-liquid-water and ice-liquid-water-porous-metal foam systems in two square enclosures with dimensions, cold- and hot-wall temperatures, and parameters akin to Runs A and C (see Table 4.4) are presented in this section. The reference porous metal foam, Foam # 1 (aluminum; 10 PPI; and  $\varepsilon = 0.95$ ), was used in this study. In the pure-conduction limit (no natural convection), this problem becomes one-dimensional, and it is possible to solve the governing equations of the two-temperature model analytically and determine the following solutions to the ice-liquid-water interface position ( $x_{int}$ ), wall Nusselt number, and flux repartition between water and foam at each wall:

$$x_{\text{int}} = \frac{H_x}{1 + \frac{T_H - T_{melt}}{T_{melt} - T_C}} , \qquad \overline{Nu}_{wall} = \frac{k_{eff_i}}{k_{l_0}} \left( 1 + \frac{T_H - T_{melt}}{T_H - T_C} \left( \frac{k_{eff_i}}{k_{eff_i}} - 1 \right) \right)$$
 4.7

$$\frac{Nu_{\text{foam left}}}{Nu_{wall}} = \frac{k_{ss} + k_{is}}{k_{eff_i}} , \qquad \frac{Nu_{\text{foam right}}}{Nu_{wall}} = \frac{k_{ss} + k_{ls}}{k_{eff_i}}$$

$$4.8$$

Since ice is more thermally conductive than liquid water, the foam contribution is always smaller at the left (cold) wall than at the right (hot) wall in the pure-conduction limit:  $Nu_{\text{foam left}} < Nu_{\text{foam right}}$ . A uniform grid with 101 x 101 nodes was used in this study. The continuation method was also necessary to achieve converged solutions. In particular, for each case, the value of  $\Delta T_{melt}$  was progressively decreased from about 1°C to the following levels, where its effect on the results was negligible (error in  $\overline{Nu}_{wall}$  less than 0.1%): for condition corresponding to Run A,  $\Delta T_{melt} = 0.01$ °C; and for conditions corresponding to Run C,  $\Delta T_{melt} = 0.002$ °C. The computed values of total Nusselt number and the heat flux repartitions for these cases on the two walls are reported in Table 4.9. The streamlines and water-ice interface positions are compared to the open-domain (no

foam) results in Fig. 4.8. Both the ice-liquid-water interface positions and the heat transfer results for the two cases with the foam show that effect of natural convection is mostly negligible: the heat transfer rates are within 1% of those in the pure-conduction limit; and the ice-liquid-water interfaces are almost superimposed on the corresponding vertical dotted lines that represent the pure-conduction-limit solutions.

	A	C		
	5.5190	5.2155		
With Reference Foam	Pure- conduction limit (analytical)	$\overline{Nu}_{wall}$	10.3359	10.3857
		Foam contribution, left wall (%)	66.1	66.1
		Foam contribution, right wall (%)	87.6	87.8
	Results obtained with FVM	$\overline{Nu}_{wall}$ (difference with respect to the pureconduction limit)	10.4006 (+0.63%)	10.4150 (+0.28%)
		Foam contribution, left wall (%)	66.1	66.1
		Foam contribution, right wall (%)	87.4	87.8

Table 4.9: Values of  $Nu_{wall}$  with and without the reference foam (aluminum, 10 PPI, 95% porosity) with the parameters corresponding to Runs A and C.

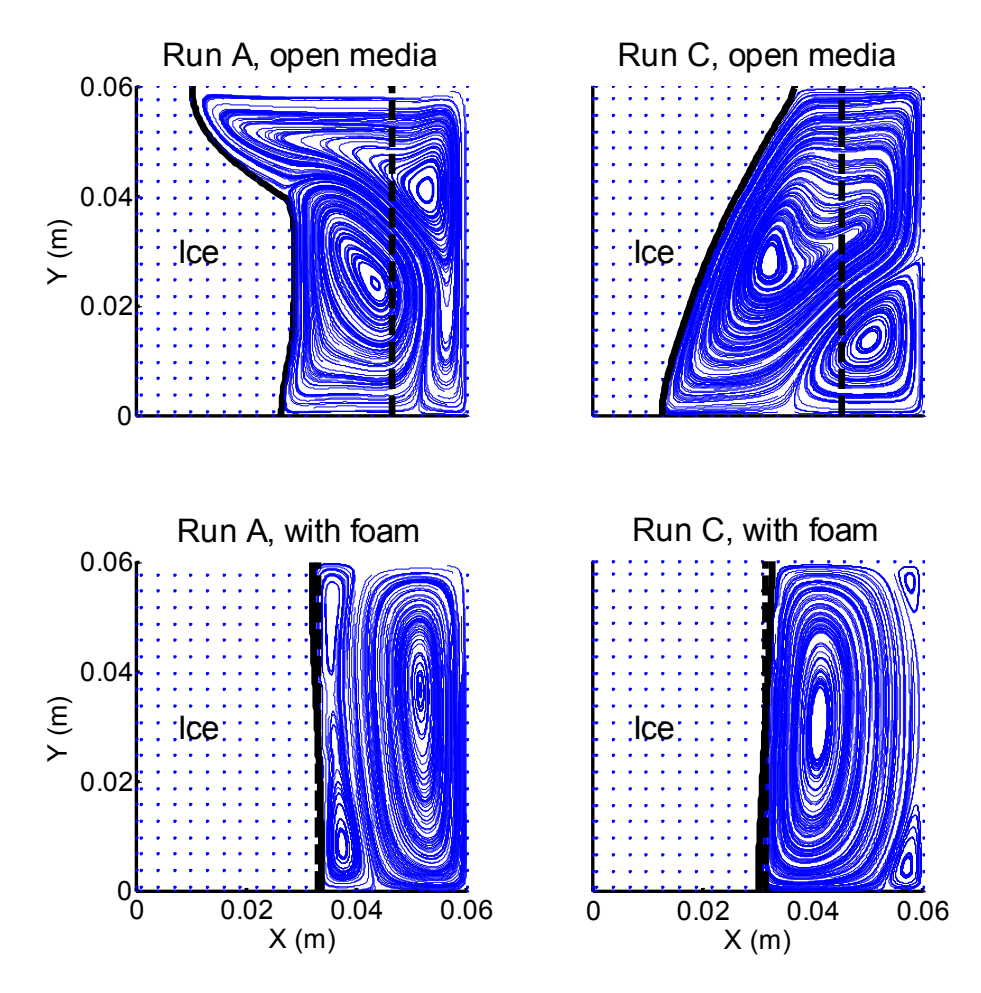


Figure 4.8: Comparison of streamlines and water-ice interface positions with and without the reference foam (aluminum, 10 PPI, 95% porosity) with the parameters corresponding to Runs A and C.

### 4.4.2 Demonstration problem

In this demonstration problem, ice-liquid-water-porous-metal-foam systems contained in rectangular enclosures were considered, with the following parameters typical of those encountered in cold-storage applications:  $\theta=0^{\circ}$ ,  $H_x=10$  cm, and 10 cm  $\leq H_y \leq 50$  cm (the aspect ratio,  $AR=H_y/H_x$ , ranged from 1 to 5). The imposed cold- and hot-wall temperatures were also similar to those typically encountered in cold-storage applications during freezing and melting operations:  $T_C=-20^{\circ}\mathrm{C}$  and  $T_H=20^{\circ}\mathrm{C}$ . The reference foam (aluminum, 10 PPI, 95% porosity) was used. The results for this demonstration problem were obtained with and without this foam, and then compared. The open-domain

(no foam) simulations were limited to values of aspect ratio that were lower than the maximum value used in case with the foam, due to convergence problems.

All the simulations were performed using uniform grids:  $101 \times 101$  grid points were used for square domains (AR = 1), while uniform grids with  $101 \times \{(100 \times AR) + 1\}$  points were used to discretized rectangular domains, with an upper limit of 301 grid points in the y direction (invoked to keep computational costs and times manageable on readily available personal computers (PCs) fitted with quad-core CPU).

The continuation method was also used in this problem to facilitate the solutions on finer grids: a simple code was written for bi-linear interpolation of the dependent-variable fields obtained from simulations with a given grid, to any finer grid, so that they could be used as starting guess values in the finer-grid simulation. The independence of the results from the values of  $\Delta T_{melt}$  (within 0.1%) was reached in all cases considered for  $\Delta T_{melt} < 0.05$ °C.

The Rayleigh number was again based on the horizontal dimension,  $H_x$ , and was, therefore, the same in all the simulations:  $Ra = 1.55 \times 10^8$ . This choice was justified by the observation that in natural convection experiments in rectangular enclosures akin to those used in this demonstration problem, the dependence of the heat transfer rate on the vertical dimension,  $H_y$ , is, in general, much weaker than its dependence on the horizontal dimension,  $H_x$  [Incropera and DeWitt (2002)]. However, increases in the vertical dimension can lead to turbulence, since the liquid water flows along vertical surfaces (right wall or the ice-liquid-water interface) have more space to develop. Thus, converged solutions in the open-media simulations could not be achieved for  $H_y > 15 \text{cm}$ .

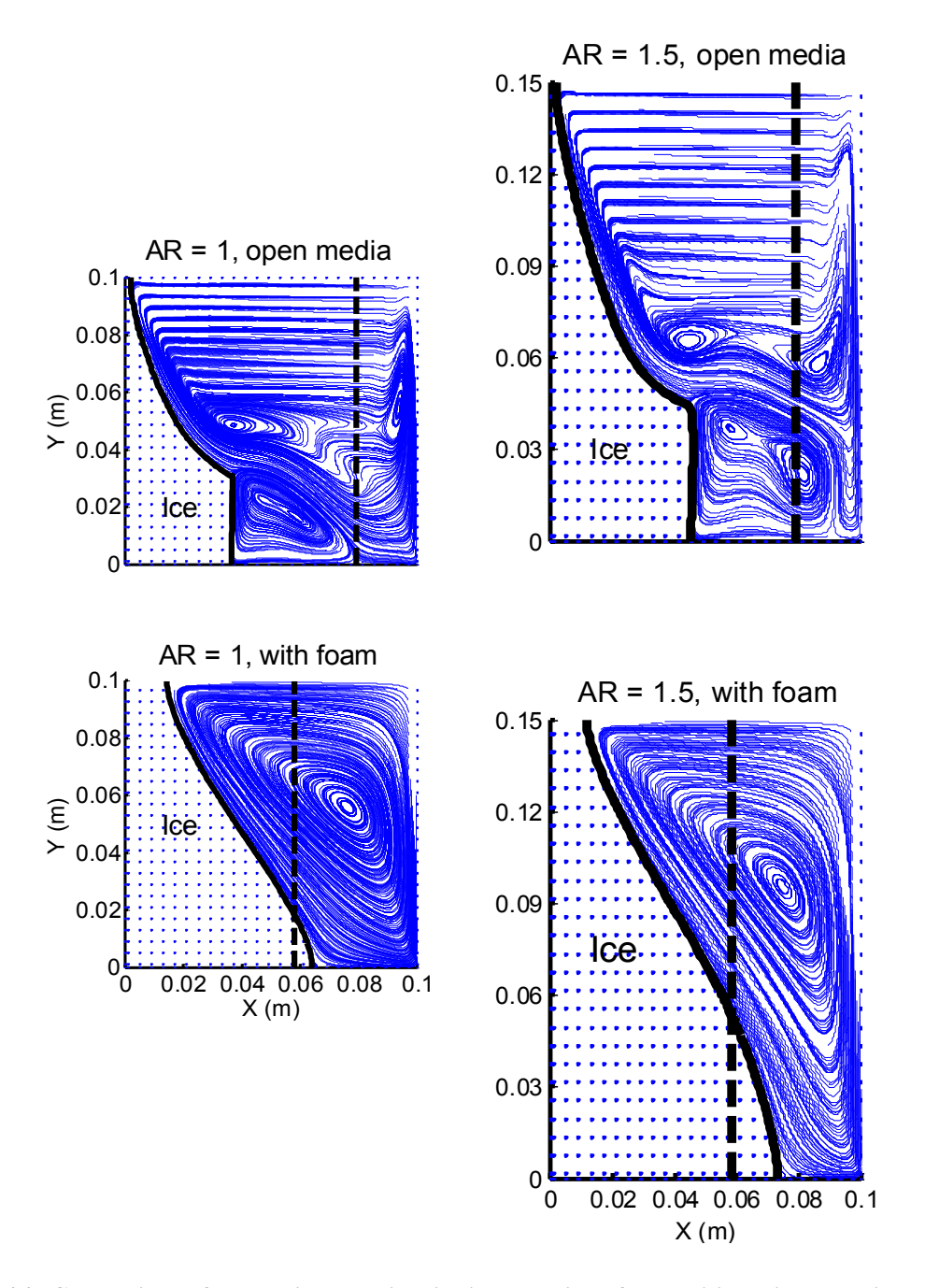


Figure 4.9: Comparison of streamlines and ice-liquid-water interface position with and without foam for AR=1 and AR=1.5 in the demonstration problem.

Comparisons of the computed streamlines and ice-liquid-water interface position with and without the foam for AR=1 and AR=1.5 in the demonstration problem are presented in Fig. 4.9. The sharp changes in the shape of the ice-liquid-water interface in the openmedia cases do not appear in the cases with the foam. Ice always occupies a bigger

portion of the calculation domain in cases with the foam, even though the position of the ice-liquid-water interface in the pure-conduction-limit is closer to the left wall with the foam (because  $k_{eff_i}/k_{eff_i} > k_{l_0}/k_{i_0}$ ). The two open-media flow fields exhibit multiple flow recirculation cells, with more such cells in the case with AR=1.5 than that in the case with AR=1.5

The wall Nusselt number is plotted as a function of the aspect ratio, with and without the foam, in Fig. 4.10. It decreases as the aspect ratio gets higher, because of boundary layer thickening along the upper portions of the right wall, and the following power-law function provides a good fit to the results for the cases with the foam:

$$\overline{Nu}_{wall} = \overline{Nu}_{wall \ square} \left(\frac{H_y}{H_x}\right)^n$$
. Despite the small number of points for the open-media cases,

a power-law function was also fitted to their results. A quantitative representation of these results is given in Table 4.10. In both cases (with and without the foam) the exponent is roughly -1/4, a value that is also found in the classical experimental correlations for open-media laminar natural convection in rectangular enclosures [Incropera and DeWitt (2002)].

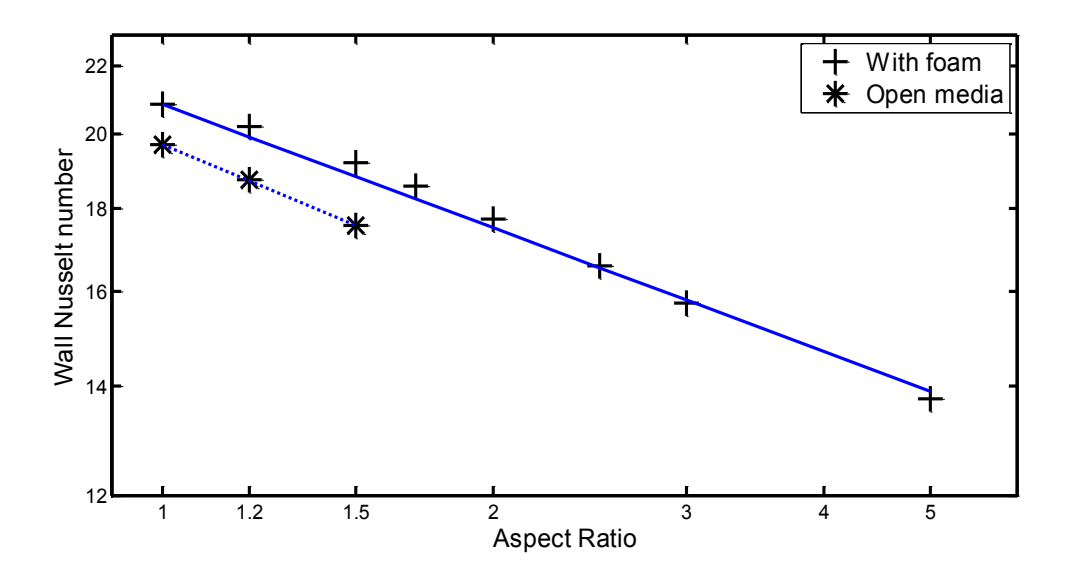


Figure 4.10: Variation of wall Nusselt number with aspect ratio and power-law fit with and without the foam for the demonstration problem

	AR range	Nu <sub>wall</sub> Square enclosure	n, exponent of the power-law	Average rms error (%)
Reference foam	1 - 5	20.84	-0.252	1.26%
Open media	1 – 1.5	19.68	~ -0.3	(not enough points)

Table 4.10: Power-law correlations for variation of wall Nusselt number with aspect ratio, with and without the foam, for the demonstration,

Streamlines and ice-liquid-water interface position for the biggest aspect ratio (AR=5, with foam) are presented in Fig. 4.11. In the central part of the vertical enclosure, the ice-liquid-water interface almost corresponds to that in the pure-conduction limit. In the upper portion of this vertical enclosure, the ice-liquid-water interface bends to the left, due to the impingement of the relative hot water coming off the right wall in this region; and the opposite phenomena take place in the lower reaches of the vertical enclosure.

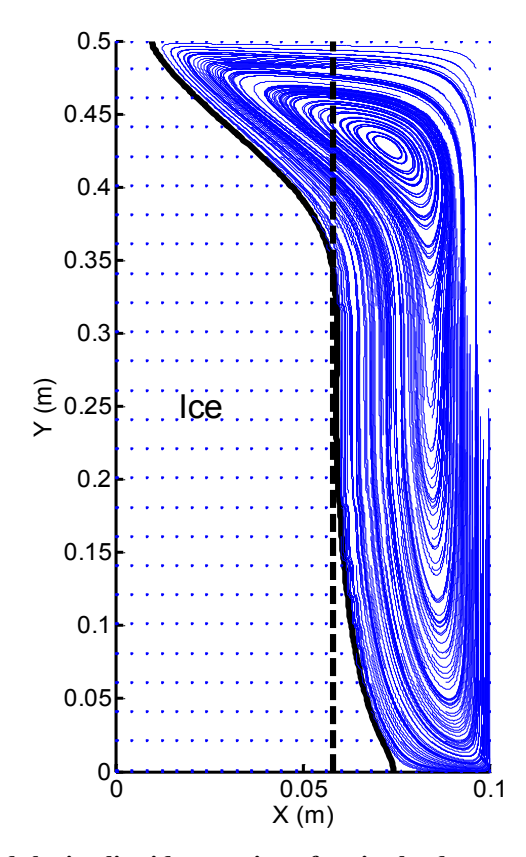


Figure 4.11: Streamlines and the ice-liquid-water interface in the demonstration problem for AR = 5. Axes are not drawn to scale.

### 4.5 Interstitial heat transfer

In this study, in all of the cases with porous metal foams, as the Rayleigh number was increased, both the flow velocity and temperature difference between foam and water increased, but there was uncertainty about whether the interstitial heat transfer is natural-convection or forced-convection domination. An observation of the computed local values of  $Gr_{d_f}/(\mathrm{Re}_{d_f})^2$  from the liquid-water simulations with foam (see Section 4.3), showed that for small Rayleigh numbers, the three interstitial convection regimes coexist: natural convection adjacent to the top and bottom walls; forced convection along the right and left walls; and mixed convection in between. As the Rayleigh number increases, the interstitial natural- and mixed-convection regions shrink and the interstitial convective heat transfer is mostly forced-convection-dominated. In all of the ice-liquid-water-metal-foam simulations discussed in Section 4.3, the interstitial convective heat transfer was found to be forced-convection-dominated, except in the top-left and bottom-right corners of the liquid-water region where the mixed convection correlation prevailed.

However, in all the simulations with the porous metal foams, the correlations for the interstitial convection Nusselt number did not influence the results because their predictions were always lower than those of the correlation for the pure-conduction-limit Nusselt number: at all points,  $Nu_{\text{convection}} < \frac{-4.1}{\ln(1-\epsilon)}$ . The highest observed local value of

 $Nu_{\rm convection}$  in the liquid-water-foam cases was 0.86, found with wall temperatures of Run # 6, the biggest cavity size, and the most porous foam ( $\varepsilon$ =0.98). This value is smaller than the minimum value of the interstitial conduction Nusselt number:  $Nu_{\rm conduction}$  = 1.05 for  $\varepsilon$ =0.98. In the ice-liquid-water-metal-foam cases,  $Nu_{\rm convection}$  locally peaked around 0.75, independently of the aspect ratio.

These rather counter-intuitive observations show the necessity of further detailed investigation of the interstitial heat transfer processes in metal foams.

# Chapter 5: Conclusion

In this final chapter, first, a brief review of the work reported in this thesis and its main contributions are presented. After that, a few suggestions regarding possible extensions of this work are proposed.

#### 5.1 Review of the work and its main contributions

In this section, a review of the work reported in this thesis and its main contributions are presented in four main parts, which correspond to the first four chapters.

- In the first chapter, first, the motivation, overall goals, and background of this work were presented. A review of the published literature relevant to this work was presented next, along with a summary of some key results and comments. Finally, the specific objectives of this work were presented.
- 2. In the second chapter, the mathematical models adopted for steady-state conduction and laminar natural convection in ice-liquid-water-metal-foam systems were presented. The Darcy-Brinkman-Forchheimer momentum equations were adapted to the particular nonlinear variation of the density of water for temperatures that span its inversion point. Empirical correlations for the permeability and the Forchheimer coefficient were taken from the work of Calmidi (1998). For the volume-averaged energy equations, a two-temperature model with isotropic thermal dispersion in the liquid water was adopted.

A semi-empirical model for effective thermal conductivity proposed by Calmidi and Mahajan (1999) was adapted for the two-temperature model, with a special modification that ensures consistency of the predictions obtained with the one-temperature and two-temperature models in the limit of local thermal equilibrium.

Novel expressions for the interstitial interfacial (foam-metal-water) heat transfer coefficients in both the conduction and convection regimes were developed. The correlation for the conduction-regime interstitial Nusselt number was determined using CVFEM simulations of steady-state heat conduction in four different

representative two-dimensional unit cells, and a critical analysis of the results. The correlation for the interstitial interfacial (foam-metal-water) Nusselt number in the convection regime was developed by adapting existing mixed convection correlations for fluid flow around solid cylinders.

- 3. In the third chapter, a well-established, fixed-grid, co-located finite volume method (FVM) for predicting fluid flow and heat transfer phenomena in open domains (no ice; no porous metal foam) was adapted for solving the mathematical models of conduction and laminar natural convection in ice-liquid-water systems in open domains (no foam) and in ice-liquid-water-metal-foam systems. A special approach involving a melting-temperature tolerance was proposed to resolve interface-oscillation and convergence issues encountered during solutions of ice-liquid-water problems, with and without the porous metal foams. Finally, a continuation method that facilitates solutions of the liquid-water, ice-liquid-water, and ice-liquid-water-metal-foam problems of interest was described.
- 4. The results obtained in this work were presented and discussed in the fourth chapter. The main points of note and the related findings are summarized below:
  - The proposed FVM was first validated by the comparing the predicted results to those obtained experimentally and numerically by Elkouh (1996) for steady-state conduction and laminar natural convection in square enclosures containing pure liquid water and ice-liquid-water systems (no foam), with temperatures spanning the density inversion point of water.

For laminar natural convection in pure liquid water (no ice), the agreement between the results obtained in this work and those of Elkouh (1996) was excellent for all cases tested, except the one in which the density inversion parameter was close to 0.5, for which satisfactory convergence could not be achieved. These simulations were conducted using a variable-property model (VPM) and also a constant-property model (CPM), with the constant fluid properties evaluated at several reference (or average) temperatures. It was found that a special zonal reference (or average)

temperature yields the lowest differences between the results yielded by the VPM and CPM.

For conduction and laminar natural convection in ice-liquid-water systems in open domains (no foam), two cases were investigated. The predicted streamlines and ice-liquid-water interface positions showed excellent agreement with the experimental and numerical results of Elkouh (1996). The continuation method was found to be critically important for achieving converged solutions to these problems.

The proposed mathematical models and FVM were used to predict laminar natural convection flow fields and average heat transfer rates at the walls in square horizontal enclosures containing liquid water and aluminum foam. The left-wall temperature was fixed at 0°C, while the right wall temperature was assigned two different values above the density inversion temperature of water. The effect of changes in the dimension of the enclosure (yielding a wide range of Rayleigh number) was investigated with no foam and the results were compared to those of simulations with five different aluminum foams.

The results showed that the addition of porous foams resulted in weaker natural convection (heat transfer due to gradients of the intrinsic-phase-average temperature of the fluid and the associated thermal conductivities) but higher conduction (heat transfer due to gradients of the intrinsic-phase-average temperature of the aluminum foam and the associated thermal conductivities). Foams with higher porosity had smaller weakening effect on the natural convection, but also a lower enhancing effect on the conduction. Foams with lower porosity had more of a weakening effect on the natural convection, but a higher enhancing effect on the conduction. In general, the resulting average total (conduction + convection) Nusselt numbers at the walls obtained with the foams were found to be comparable to those obtained in corresponding cases for open domains (no foam).

In all these simulations, the variation of the average total Nusselt number with Rayleigh number, when natural convection was well established (at high enough values of Ra), was found to follow a power-law:  $\overline{Nu_{wall}} = C \times Ra^n$ . The value of n was found to be common to all foams tested, around 0.22. With no foam, the best fit was found for n=0.29.

The influences of the Forchheimer drag term in the momentum equations and the thermal dispersion in the energy equation were investigated. Their local contributions to the volumetric-drag and heat-conduction terms in the governing momentum and energy equations, respectively, were shown to be proportional to the local permeability Reynolds number.

 Finally, the proposed mathematical models and FVM were applied to problems involving conduction and laminar natural convection in iceliquid-water-porous-metal-foam systems contained in vertical rectangular enclosures.

First, two cases studied earlier by Elkouh (1996) and also in this work for ice-liquid-water systems in an open enclosure (no foam) were investigated with the inclusion of a porous metal foam. In both cases, with the inclusion of the porous metal foam, the results were very close to the pure-conduction limit, in terms of ice-liquid-water interface position and values of the average total Nusselt number on the walls.

Then, a demonstration problem with a representative porous foam made of aluminum, and other parameters in ranges relevant to seasonal cold-storage applications, was investigated. The rectangular enclosure was maintained in a vertical position with respect to the gravitational acceleration vector. Its width in the horizontal direction was 10 cm, its height was varied between 10 to 50 cm, and the imposed cold and hot wall temperatures were -20°C and 20°C, respectively. The Rayleigh number was maintained constant at  $Ra = 1.55 \times 10^8$ . The computed streamlines, water-ice interface positions, and wall heat transfer rates were compared to

the corresponding results obtained with open domains (no foam), to the extent possible (without the foam, convergence could not be achieved for AR > 1.5, and the appearance of multiple recirculating flow cells and chaotic flow fields during the iterative solution process indicated possible transition to turbulence). In cases for which converged solution could be obtained with and without the foam, comparable values of the average total wall Nusselt number were obtained. This Nusselt number was found to decrease as the aspect ratio (AR) increased, and a power-law function with an exponent of -0.252 gave a good fit to the results.

• Finally, the values of the computed interfacial (foam-metal-water) Nusselt number were checked a posteriori. In all of the liquid-water-metal-foam and ice-liquid-water-metal-foam simulations undertaken in this work, the interstitial interfacial (foam-metal-water) heat transfer was found to be conduction-dominated throughout the calculation domain.

## 5.2 Suggestions for extensions of this work

A few suggestions for extensions of this work are listed in this section.

As was mentioned in Chapter 2, cost-effective volume-averaged mathematical models of fluid flow and heat transfer in porous metal foams are quite complex to formulate rigorously, and some improvements in the semi-empirical inputs to these models would be useful. Correlations that bring in the influence of the structure of the porous metal foam could be improved to better account for non-uniformities of pore-diameter and variations in the shape of the ligament cross-section. Approaches akin to those proposed by Wang and Pan (2008) and Bodla et al. (2010) would provide a good starting point in this regard. The treatment of interfacial (foam-metal-water) heat transfer coefficients could be improved by undertaking simulations with three-dimensional unit-cell models of the foam. Furthermore, the transition between conduction and mixed-convection regimes in the interstitial interfacial heat transfer should be fundamentally investigated.

For designing and optimizing cold-storage systems, the implementation of an unsteady numerical model for simulating thermal-energy charging and discharging periods is necessary. Unsteady phase-change problems need to be treated with adapted techniques such as interface-tracking or the enthalpy method [Crank (1988)]. These techniques should be adapted to ice-liquid-water-metal-foam systems. Such models could then be applied to practical cold-storage units, and the best unit size and foam type (porosity and pore diameter) could be determined using suitable optimization techniques.

Finally, complementary experimental investigations of fluid flow and heat transfer in iceliquid-water-metal-foams systems contained within rectangular enclosures would be very useful for checking and refining the proposed mathematical models and numerical solution methods.

# List of References

Abhat, A. (1983), "Low temperature latent heat thermal energy storage: Heat storage materials", *Solar Energy*, Vol.30, pp. 313-332.

Alkan, C., Sari, A., Karaipekli, A. and Uzun, O. (2009), "Preparation, characterization, and thermal properties of microencapsulated phase change material for thermal energy storage", *Solar Energy Materials and Solar Cells*, Vol. 93, pp. 143-147.

Angell, C.A. (1983), "Supercooled water", *Annual review of Physical Chemistry*, Vol. 34, pp. 593-630.

Ashby M.F., Evans A.G., Fleck N.A., Gibson L.J., Hutchinson J.W. and Wadley H.N.G. (2000), *Metal Foams: A design Guide*, Boston: Butterworth–Heinemann.

Ashby, M.F. and Lu, T.J. (2003), "Metal Foams: A survey", *Science in China Series B-Chemistry*, Vol. 46, pp. 521-532.

ASHRAE Handbook, HVAC Applications (2007), New York.

Baliga, B.R. and Atabaki, N. (2006), "Control-volume-based Finite Difference and Finite Element Methods", in *Handbook of Numerical Heat Transfer (2<sup>nd</sup> Ed.)*, W.J. Minkowycz, E.M. Sparrow, and J.Y. Murthy, Chapter 6, John Wiley & Sons, New York.

Banhart, J. (2001), "Manufacture, characterisation and application of cellular metals and metal foams", *Progress in Materials Science*, Vol. 46, pp. 559-U3.

Bear, J. (1988), Dynamics of Fluids in Porous Media, Dover Publications, New York.

Beckermann, C. and Viskanta, R. (1988), "Natural convection solid/liquid phase change in porous media", *International Journal of Heat and Mass Transfer*, Vol. 31, pp. 35-46.

Bhattacharya, A., Calmidi, V.V., Mahajan and R.L. (2002), "Thermophysical properties of high porosity metal foams", *International Journal of Heat and Mass Transfer*, Vol. 45, pp. 1017-1031.

Bodla, K.K., Murthy, J.Y. and Garimella S.V. (2010), "Resistance network-based thermal conductivity model for metal foams", *Computational Materials Science*, Vol. 50, pp. 622-632.

Boomsma, K. and Poulikakos, D. (2001), "On the effective thermal conductivity of a three-dimensionally structured fluid-saturated metal foam", *International Journal of Heat and Mass Transfer*, Vol. 44, pp. 827-836.

Cabeza, L.F., Badia, F., Illa, J., Roca, J., Mehling, H., Ziegler, F. (2001), "Corrosion experiments on salt hydrates used as phase change materials in cold storage", IEA, ECES IA Annex 17Kick-off Workshop, Lleida (Spain).

Cabeza, L.F., Mehling, H., Hiebler, S. and Ziegler, F. (2002), "Heat transfer enhancement in water when used as PCM in thermal energy storage", *Applied Thermal Engineering*, Vol. 22, pp. 1141-1151.

Calmidi, V.V. (1998) "Transport Phenomena in High Porosity Metal Foams", Ph.D. thesis, University of Colorado, Boulder, CO.

Calmidi, V.V. and Mahajan, R.L. (1999), "The effective thermal conductivity of high porosity fibrous metal foams", *Journal of Heat Transfer*, Vol. 121, pp. 466-471.

Calmidi, V.V. and Mahajan, R.L. (2000), "Forced convection in high porosity metal foams", *Journal of Heat Transfer*, Vol. 122, pp. 557-565.

Churchill, S.W. and Chu, H.H.S. (1975), "Correlating equations of laminar and turbulent convection from a horizontal cylinder", *International journal of Heat and Mass Transfer*, Vol. 18, pp. 1049-1053.

Crank, J. (1988), *Free and Moving Boundary Problems*, Oxford University Press, Oxford.

Debenedetti, P.G. and Stillinger, F.H. (2001), "Supercooled liquids and the glass transition", *Nature*, Vol. 410, pp. 259-267.

Dinçer, I. and Rosen, M. (2002), *Thermal energy storage, Systems and Applications*, John Wiley & Sons, Chichester (England).

Du Plessis, P., Montillet, A., Comiti, J. and Legrand, J. (1994), "Pressure drop prediction for flow through high porosity metallic foams", *Chemical Engineering Science*, Vol. 49, pp. 3545-3553.

Elkouh, N. (1996), "Laminar natural convection and interfacial heat flux distributions in pure water-ice Systems", Ph.D. thesis, McGill University, Montréal, Québec Canada.

Farid, M.M., Khudhair, A.M., Razack, S.A.K., and Al-Hallaj, S. (2004), "A review on phase change energy storage: materials and applications", *Energy Conversion and Management*, Vol. 45, pp. 1597-1615.

Frusteri, F., Leonardi, V., Vasta, S. and Restuccia, G. (2004), "Thermal conductivity measurement of a PCM based storage system containing carbon fibers", *Applied Thermal Engineering*, Vol. 25, pp. 1623-1633.

Fukai, J., Hamada, Y., Morozumi, Y. and Miyatake, O. (2002), "Effect of carbon-fiber brushes on conductive heat transfer in phase change materials", *International Journal of Heat and Mass Transfer*, Vol. 45, pp. 4781-4792.

Günther, E., Mehling, H. and Hiebler, S. (2007), "Modeling of subcooling and solidification of phase change materials", Modelling and Simulation in Materials Science Engineering, Vol. 15, pp. 879-892.

Hawlader, M.N.A., Uddin, M.S., and Khin, M.M. (2003), "Microencapsulated PCM thermal-energy storage system", *Applied Energy*, Vol. 74, pp. 195-202.

Hong, Ye, Xin-shi, Ge (2000), "Preparation of polyethylene-paraffin compound as a form-stable solid-liquid phase change material", *Solar Energy Materials and Solar Cells*, Vol. 64, pp. 37-44.

Hunt, M.L. and Tien, C.L. (1988), "Effects of thermal dispersion on forced convection in fibrous media", *International Journal of Heat and Mass Transfer*, Vol. 31, pp. 301-309.

Incropera, F.P. and DeWitt, D.P. (2002), Fundamentals of Heat and Mass Transfer (5<sup>th</sup> edition), Wiley and Sons, New York.

Jagjiwanram and Singh R. (2004), "Effective thermal conductivity of highly porous two-phase media", *Applied Thermal Engineering*, Vol. 24, pp. 2727-2735.

Jegadheeswaran, S., Pohekar, Sanjay D. (2009), "Performance enhancement in latent heat thermal storage system: A review", *Renewable and Sustainable Energy Reviews*, Vol. 13, pp. 2225-2244.

Kaviany, M. (1999), *Principles of heat transfer in porous media* (2<sup>nd</sup> edition), Springer, Berlin.

Kuwahara, F., Shirota, M. and Nakayama, A. (2001), "A numerical study of interfacial convective heat transfer coefficient in two-energy equation model for convection in porous media", *International Journal of Heat and Mass Transfer*, Vol. 44, pp. 1153-1159.

Kazmierczak, M., Poulikakos, D. and Pop, I. (1986), "Melting from a flat plate embedded in a porous medium in the presence of steady natural convection", *Numerical Heat Transfer*, Vol. 10, pp. 571-582.

Khudhair, A.M. and Farid, M.M. (2004), "A review on energy conservation in building applications with thermal storage by latent heat using phase change materials", *Energy Conversion and Management*, Vol. 45, pp. 264-275.

Krishnan, S., Murthy, J.Y. and Garimella, S.V. (2005), "A two-temperature model for solid-liquid phase change in metal foams", *Journal of Heat Transfer - Transactions of the ASME*, Vol. 127, pp. 995-1004.

Kukulka, D.J., Gebhart, B. and Mollendorf, J.C. (1987), "Thermodynamic and transport properties of pure and saline water", *Advances in Heat Transfer*, Vol. 18, pp. 325-363.

Lafdi, K., Mesalhy, O. and Elgafy, A. (2008), "Graphite foams infiltrated with phase change materials as alternative materials for space and terrestrial thermal energy storage applications", *Carbon*, Vol. 46, pp. 159-168.

Lazaridis, A. (1970), "A numerical solution to the multidimensional solidification (or melting) problem", *International Journal of Heat and Mass Transfer*, Vol. 13, pp. 1459-1477.

Mehling, H. and Cabeza, L.F. (2008), *Heat and cold storage with PCM: an up to date introduction into basics and applications*, Springer, Berlin.

Mesalhy, O., Lafdi, K., Elgafy, A., Bowman, K. (2004), "Numerical study for enhancing the thermal conductivity of phase change material (PCM) storage using high thermal conductivity porous matrix", *Energy Conversion and Management*, Vol. 46, pp. 847-867.

Mettawee, E.B.S. and Assassa, G.M.R. (2007), "Thermal conductivity enhancement in a latent heat storage system", *Solar Energy*, Vol. 81, pp. 839-845.

Minkowycz, W.J., Sparrow, E.M., and Murthy, J.Y. (2006), *Handbook of Numerical Heat Transfer (2<sup>nd</sup> Edition)*, John Wiley & Sons, New York.

Mishima, O. and Stanley, H.E. (1998), "The relationship between liquid, supercooled and glassy water", *Nature*, Vol. 396, pp. 329-335.

Nield, D.A. and Bejan, A. (2006), *Convection in porous media* (3<sup>rd</sup> edition), Springer, New York.

Özturk, H.H. (2005), "Experimental evaluation of energy and exergy efficiency of a seasonal latent heat storage system for greenhouse heating", *Energy Conversion and Management*, Vol. 46, pp. 1523-1542.

Patankar, S.V. (1980), Numerical Heat Transfer and Fluid Flow, McGraw-Hill, New York.

Pasupathy, A., Velraj, R. and Seeniraj, R.V. (2008), "Phase change material-based building architecture for thermal management in residential and commercial establishments", *Renewable and Sustainable Energy Reviews*, Vol. 12, pp. 39-64.

Pedras, M.H.J, and De Lemos, M.J.S (2008), "Thermal dispersion in porous media as a function of the solid-fluid conductivity ratio", *International Journal of Heat and Mass Transfer*, Vol. 51, pp. 5359-5367.

Phanikumar, M. S. and Mahajan, R. L. (2002), "Non-Darcy natural convection in high porosity metal foams", *International Journal of Heat and Mass Transfer*, Vol. 45, pp. 3781-3793.

Quintard, M. and Whitaker, S. (1995), "Local thermal equilibrium for transient heat conduction: theory and comparison with numerical experiments", *International Journal of Heat and Mass Transfer*, Vol. 38, pp. 2779-2796.

Regin, A. F., Solanki, S. C. and Saini, J. S. (2008), "Heat transfer characteristics of thermal energy storage system using PCM capsules: A review", *Renewable and Sustainable Energy Reviews*, Vol. 12, pp. 2438-2458.

Rhie, C.M. and Show, W.L. (1983), "Numerical study of the turbulent flow past an air foil with trailing edge separation", *AIAA*, Vol. 21, p. 1525.

Saito, A., Okawa, S., Tojiki, A., Une H.and Tanogashira, K. (1992), "Fundamental research on external factors affecting the freezing of supercooled water" *International Journal of Heat and Mass Transfer*, Vol. 35, pp. 2527–2536.

Saito, A. (2002), "Recent advances in research on cold thermal energy storage", *International Journal of refrigeration*, Vol. 25, pp. 177-189.

Sari, A. (2004), "Form-stable paraffin/high density polyethylene composites as solid-liquid phase change material for thermal energy storage: preparation and thermal properties", *Energy Conversion and Management*, Vol. 45, pp. 2033-2042.

Sharma, A., Tyagi, V.V., Chen, C.R. and Buddhi, D. (2009), "Review on thermal energy storage with phase change materials and applications", *Renewable and Sustainable Energy Reviews*, Vol. 13, pp. 318-345.

Singh, R. and Kasana, H.S. (2004), "Computational aspects of effective thermal conductivity of highly porous metal foams, *Applied Thermal Engineering*, Vol. 24, pp. 1841-1849.

Tadrist, L., Miscevic, M., Rahli, O. and Topin, F. (2004), "About the use of fibrous materials in compact heat exchangers", *Experimental Thermal and Fluid Science*, Vol. 28, pp. 193-199.

Vafai, K. (2000), *Handbook of porous media*, Marcel Dekker, New York.

Velraj, R., Seeniraj, R. V., Hafner, B., Faber, C. and Schwarzer, K. (1999), "Heat transfer enhancement in latent heat storage system", *Solar Energy*, Vol. 65, pp. 171-180.

- Viskanta, R. (1985), "Natural Convection in Melting and Solidification", *Natural Convection: Fundamentals and Applications*, Kakac S. et al., Hemisphere, Washington, DC, pp. 845-877.
- Wakao, N., Kaguei, S. and Funazkri, T. (1979), "Effect of fluid dispersion coefficients on particle-to-fluid heat transfer coefficients in packed beds: Correlation of Nusselt numbers", *Chemical Engineering Science*, Vol. 34, pp. 325-336.
- Wang, M. and Pan, N. (2008), "Modeling and prediction of the effective thermal conductivity of random open-cell porous foams", *International Journal of Heat and Mass Transfer*, Vol. 51, pp. 1325-1331.
- Warnock, J., Awschalom, D.D. and Shafer, M.W. (1986), "Geometrical Supercooling of Liquids in Porous-Glass", *Physical Review Letters*, Vol. 57, pp. 1753-1756.
- Whitaker, S. (1999), *The method of volume averaging*, Kluwer Academic, Boston.
- Xiao, M., Feng, B. and Gong, K. (2002), "Preparation and performance of shape stabilized phase change thermal storage materials with high thermal conductivity", *Energy Conversion and Management*, Vol. 43, pp. 103-108.
- Yang, Z. and Garimella, S.V. (2010), "Melting of phase change materials with volume change in metal foams", Journal of Heat Transfer, Vol. 132, pp. 062301-11.
- Zalba, B., Marín, J.M., Cabeza, L.F. and Mehling, H. (2003), "Review on thermal energy storage with phase change: materials, heat transfer analysis and applications", *Applied Thermal Engineering*, Vol.23, pp. 251-283.
- Zhang, Y. P., Lin, K. P., Yang, R., Di, H. F., and Jiang, Y. (2006), "Preparation, thermal performance and application of shape-stabilized PCM in energy efficient buildings", *Energy and Buildings*, Vol. 38, pp. 1262-1269.
- Zhang, Y.P., Zhou, G.B., Lin, K.P., Zhang, Q.L. and Di, H.F. (2007), "Application of latent heat thermal energy storage in buildings: State-of-the-art and outlook", *Building and Environment*, Vol. 42, pp 2197-2209.
- Zhao, C.Y., Lu, T.J. and Hodson, H.P. (2005), "Natural Convection in metal foams with open cells", *International Journal of Heat and Mass Transfer*, Vol. 48, pp. 2452-2463.
- Zhao, C.Y., Lu, W. and Tassou, S.A. (2006), "Thermal analysis on metal-foam filled heat exchangers. Part II: Tube heat exchangers", *International Journal of Heat and Mass Transfer*, Vol. 49, pp. 2762-2770.
- Zukauskas, A.A (1987), "Convective Heat Transfer in Cross-Flow", *Handbook of Single-Phase Heat Transfer*, Kakac, S. et al., Wiley, New York.